JYU DISSERTATIONS 84

Riia Annala

Conformational Properties and Anion Complexes of Aromatic Oligoamide Foldamers

UNIVERSITY OF JYVÄSKYLÄ
FACULTY OF MATHEMATICS
AND SCIENCE

JYU DISSERTATIONS 84

Riia Annala

Conformational Properties and Anion Complexes of Aromatic Oligoamide Foldamers

Esitetään Jyväskylän yliopiston matemaattis-luonnontieteellisen tiedekunnan suostumuksella
julkisesti tarkastettavaksi yliopiston Ylistönrinteen salissa YlistöKem4
toukokuun 10. päivänä 2019 kello 12.

Academic dissertation to be publicly discussed, by permission of
the Faculty of Mathematics and Science of the University of Jyväskylä,
in Ylistönrinne, auditorium YlistöKem4, on May 10, 2019 at 12 o'clock noon.

JYVÄSKYLÄN YLIOPISTO
UNIVERSITY OF JYVÄSKYLÄ

JYVÄSKYLÄ 2019

Editors
Maija Nissinen
Department of Chemistry, University of Jyväskylä
Ville Korkiakangas
Open Science Centre, University of Jyväskylä

Permanent link to this publication: http://urn.fi/URN:ISBN:978-951-39-7767-2

ISBN 978-951-39-7767-2 (PDF)
URN:ISBN:978-951-39-7767-2
ISSN 2489-9003

ABSTRACT

Annala, Riia
Conformational properties and anion complexes of aromatic oligoamide foldamers
Jyväskylä: University of Jyväskylä, 2019, 80 p.
(JYU Dissertations
ISSN 2489-9003; 84)
ISBN 978-951-39-7767-2 (PDF)

In this work, the conformational properties and anion binding of aromatic oligoamide foldamers with 4-9 aromatic units are described. Single crystal X-ray diffraction, NMR experiments, mass spectrometry and CD spectroscopy were used to study the conformations and structures of the foldamers, while ^{1}H NMR and ITC titrations were used to elucidate the anion binding of the foldamers. The literature review focuses on the anion binding of foldamers.

The structural analysis of five extended foldamers with 7-9 aromatic units showed that the folding motifs are similar to shorter foldamers. The folding is, therefore, predictable and relies mainly on intramolecular hydrogen bonding. The helical and open conformations are retained when foldamers with 5 aromatic units are extended to 7 or 9 aromatic units. A variety of other structures can be obtained by changing the type of a spacer group between the pyridine rings in the foldamer backbone.

The binding of small halides is facilitated by the helical preorganization of the foldamers. Five crystal structures of fluoride complexes were obtained. In the complexes, the fluoride is located at the center of a helix. One of the crystal structures was chiral and even exhibited symmetry breaking in the bulk sample.

Anion complexes were in line with solid state structural studies. The shorter foldamers with 5 aromatic units had the best affinity to chloride in acetone. A slight increase in the affinity was observed for foldamers with electron withdrawing groups. A favorable entropy increase was the main driving force in the 1:1 chloride complexation. For foldamers with two nitro groups at the foldamer ends, a 1:2 host:guest complex was also unexpectedly observed.

Ion mobility mass spectrometry results show that the deprotonated and protonated foldamers and their Cl^- and Na^+, K^+ and Cs^+ complexes have only one preferential conformation in the gas phase. Several cation complexes had conformations where the guest did not affect the size of the conformation, but further comparisons to molecular models are needed to make conclusions about the conformations of the complexes.

Keywords: foldamers, anion binding, supramolecular chemistry, X-ray diffraction, NMR spectroscopy, ion mobility mass spectroscopy

Author's address

Riia Annala
Department of Chemistry
Nanoscience Center
University of Jyväskylä
P.O. Box 35
FI-40014 University of Jyväskylä
Finland
riia.annala@jyu.fi

Supervisor

Professor Maija Nissinen
Department of Chemistry
Nanoscience Center
P. O. Box 35
FI-40014 University of Jyväskylä
Finland

Reviewers

Professor Ngong Kodiah Beyeh
Department of Chemistry
Oakland University
Michigan, USA

Dr. Gilles Guichard
Institut Européen de Chimie et Biologie
Université de Bordeaux
France

Opponent

Professor Antonella Dalla Cort
Dipartimento di Chimica
Università La Sapienza
Roma, Italy

PREFACE

This thesis work was conducted at the Departement of Chemistry, Nanoscience Center, University of Jyväskylä between 2015 and 2019. The work was funded by the University of Jyväskylä Graduate School for Doctoral Studies and the Otto A. Malm Foundation. Additional grants, awards and bursaries given by the Department of Chemistry, the Finnish Concordia Fund, the Alfred Kordelin Foundation Gust. Komppa Fund, the International Union of Crystallography, the 15th BCA/CCG Intensive Teaching School in X-ray Structure Analysis, and the 10th ISMSC-2015, have enabled me to visit international schools and conferences. I sincerely appreciate the experience and knowledge these travels have given me.

I want to express my sincerest gratitude to my supervisor Professor Maija Nissinen. I'm deeply grateful for you, for letting me work in your group and for letting me have this interesting project. I really appreciate the expertise and insight to supramolecular chemistry you have shared with me. I would also like to thank colleagues Dr. Aku Suhonen for helping me get started with foldamers and X-ray crystallography, Dr. Kaisa Helttunen for guidance with the NMR titrations and Dr. Elina Kalenius for her kind advice with the MS and IM-MS methods.

Also, a huge thanks goes to collaborators Prof. Perttu Permi, Dr. Elisa Nauha, Juho Iloniemi, Heikki Lakkonen, Dr. Juha Linnato, Dr. Gemma Aragay, Prof. Pablo Ballester and Prof. Heikki M. Tuononen for their good work. I would like to collectively thank the laboratory technicians, the coworkers and the administrative personnel in the Nanoscience Center and in the Department of Chemistry. Thank you for the positive work environment and assistance during these years. I especially appreciate the interesting and fun discussions during breaks at the NSC coffee room.

I would like to thank the reviewers of this thesis Prof. Ngong Kodiah Beyeh and Dr. Gilles Guichard for their valuable comments. I'm also incredibly grateful that I was able have a two-month research exchange during my PhD studies and would like to thank Prof. Mir Wais Hosseini and his group for so warmly welcoming me in Strasbourg. Special thanks goes to Donata for her friendship during and after the visit.

My work would not have been possible without the support of my friends and family. Thanks to my parents Marja-Liisa and Pauli, my sisters Reeta and Sallamari, and for my best friend Iida for always being there. I'm super grateful to all of my "nanomaisterit" friends Annika, Jenna A., Jenna T., Joakim, Juuli, Karolina, Karoliina, Lasse R., Lasse V., Lauri, Minna, Noora, Ossi, Sonja, Tero and Ville for all the relaxing and fun times we have had. Finally, I wish to thank my dear boyfriend Aatu for all the love, help, and friendship he has given me.

Jyväskylä 25.4.2019
Riia Annala

LIST OF ORIGINAL PUBLICATIONS

This dissertation is based on the original publications listed below and they are referred to by their Roman numerals.

I Riia Annala, Aku Suhonen, Heikki Laakkonen, Perttu Permi and Maija Nissinen, Structural Tuning and Conformational Stability of Aromatic Oligoamide Foldamers, *Chem. Eur. J.*, **2017**, *23*, 16671–16680.

II Kaisa Helttunen, Riia Annala, Aku Suhonen, Elisa Nauha, Juha Linnanto and Maija Nissinen, Supramolecular Chirality and Symmetry Breaking of Fluoride Complexes of Achiral Foldamers, *CrystEngComm*, **2017**, *19*, 5184–5187.

III Kaisa Helttunen, Riia Annala, Aku Suhonen, Juho Iloniemi, Elina Kalenius, Gemma Aragay, Pablo Ballester, Heikki M. Tuononen and Maija Nissinen, Oligoamide Foldamers as Helical Chloride Receptors – the Influence of Electron-Withdrawing Substituents on Anion-Binding Interactions, *Chem. Asian J.*, **2019**, *14*, 647–654.

The author is the primary author for paper I, for which she carried out the crystallographic data analysis and part of the synthesis, characterization, crystallization, X-ray diffraction measurements, and NMR measurements. She has carried out part of the synthesis and crystallography work for paper II and part of the NMR and MS measurements for paper III. The author is the primary investigator and author for the unpublished, preliminary IM-MS studies presented at the end of this work.

ABBREVIATIONS

Ac	acetone
Boc	*tert*-butyloxycarbonyl
CCS	collision cross section
CD	circular dichroism
CPL	circularly polarized luminescence
DCM	dichloromethane
DFT	density functional theory
DMA	dimethylacetamide
DMF	*N,N*-dimethylformamide
DMSO	dimethyl sulfoxide
DOSY	diffusion-ordered spectroscopy
DT	drift tube
EDC	1-ethyl-3-(3-dimethylaminopropyl)carbodiimide
ESI	electrospray ionization
EtOAc	ethylacetate
equiv	equivalence
IM	ion mobility
IM-MS	ion mobility mass spectrometry
ITC	isothermal calorimetry
Me	methyl
MeCN	acetonitrile
MS	mass spectrometry
NMR	nuclear magnetic resonance
NOE	nuclear Overhauser effect
NOESY	nuclear Overhauser effect spectroscopy
Ph	phenyl
TBA	tetrabutylammonium
TBAF	tetrabutylammonium fluoride
t-Bu	*tert*-butyl
TFA	trifluoroacetic acid
THF	tetrahydrofuran
UV	ultraviolet
UV-vis	ultraviolet-visible
XB	halogen bond
XRD	X-ray diffraction

CONTENTS

1 REVIEW OF THE LITERATURE

1.1 Introduction

1.1.1 Foldamers

Foldamers are scientists' attempt to not only mimic the functions of natural biopolymers but to discover new functions. Gellman[1] coined the term foldamers to mean artificial oligomers with "well-defined secondary structural preferences." In this case, the expression "well-defined" means that the conformational preferences of moderate length oligomers should be detectable in solution.

Foldamers can be categorized into two categories: biotic foldamers and abiotic foldamers. In biotic foldamers, the building blocks are natural, such as nucleotides and α- and β-peptides, or the oligomers follow the same folding principles as biopolymers.[2,3] Abiotic foldamers have unnatural backbones and different types of folding modes. Many abiotic foldamers, for example, have aromatic backbones.[4] Heterogeneous foldamers are generated by mixing different types of building blocks.[5,6]

A helix is the most sought out folding mode in foldamer design because of the prevalence of helicity in biological molecules and its potential optical properties due to the chirality of the helix.[7,8] In addition to helices, foldamers can fold into other conformations, such as sheets.[9] The desired conformational preference can be created in multiple different ways.[10] The foldamer can be rigidified by local conformational preferences and interactions[11] or remote intrastrand interactions of the backbone[12]. The conformation can also be induced by solvophobic effects[13,14], metal coordination[15], binding of a guest[16], or other external stimuli[17].

1.1.2 Foldamers as supramolecular hosts and receptors

Due to the prevalence of helical folding, foldamers can form an internal helical cavity, which is ideal for small guests, or they are helically preorganized to accept guests.[18] Alternatively, the ionic or neutral guests can induce foldamers to

adopt a certain conformation.[19] Metal coordination assisted folding of rigid foldamers can also help in the encapsulation of the guest.[20] Foldamers can change their conformation to bind to a guest and in that regard have significant advantage to rigid macrocycle receptors.[21] The control of the foldamer conformation via a guest has many potential applications,[22] for example, in colorimetric anion detection[23] and in creating cell penetrating vectors[24,25].

By careful design, a foldamer can be made to act as a container for specific guests.[26] Huc *et al.*[27], for example, have recently managed to iteratively design[28] a foldamer capsule that can selectively bind disaccharide xylobiose (FIGURE 1). Capsules have wider diameter at the center so that the guest molecule is completely enclosed inside.

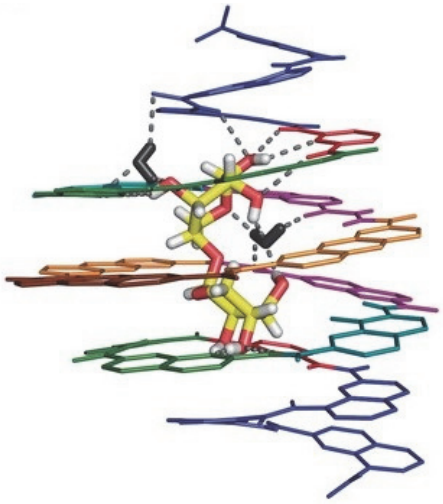

FIGURE 1 Crystal structure of the xylobiose binding foldamer capsule. Figure used with permission from ref. 27. Copyright (2018) Wiley.

Foldamer receptors that bind or release upon external stimuli, such as metal coordination[29] or pH[30-32], could be used as transmembrane channels and transporters or in other stimuli responsive materials. Foldamer receptors have also other potential functions, for example, as catalysts[33], molecular receptors[34,35], luminescent materials[36], and chemical sensors[37].

1.1.3 Anion binding receptors

The properties of anions, such as hydrophilicity or hydrophobicity, hydrogen bonding with the solvent, low charge to radius ratio, sensitivity to pH, and different anion geometries, make the design of anion receptors challenging.[38] Despite inherent difficulties, several acyclic and cyclic anion receptors have been developed that utilize hydrogen bonds, halogen bonding and anion···π interactions in binding.[39] The preorganization and rigidity of cyclic and bicyclic receptors make them suitable for selective binding of small anions and the anions, can also be used as templates in the synthesis of macrocycles.[40] Anion coordination

also has been used to self-assemble knots, molecular cages, and other supramolecular structures.[41]

Anion binding receptors have a great variety of potential applications.[42] Sensor or optical and electronic materials development can benefit from receptors that show optical properties change upon anion guest binding.[43] Anion extraction is important in waste treatment to prevent anions, such as nitrates and phosphates, from causing eutrophication[44], or other harmful anions getting into the environment.[45] Selective receptors can facilitate the selective transport of ions through membranes or enable the separation of mixtures of anions.[46] For example, a potential treatment for cystic fibrosis could be found from artificial chloride transport systems, since the disease is caused by the lack of chloride transport through the natural ion channels.[47]

1.2 Anion binding foldamers

Anion binding is one aspect where foldamers mimic and are inspired by nature. Various substituent groups have been used to bind anions to foldamers, mainly through hydrogen bonds. Quite often, the anion induces the folding of the foldamer into a helical conformation,[22] but the guest anion can also force the foldamer to uncoil from that helical conformation.[48] In the third type of complex, a preorganized foldamer binds the guest.[49]

The anion binding of foldamers has been studied with halide anions (F^-, Cl^-, Br^-, and I^-) and with molecular anions, such as NO_3^-, PF_6^-, CN^-, N_3^- AcO^-, $PhCO_2^-$, HSO_4-, $H_2PO_4^-$, and CH_3COO^-. The binding affinities have been studied by ^1H NMR, ITC, UV-vis, and fluorescence spectroscopic titration. The structures of the complexes have been studied by single crystal XRD, NMR spectroscopic methods, and CD spectroscopy.

1.2.1 Triazole-based foldamers

Triazole-based foldamers utilize the hydrogen bond donor properties of the CH group in the polarized 1,2,3-triazole ring (FIGURE 2).[50] W. D. Kumler[51] first reported CH-based hydrogen bonds in 1935. The existence of CH hydrogen bonds was largely overlooked until the evidence of CH hydrogen bonds in the crystal structures came forth.[52,53] The 1,2,3-triazole motif is selectively formed by a so-called "click reaction," a CuI-catalyzed cycloaddition of organic azides.[54] The click reaction is so fast and efficient that at first it was mainly used to connect other functional groups together.[55] Since then, the anion binding function of triazoles have been used in receptors varying from macrocycles to rotaxanes.[50]

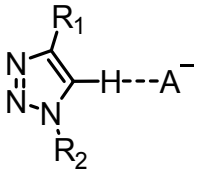

FIGURE 2 A schematic presentation of anion (A^-) binding mode of 1,2,3-triazole ring.

1.2.1.1 Preorganized triazole-based foldamers

Different methods to introduce preorganization to aryl triazole foldamers have been successfully attempted. Meudtner and Hecht[55,56] were the first to study the anion recognition of aryl triazole foldamers. The chiral helical conformation of these foldamers is based on the chiral side groups and intramolecular hydrogen bonds between CH of the triazole and the nitrogen of the pyridine rings in every other aryl ring. Amazingly, according to the CD spectrum, the chiral foldamer **1** can change its helicity when achiral chloride and bromide anions are present, whereas in the presence of fluoride, it retains its helicity (FIGURE 3). The recognition interactions were not studied further, but low pH seemed to intensify the effect.

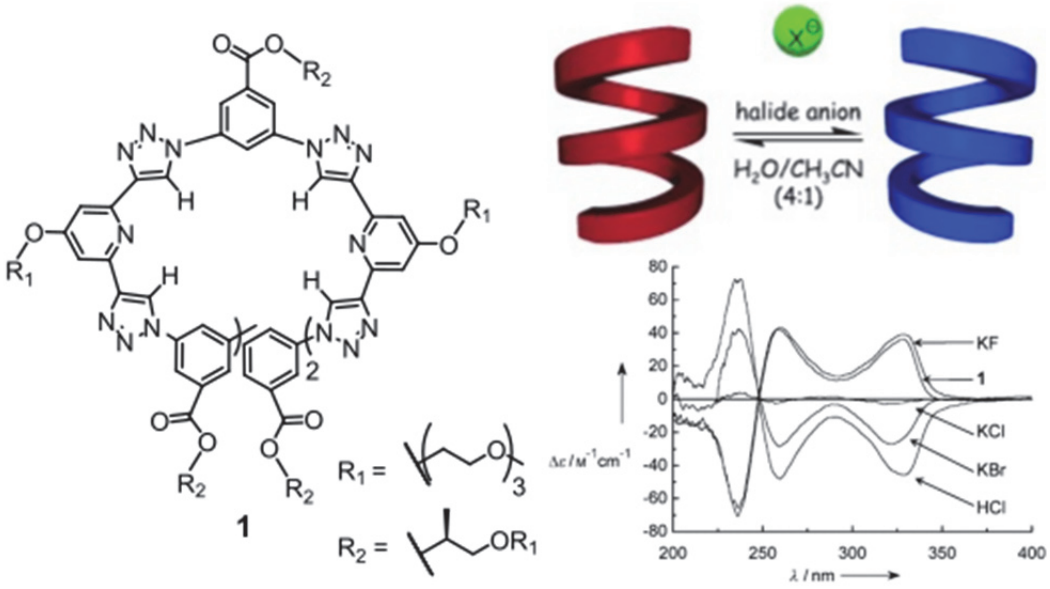

FIGURE 3 Foldamer **1** can change its chirality when binding to anions. Figures used with permission from ref. 56. Copyright (2008) Wiley.

Flood *et al.*[57] also used intramolecular hydrogen bonds for preorganization. The OH···N hydrogen bond forms on the outer rim of short crescent foldamer **2a**, leaving the CH groups free for anion binding (FIGURE 4). This preorganization resulted in approximately a fifty-fold increase in binding of chloride compared with the non-preorganized foldamer **2b** (4.7×10^4 M^{-1} vs. 1.0×10^3 M^{-1}, ^1H NMR titrations in CD_2Cl_2).

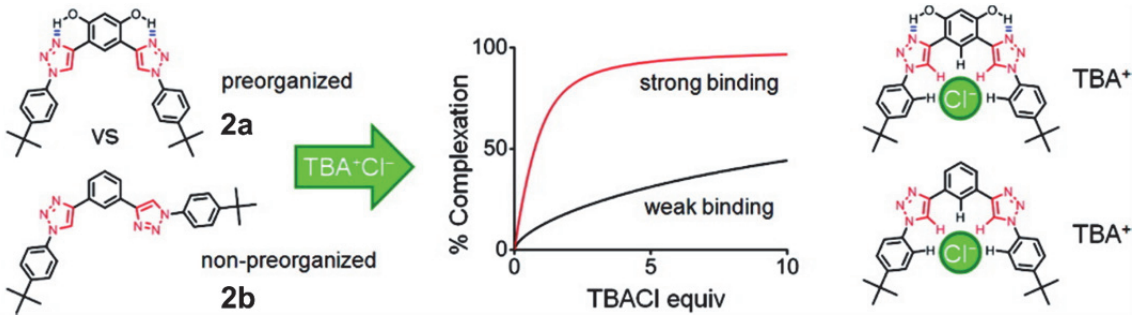

FIGURE 4 The preorganized foldamer **2a** exhibits stronger binding to chloride than the non-preorganized **2b**. Figure is reprinted with permission from ref. 57. Copyright (2010) American Chemical Society.

The same design principle, where the intramolecular hydrogen bonds are on the outer ring, was used in foldamers **3a-b** (FIGURE 5) to create a capsule for chloride.[58] Foldamer **3a** has chiral side chains, and it produced the crystal structure of **3a·Cl⁻·Na⁺** complex with an M helix. Based on the chemical shifts in NMR titrations ($CDCl_2$, CD_3CN), foldamers **3a-b** also formed helical duplex capsule complexes (**3a/b)$_2$·Cl⁻**. Binding constants for foldamer **3b**, which has solubility increasing side chains, were determined by UV-vis spectroscopic titration. The formation stability of the duplex increased when water was added to MeCN (K_2: 500 000 M^{-1} in pure MeCN and 38 000 000 M^{-1} in 1:1 H_2O:MeCN), and the foldamer **3b** can bind chloride even when 50 % water is present. Similarly to biomolecules, hydrophopic effects play an important part in formation of the 2:1 foldamer:chloride complex. Molecular models show that the duplex conformation efficiently protects the triazole hydrogen bond donors from solvents.

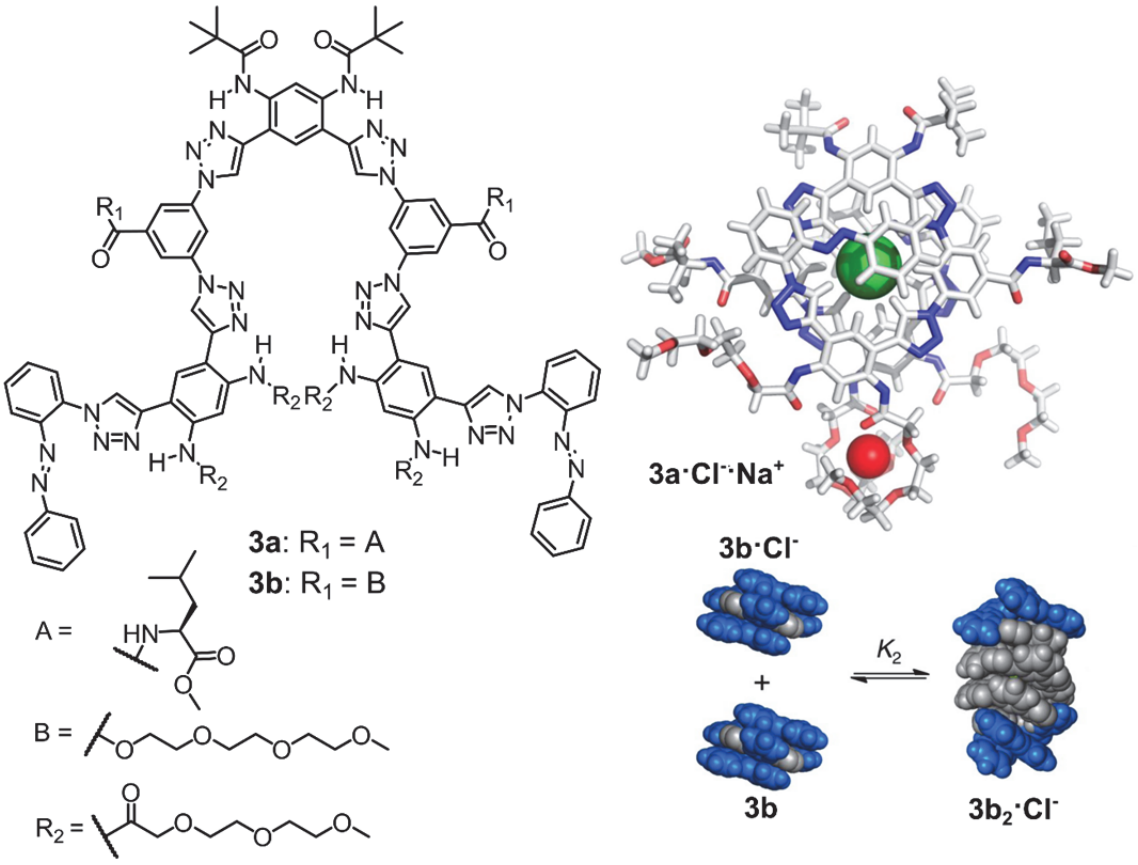

FIGURE 5 Schematic representation of foldamers **3a-b** (left), the crystal structure of **3a·Cl⁻·Na⁺** complex (top right), and molecular model of the duplex (bottom right). The figures on the right are reprinted (adapted) with permission from ref. 58. Copyright (2013) American Chemical Society.

Jiang *et al.*[49] discovered that the preorganized foldamer **4a** was a more efficient transporter of Cl^- across a lipid membrane than partially preorganized foldamer **4b**. ^1H NMR titrations revealed that foldamer **4a** also had higher affinity to halide anions (Cl^-, Br^-, and I^-) in DCM than foldamer **4b** in chloroform (FIGURE 6).

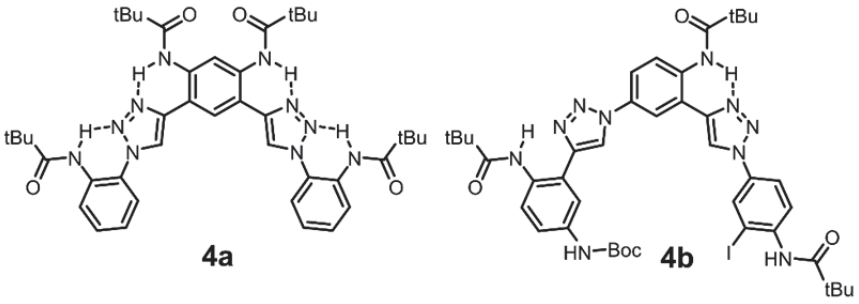

Anion	K_a of **4a** in CD_2Cl_2 [M^{-1}]	K_a of **4b** in $CDCl_3$ [M^{-1}]
Cl^-	757	91
Br^-	367	109
I^-	134	68

FIGURE 6 Schematic representation of foldamers **4a** and **4b** and their binding affinities.

A ruthenium(II) complex was incorporated into the backbone of foldamers **5a-b** to make the foldamers partially preorganized for the helical binding of anions (FIGURE 7).[59] The ROESY measurements of foldamer **5a** in acetone-d_6 confirmed that the foldamer is folded when in presence of Cl^-. The binding of chloride, bromide, iodide, and nitrate anions to foldamer **5a** was studied by NMR, UV-vis, and fluorescence titration experiments. Binding affinities could not be determined from the UV-vis titrations, but the binding constants from the NMR and fluorescence titrations are presented in TABLE 1. The NMR chemical shifts induced by chloride in acetone-d_6 indicated that a 2:1 complex, where the chloride is sandwiched between two foldamers, forms in addition to the 1:1 complex. In DMSO-d_6, however, only a 1:1 complex was observed. The data from NMR and ITC titrations in DMSO suggested 2:1 foldamer:anion binding and duplex formation for foldamer **5b**.

TABLE 1 Binding constants for foldamers **5a-b.**

Foldamer **5a**

Anion	K_a in acetone $[M^{-1}]$[a]	K_a in D_2O/acetone-d_6 (5/95) $[M^{-1}]$[b]	K_a in DMSO-d_6 (5/95) $[M^{-1}]$[b]
Cl^-	$K_{11} = (5.09\pm0.17)\times10^5$ K_{21}[c] -	$K_{11} = (4.3\pm0.2)\times10^3$ $K_{21} = (2.9\pm0.2)\times10$	$K_{11} = (2.1\pm0.17)\times10^2$
Br^-	$K_{11} = (1.15\pm0.05)\times10^6$ $K_{21} = (9.73\pm1.11)\times10^4$	$K_{11} = (4.8\pm0.4)\times10^3$ $K_{21} = (3.6\pm0.9)\times10$	$K_{11} = (8.3\pm0.02)\times10$
I^-	$K_{11} = (2.86\pm0.07)\times10^4$ $K_{21} = (5.03\pm0.75)\times10^4$	$K_{11} = (5.9\pm0.5)\times10^3$ $K_{21} = (2.4\pm0.3)\times10$	$K_{11} = 7.1\pm0.9$
NO_3^-	$K_{11} = (1.93\pm0.01)\times10^5$ K_{21}[c] -	$K_{11} = (1.5\pm0.2)\times10^3$ $K_{21} = (4.5\pm0.7)\times10$	-[d]

[a] Fluorescence titration. [b] NMR titration. [c] Could not be determined.
[d] No complexation.

Foldamer **5b**

Anion	K_a in DMSO-d_6 $[M^{-1}]$[a]	K_a in D_2O/acetone-d_6 (5/95) $[M^{-1}]$[b]
Cl^-	$K_{11} = (6.08\pm0.30)\times10^3$ $K_{21} = (1.38\pm0.12)\times10^3$	$K_{11} = (2.41\pm0.22)\times10^3$ $K_{21} = (2.15\pm0.22)\times10^3$
Br^-	$K_{11} = (6.05\pm0.38)\times10^2$ K_{21}[c] -	$K_{11} = (6.30\pm0.67)\times10^2$ $K_{21} = (4.69\pm0.54)\times10^3$
I^-	$K_{11} = (3.20\pm0.32)\times10^2$ K_{21}[c] -	$K_{11} = (4.10\pm0.47)\times10^2$ $K_{21} = (8.56\pm1.1)\times10^3$
NO_3^-	$K_{11} = (5.5\pm2.3)\times10$ K_{21}[c] -	-[c]

[a] NMR titration. [b] ITC. [c] Could not be determined.

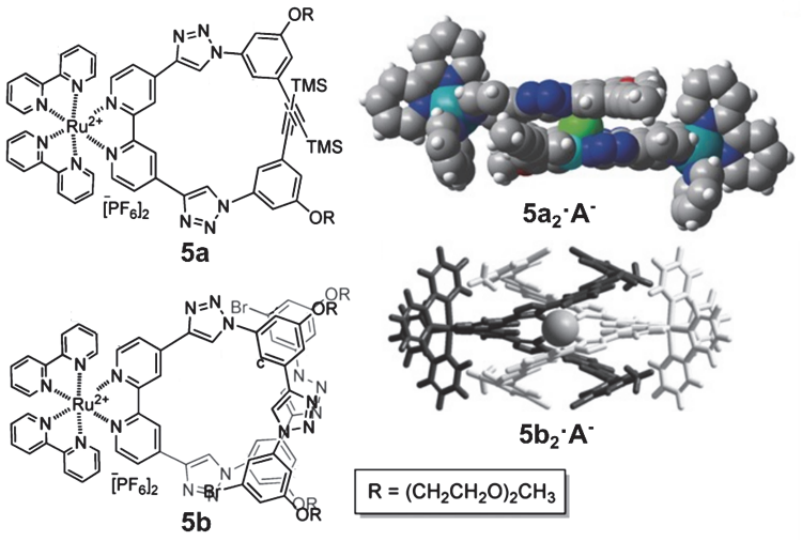

FIGURE 7 Schematic representation of foldamers **5a-5b** and molecular models of their 2:1 anion complexes. The figures are used with permission from ref. 59. Copyright (2016) Wiley.

Cationic side chains were used to induce helical folding of a triazole containing foldamer in a water:methanol solvent mixture.[60] The foldamer **6** (FIGURE 8) can bind chloride and fluoride ions even in aqueous solution (water:methanol 75:25) through the internal helical cavity. The binding prevents the aggregation of the foldamer.

Foldamers **7a** and **7b** constitute of cationic methylpyridinium groups between the triazole units (FIGURE 8).[61] ^{1}H NMR titration was used to study the binding of chloride, bromide, and iodide in an aqueous solvent mixture (6:94 D_2O/pyridine-d_5). The binding was nonselective, and the association constants were in the order of 10^3 M^{-1} for **7a** and 10^4 M^{-1} for **7b**.

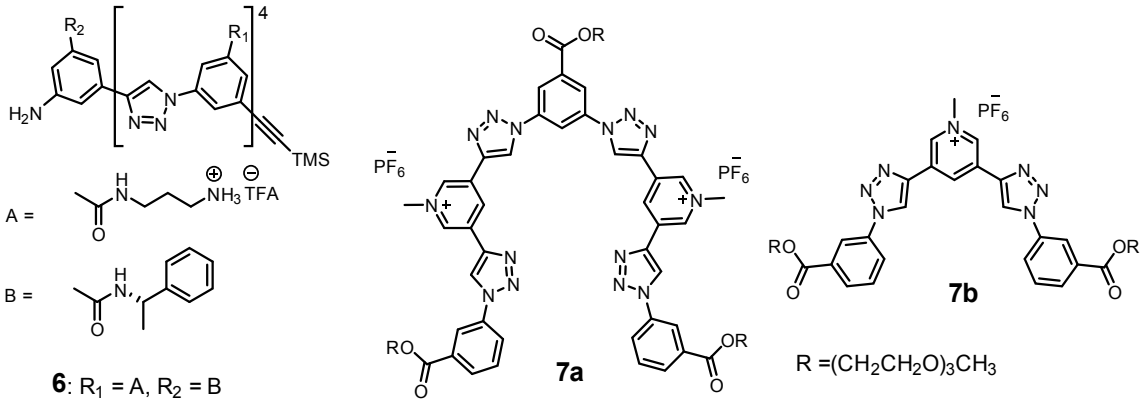

FIGURE 8 Cationic foldamers **6** and **7a-b** that can bind halide anions in aqueous solvent mixtures.

Photoswitchable azobenzene moiety in triazole foldamer **8** backbone was used to influence the binding conformation (FIGURE 9).[62] In this foldamer receptor, the binding affinity increased 4-fold for Cl^- (from 70 M^{-1} to 290 M^{-1}, ^{1}H NMR titration in acetone-d_6) when the azobenzene was irradiated with UV light to adopt the *cis* form.

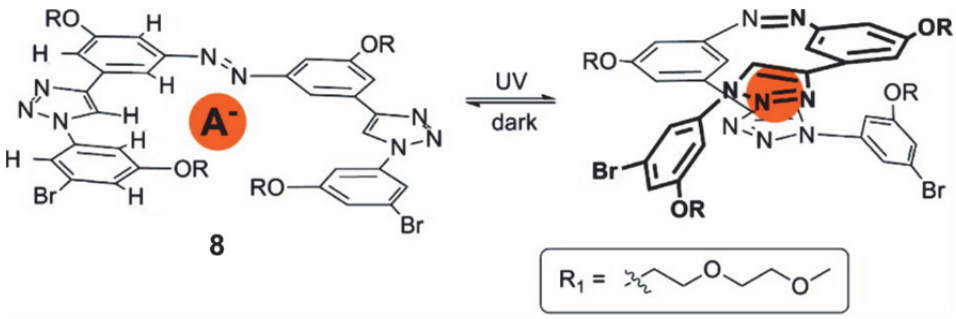

FIGURE 9 The photoswitchable foldamer **8**. Figure is reprinted (adapted) with permission from ref. 62. Copyright (2010) American Chemical Society.

In the light active foldamers **9a-c** (FIGURE 10), the chloride binding conformation is stabilized by π-π stacking interactions when the azobenzene end groups are in *trans* conformation.[63,64] The binding constant for foldamer **9a** de-

termined by UV-vis titration in 50% MeCN/THF was 40300 M^{-1}. For foldamer **9b,** which has added aromatic groups that increase the π-π stacking interactions, the binding affinity increased to 126000 M^{-1} in the same conditions. To further increase the chloride affinity, the helical conformation of foldamer **9c** was stabilized with side chains that form β-sheet-like hydrogen-bonding arrays with each other and, therefore, interlock the ends of the foldamer together (FIGURE 10). This resulted in a binding constant of 970000 M^{-1}. The chloride can be released by irradiating the azobenzene groups to *cis* conformation, which breaks the π···π contacts.

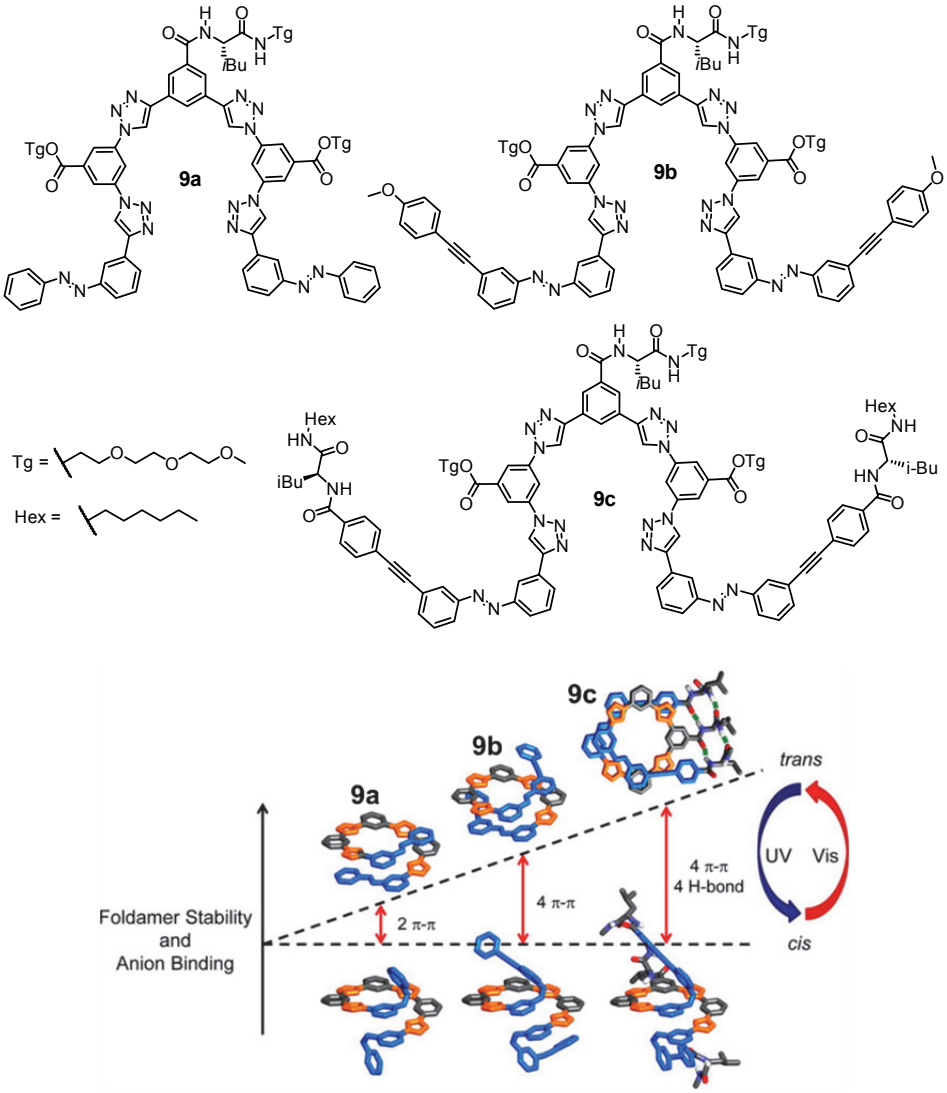

FIGURE 10 Photoswitchable foldamers **9a-c.** The foldamer conformational stability and anion binding increases with higher preorganization via π-π stacking interactions or intramolecular hydrogen bonds. When the azobenzene groups are switched to *cis* conformation, the preorganization interactions are lost. Figure is reprinted (adapted) with permission from ref. 64. Copyright (2014) American Chemical Society.

Aryltriazole foldamer **10** with a resorcinol group in its backbone can also be switched between preorganized helical halide binding conformation and w-shaped weakly binding conformation by protonating and de-protonating the resorcinol OH groups (FIGURE 11).[65] Binding of Cl^-, Br^-, and I^- was nonselective and the binding constants in 6:94 (v/v) $[D_6]DMSO/CDCl_3$ solution were 1-2 orders of magnitude larger for the helical conformation (Cl^-: 8.1×10^4 M^{-1}, Br^-: 1.8×10^4 M^{-1}, I^-: 3.1×10^3 M^{-1}) than for the w-shaped conformation (Cl^-: 3.1×10^2 M^{-1}, Br^-: 2.7×10^2 M^{-1}, I^-: 2.1×10^2 M^{-1}).

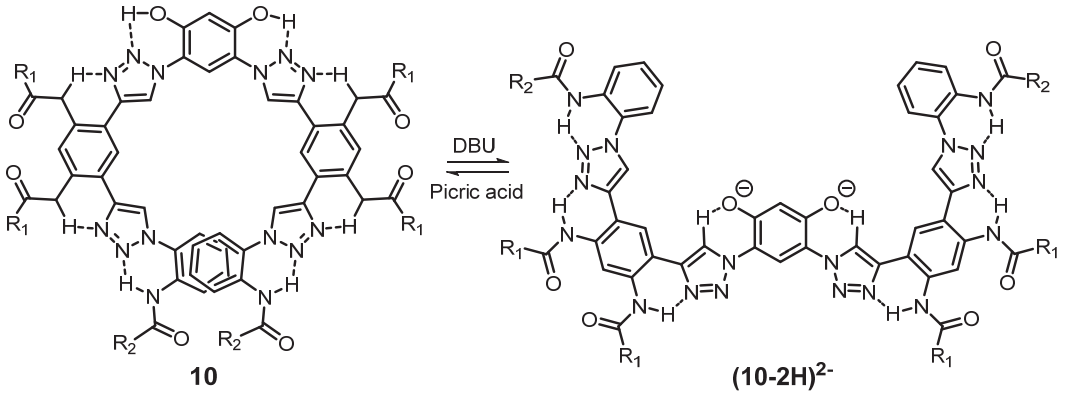

FIGURE 11 The pH-switchable foldamer **10** and the conformational change from helical to w-shape.

Preorganization can also hinder anion binding as is the case with helical triazole-based foldamers (**11,** FIGURE 12**)** where no binding of chloride or iodide could be seen.[66] The conformation is too strongly stabilized by intramolecular CH···F bonding, which prevents the triazole CH groups from hydrogen bonding to the anions.

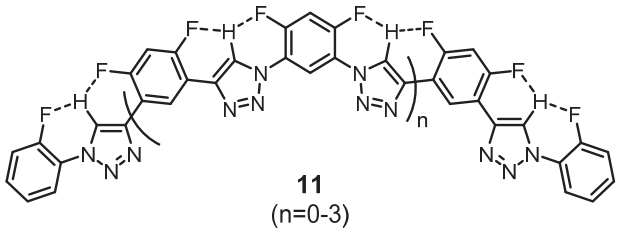

FIGURE 12 The strong CH···F hydrogen bonds prevent foldamers **11** from binding anions.

1.2.1.2 Anion induced folding in triazole-based foldamers

The research group of Craig[67] was the first to demonstrate that CH···anion binding can induce aryl triazole foldamers to fold into a helical conformation (FIGURE 13). The helicity is caused by directional CH···halide interactions in the 1:1 foldamer-anion complexes, and the interactions are strong enough to be observed by ^1H NMR spectroscopy. The binding constants for chloride complexes of the foldamers **12** and **13** ($K= 1.7\times10^4$ M^{-1} and 1.3×10^3 M^{-1}, respectively) were determined by ^1H NMR titration in deuterated acetone. Further studies of

foldamers **12** and **13** with different anions (Br^-, I^-, $PhCO_2^-$, HSO_4^-, NO_3^- and PF_6^-) and in different solvents and solvent mixtures revealed that the binding is weaker if the solvents have good hydrogen bond donor ability.[68] Anions with small ionic radius have greater binding affinity, and increasing the number of triazole CH···anion hydrogen bond donors to the foldamer backbone has a positive effect on binding.

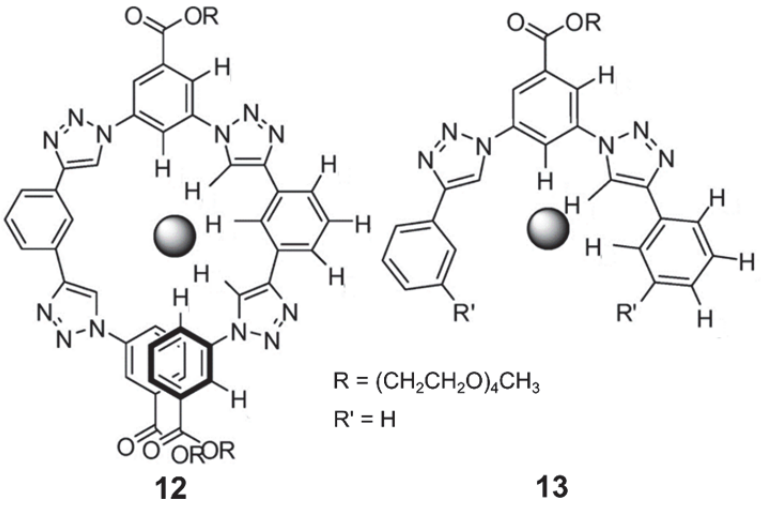

FIGURE 13 Foldamers **12** and **13** and their assumed anion binding mode. The figure is reprinted (adapted) with permission from ref. 68. Copyright (2009) American Chemical Society.

Foldamer **14** (FIGURE 14) can helically wrap around large halides, such as Br^- and I^-.[69] The binding of Cl^- ($K = 6.9\ M^{-1}$), Br^- ($K = 2.7\times10^2\ M^{-1}$), and I^- ($K = 2.1\times10^2\ M^{-1}$) in deuterated DCM, however, was 2 to 6 orders of magnitudes weaker than with the comparable macrocycles ($K = 1.1\times10^7\ M^{-1}$ for Cl^-, $K = 7.5\times10^6\ M^{-1}$ for Br^- and $K = 1.7\times10^4\ M^{-1}$ for I^-, determined using UV spectroscopy).[69,70] Foldamers **15a-c** (FIGURE 14), with alternating triazole and amide groups, also fold into helical conformations when binding halide ions (Cl^-, Br^-, I^-).[71] The host:guest stoichiometry was 1:1 for short oligomer **15a** and 1:2 for longer oligomers **15b** and **15c**. To bind two halides, the helical pitch of the foldamers increases so that the distance between the electrostatically repulsive anions increases as well.

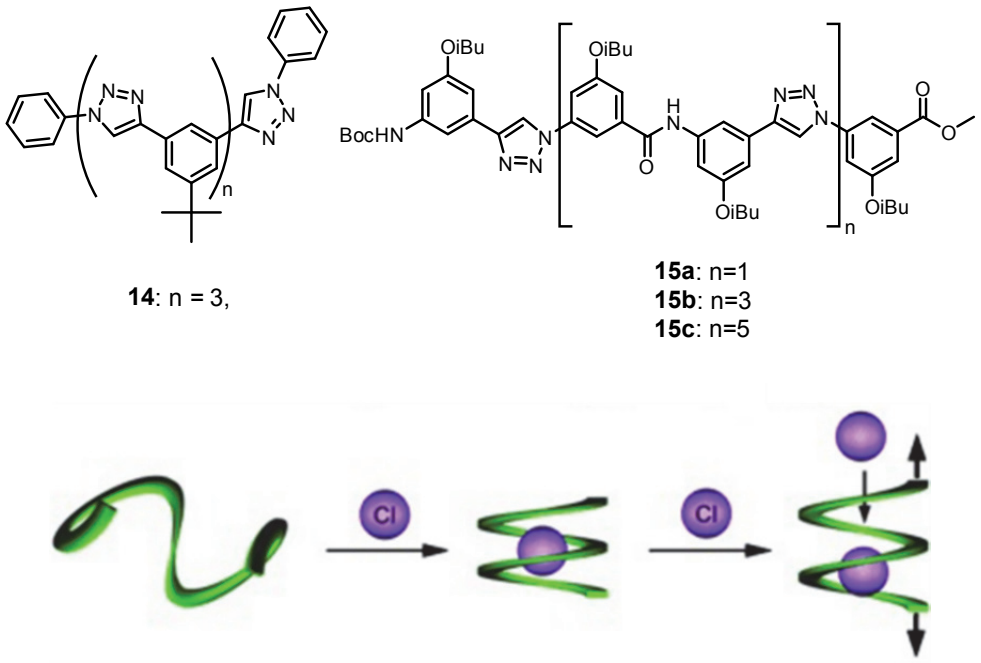

FIGURE 14 Foldamers **14** and **15a-c** (top). The anion binding induces a helical conformation and the helical pitch of the foldamers increases to accommodate second chloride (bottom, figure used with permission from ref. 71. Copyright (2010) Wiley).

Halide induced folding can be monitored by placing fluorescent 1,8-naphthalimide motifs at the triazole foldamer **16** terminus (FIGURE 15) because the binding of halide either changes or quenches the fluorescent emission.[72] The strong π-π stacking of the aromatic terminal groups in foldamer **16** enhances the non-selective binding to halides (Cl^-, Br^-, I^-, $K = 10^5\ M^{-1}$, determined by fluorescent titration in THF). The binding to chloride brings the naphthalimide motifs closer together to create a π-π stacked excimer, whose emission is detectable at 480 nm. In foldamers **17a-d**, the π-π stacking interaction of terminal groups only slightly affects the nonselective binding of Cl^-, Br^-, and I^-.[73] Instead, the amide H-bond donor enables the binding in foldamers **17c-d** ($K = 10^1$-$10^2\ M^{-1}$ in 15:85 (v/v) DMSO-d_6/$CDCl_3$, ^1H NMR titrations), while **17a** does not bind halides at all.

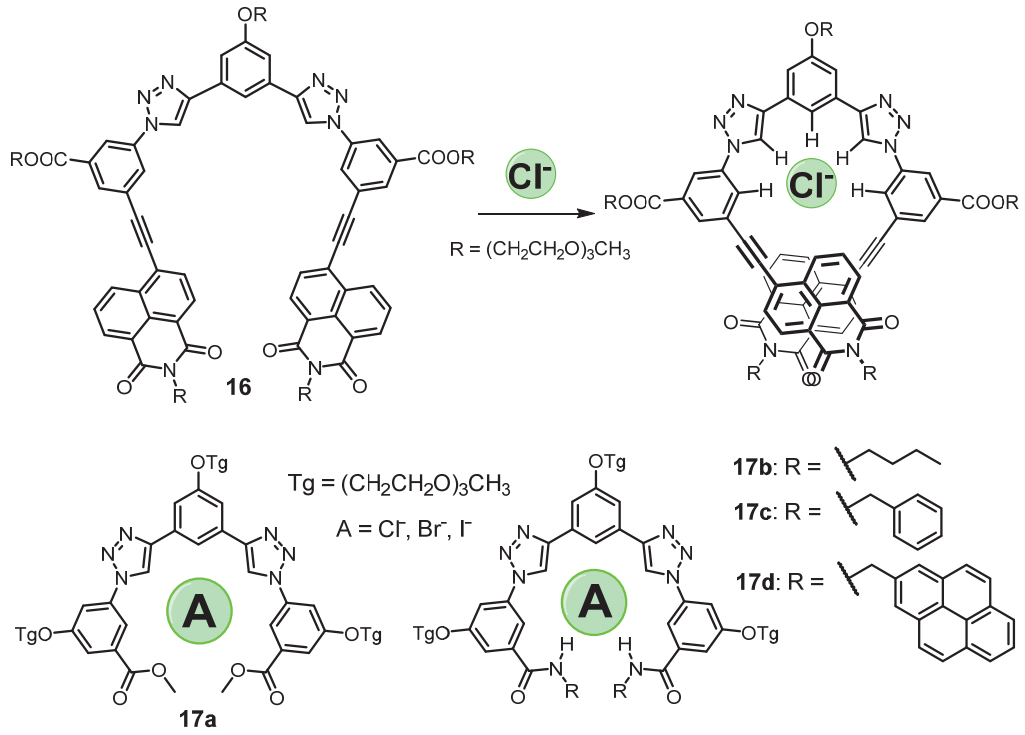

FIGURE 15 The anion induced folding of foldamer **16** can be monitored by fluorescence spectroscopy (top). Halide binding modes of foldamers **17a-d** (bottom).

Foldamers 1**8a-b** (FIGURE 16) have high affinity to various anions but low selectivity.[74] The binding affinities for Cl^-, Br^-, I^-, NO_3^-, HSO_4^-, $H_2PO_4^-$, and AcO^- were all in the range of 10^6-10^5 M^{-1} (in 10:90 (v/v) DMSO/THF, as determined by UV-vis titration).

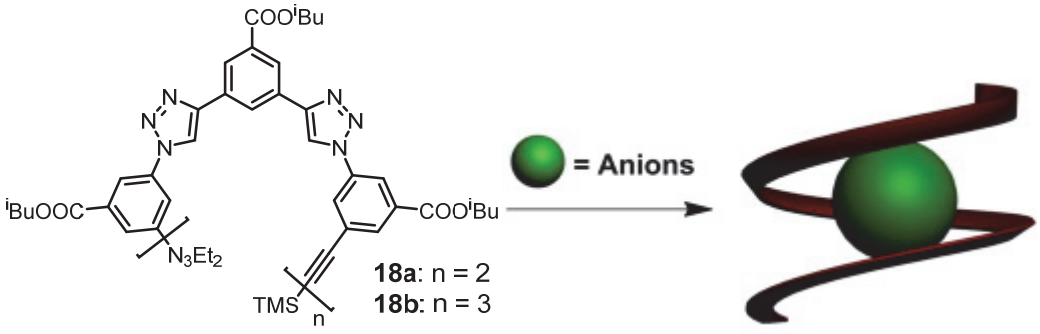

FIGURE 16 **18a-b** has low selectivity but high affinity to several anions. The binding induces a helical folding (right, image reprinted from ref. 74, Copyright (2016), with permission from Elsevier).

Foldamers **19a-b** (FIGURE 17) have three triazolecarboxamide units in their backbone and the best affinity toward sulfate anion (K = 1300 M^{-1} and 2200 M^{-1}, respectively in CD_2Cl_2).[75] For F^-, Cl^-, Br^-, AcO^-, and $H_2PO_4^-$, the binding affinities with **19a** were 1 to 3 orders of magnitude smaller. NOESY NMR studies of the stable **19a**·SO_4^{2-} complex indicated a helical conformation around the anion.

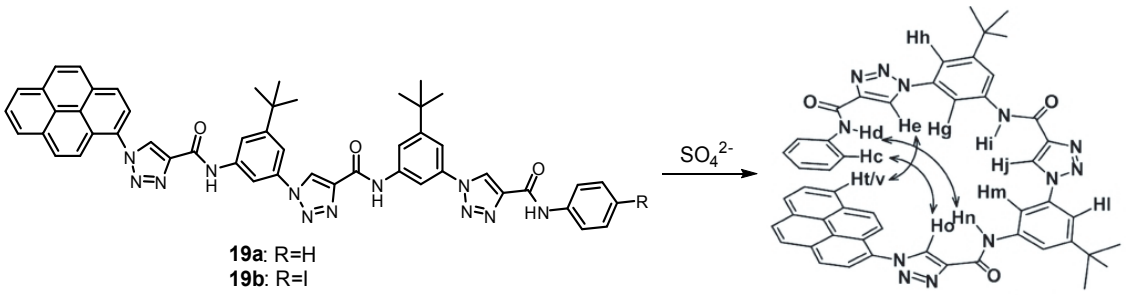

FIGURE 17 Foldamer **19** wraps around sulfate anions in helical conformation as evidenced by NOESY NMR studies. Proton correlations are shown with arrows. Figure used with permission from ref 75. Copyright (2014) Wiley.

Instead of hydrogen bonds, Beer *et al.*[76] used halogen bonds to bind anions in their 5-iodo-1,2,3-triazole-based foldamers **20a-d**, where the CH proton is replaced by iodide (FIGURE 18). These four dentate foldamers had a greater affinity especially toward larger halides, such as I^-, compared with the analogus hydrogen bond based triazole foldamer receptors **21a-d**. The crystal structure of **20c·NaI** shows that the foldamer is not tightly wrapped around the I^- due to the large size of iodine XB donor atoms. Instead, the iodotriazoles are tilted towards the I^- situated 3 Å above the mean plane of the foldamer backbone (FIGURE 18).

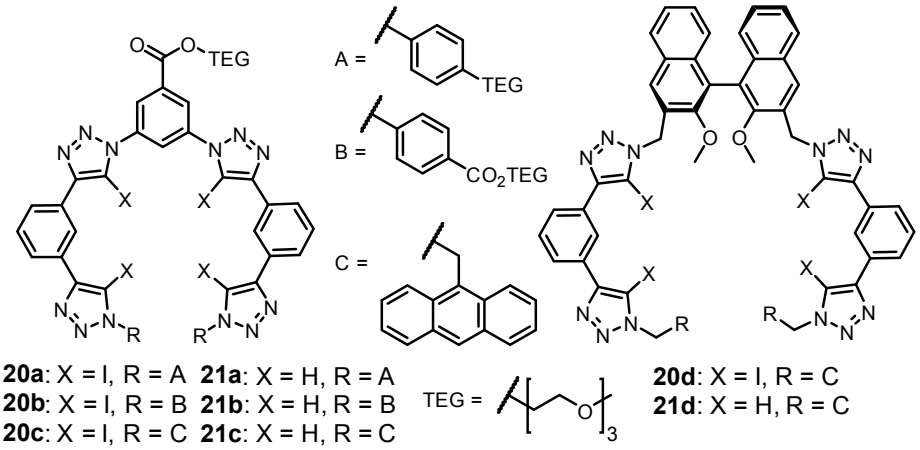

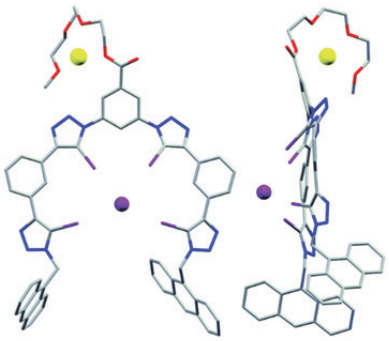

FIGURE 18 The 5-iodo-1,2,3-triazole-based foldamers **20a-d** and the equivalent hydrogen bond based triazole foldamer receptors **21a-d** (top)**.** The crystal structure of **20c·NaI** shows how the foldamer binds to iodide by halogen bonds (bottom).

Mancheño *et al.*[77] have designed chiral chloride binding foldamer **22** (FIGURE 19) as helical anion-binding catalysts. The catalyst dearomatized quinolones asymmetrically with high enantioselectivity. Similarly, the principle has been used with shorter triazolium cation receptors to catalyze asymmetric alkylation of oxindoles.[78]

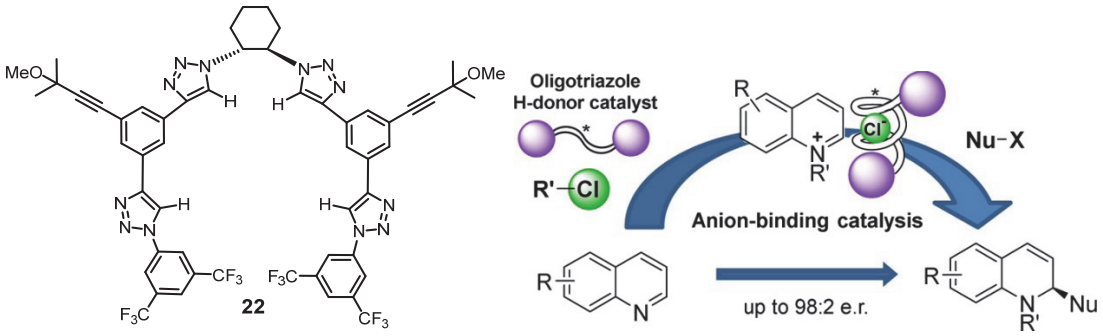

FIGURE 19 The chloride complex of chiral foldamer **22** catalyses the dearomatization of quinoles enantioselectively. Figure on right reprinted (adapted) with permission from ref. 77. Copyright (2014) American Chemical Society.

1.2.2 Hydrazine foldamers

Hydrazine foldamers have been used to bind neutral saccharides[79-81], but the hydrazine foldamers **23a-b** (FIGURE 20) can also bind halide anions and saccharides separately or even simultaneously.[82] The Cl^- and Br^- complexes both have 1:2 foldamer:halide stoichiometry confirmed by Job's plot, and the association constants are higher for chloride (K_1 = 133 M^{-1}, K_2 = 89 M^{-1} vs. K_1 = 75 M^{-1}, K_2 = 18 M^{-1} for **23b·Cl₂** and **23b·Br₂**, respectively, in $CDCl_3$). The synergistic binding of saccharides and chloride was investigated by CD spectroscopy. The addition of chloride to the **23a**:saccharide complex greatly increased the CD signal, indicating that the binding of the chiral saccharide to the achiral foldamer is amplified by the chloride binding.

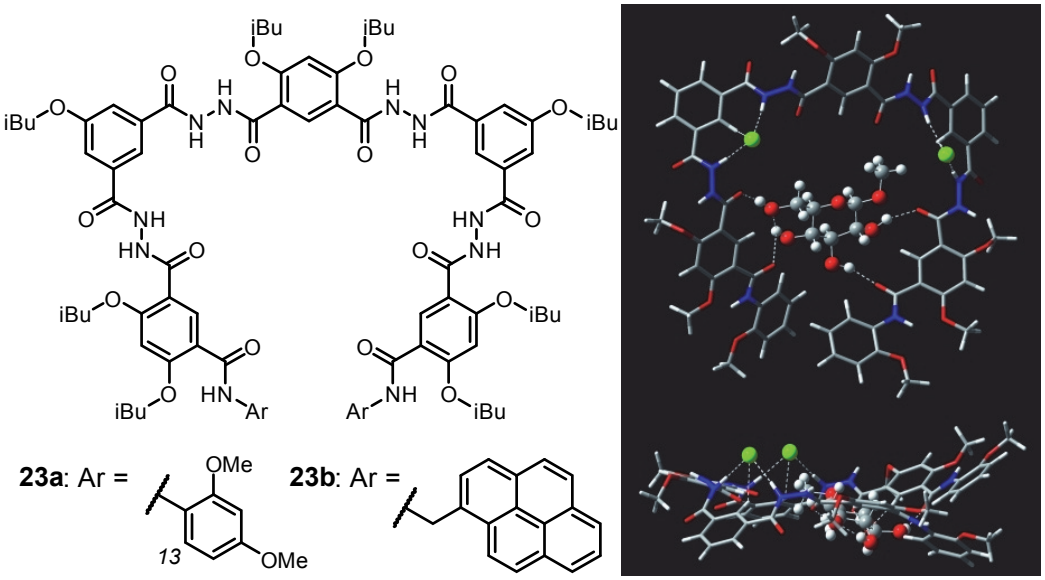

FIGURE 20 Foldamers **23a** and **23b** and DFT optimized model of **23a·2Cl⁻·saccharide** complex. Figure used with permission from ref. 82. Copyright (2013) Wiley.

1.2.3 Oligoindole foldamers

Oligoindoles use the NH group of indoles as hydrogen bond donors to bind anions. Typically, the oligoindole-based foldamers exists as a random coil, and the folding is induced by the anion.[83] Kyu-Sung Jeong *et al.*[84] introduced oligoindole foldamers **24a-c** (FIGURE 21) that fold into a helical conformation when binding to chloride. Similar foldamers **25a-d** are fluorescent and express fluorescent color change upon binding of an anion.[85] The association constants for foldamers **25c** and **25d** with a series of anions were determined by fluorescence spectroscopy in 20 % (v/v) MeOH/DCM (FIGURE 21). Both **25c** and **25d** had the highest affinity for fluoride. For foldamers **25a** and **25b**, only the chloride binding was tested, which resulted in association constants of <1 M^{-1} and 630 M^{-1}, respectively.

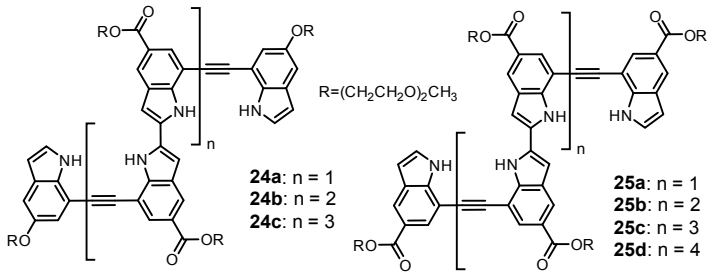

Anion	K_a of **25c** [M^{-1}]	K_a of **25d** [M^{-1}]
F^-	5.1×10^5	1.2×10^6
Cl^-	1.1×10^5	2.9×10^5
Br^-	1.6×10^4	5.0×10^4
I^-	4.0×10^3	2.1×10^4
CN^-	8.5×10^4	1.1×10^5
N_3^-	6.0×10^4	1.2×10^5
NO_3^-	4.8×10^3	8.0×10^4
AcO^-	2.9×10^4	9.4×10^4

FIGURE 21 Schematic presentation of foldamers **24a-c** and **25a-d** (left) and the association constants of foldamers **25c** and **25d** in 2:8 (v/v) MeOH/DCM mixture (right).

Chiral oligoindole foldamers **26a-e** have a preference to fold upon binding to anions either into M-helix or P-helix based on which of the chiral phenylethylamine (R or S, respectively) is incorporated at the ends of the foldamers.[86,87]

The helicity is observed in CD spectra when TBACl is added to foldamers **26a-e** in $CDCl_2$ or in 1:1 (v/v) CH_3CN/DCM. NOESY spectra of **26a·Cl**$^-$ and **26c·Cl**$^-$ complexes supported the helical conformation. The binding of foldamer **26a** with Cl^-, Br^-, I^-, NO_3^-, and N_3^- was studied with UV-vis titration in 99:1 (v/v) DCM/MeOH. The best affinity was for N_3^- with binding constant of 8.5×10^5 M^{-1}, and the weakest affinity was to I^- (K_a = 2.6×10^2 M^{-1}). The binding constants for Cl^-, Br^- and NO_3^- were 2.9×10^5 M^{-1}, 6.2×10^4 M^{-1} and 4.4×10^4 M^{-1}, respectively.

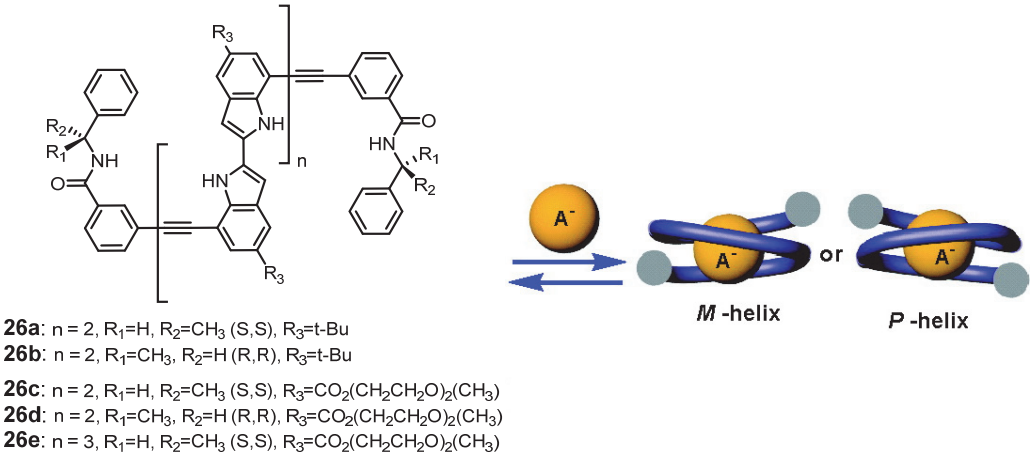

26a: n = 2, R_1=H, R_2=CH_3 (S,S), R_3=t-Bu
26b: n = 2, R_1=CH_3, R_2=H (R,R), R_3=t-Bu
26c: n = 2, R_1=H, R_2=CH_3 (S,S), R_3=$CO_2(CH_2CH_2O)_2(CH_3)$
26d: n = 2, R_1=CH_3, R_2=H (R,R), R_3=$CO_2(CH_2CH_2O)_2(CH_3)$
26e: n = 3, R_1=H, R_2=CH_3 (S,S), R_3=$CO_2(CH_2CH_2O)_2(CH_3)$

FIGURE 22 Chiral foldamers **26a-d** fold to M- or P-helices upon anion binding depending on the chirality of the substituent R_2. Figure on the right is reprinted (adapted) with permission from ref. 86. Copyright (2008) American Chemical Society.

Jang *et al.*[88] synthesized molecular tweezers **27** (FIGURE 23) that fold when either chloride anion or 1,4□diazabicyclo[2.2.2]octane (DABCO) is bound in different binding sites. The tweezers can also bind both guests at the same time. UV-vis titration in THF resulted in a binding constant of 4.93×10^4 M^{-1} for the **27·Cl**$^-$ complex. The **27**·DABCO complex made the chloride binding site suitably preorganized so that the binding of chloride increased significantly (K_a = 7.10×10^5 M^{-1}) in the presence of DABCO.

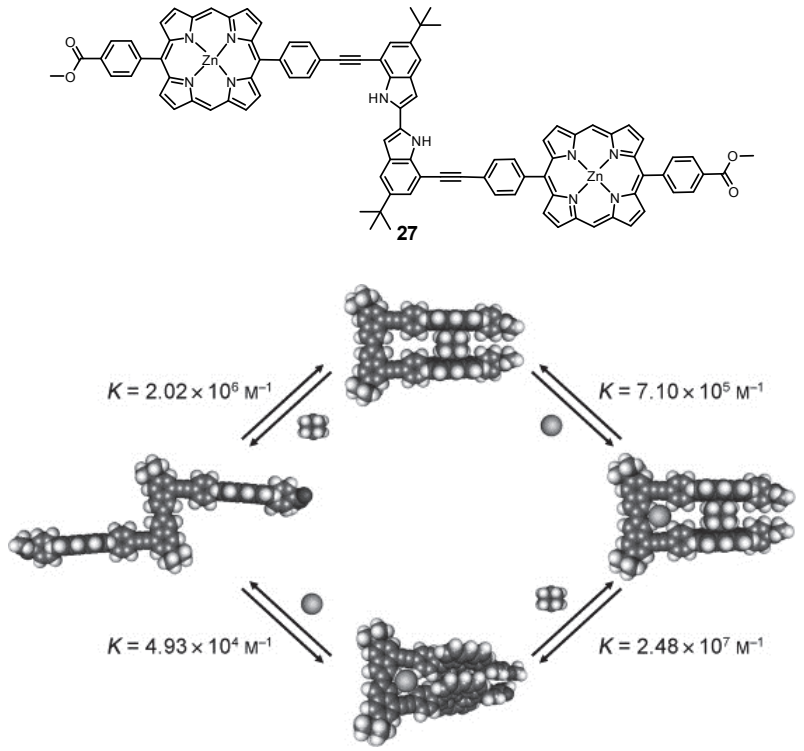

FIGURE 23 Schematic presentation of foldamer **27** (top). Energy-minimized molecular models of foldamer **27** complexes and their respective association constants determined by UV-vis titration in THF (bottom, the figure used with permission from ref. 88. Copyright (2009) Wiley).

The research group of Jurczak[89] combined indole groups with urea hydrogen bond donors in their foldamer **28** (FIGURE 24). The foldamer could bind $H_2PO_4^-$ in MeOH-d_3 with a binding constant of 235 M^{-1}. For HSO_4^-, $PhCO_2^-$, Cl^-, and Br^- anions, the binding constants were one order of magnitude smaller. The crystal structure of the **28**·HPO_4^- complex shows that the HPO_4^- is bound to the foldamer by eight hydrogen bonds (FIGURE 24).

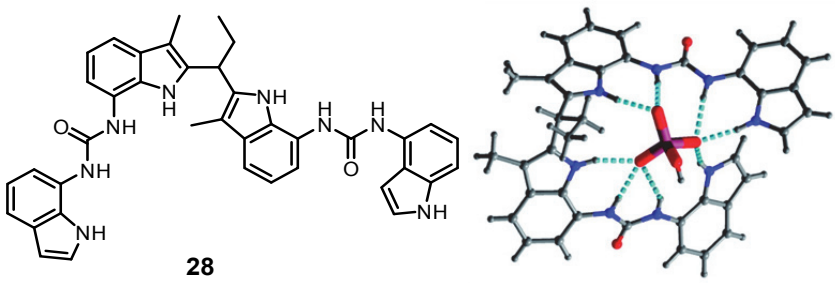

FIGURE 24 Foldamer **28** and the crystal structure of **28**·HPO_4^- complex. Reprinted (adapted) with permission from ref. 89. Copyright (2010) American Chemical Society.

1.2.4 Indolocarbazole-based foldamers

The indolocarbazole unit is useful for making internal cavities inside helically folded foldamers due to its large size.[90] Increasing the length of indolocarbazole foldamers **29a-d** increased the binding constants with chloride.[91] The binding constants 11 M^{-1} for **29a·Cl**$^-$ and 560 M^{-1} for **29b·Cl**$^-$ were determined by NMR titration in 4:1 (v/v) DMSO-d_6/MeOH-d_3. For chloride complexes of **29c** and **29d,** the binding constants of 37000 M^{-1} and 140000 M^{-1}, respectively, were determined by fluorescence spectroscopy in 4:1 (v/v) DMSO/MeOH.

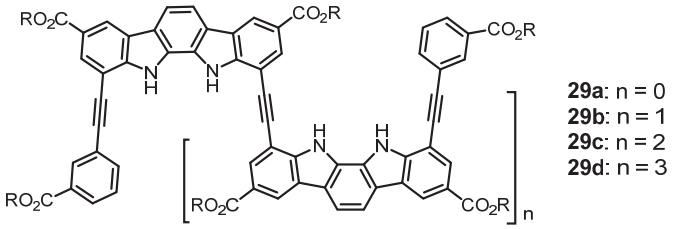

FIGURE 25 Schematic representation of foldamers **29a-d**.

A water soluble foldamer **30a** with an internal cavity and hydrolyzed ester side chains (FIGURE 26) can bind halides in the order $Cl^- > F^- > Br^-$, (K = 65, 46 and 19 M^{-1}, respectively, determined by NMR titration in D_2O).[92] In organic solvents (4:1 DMSO:MeOH), however, the affinity is stronger for F^- than for Cl^- (FIGURE 26). Further proof about helical folding upon binding was later obtained from a crystal structure and solution studies of indolocarbazole foldamer **30b**.[93] The foldamer **30b** has a high selectivity toward sulfate (640000 M^{-1}) determined by fluorescence spectroscopy in 10% (v/v) MeOH:CH_3CN. The binding affinity of **30b** to $H_2PO_4^-$, Cl^-, Br^-, $CH_3CO_2^-$, and CN^- was two orders of magnitude smaller.

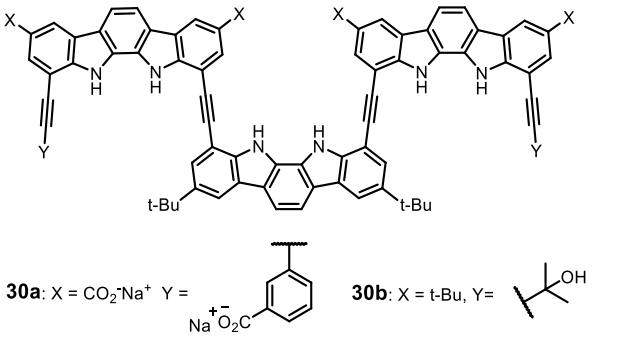

Anion	K_a of **30a** [M^{-1}]
F^-	183 000
Cl^-	36 800
Br^-	1350
I^-	86

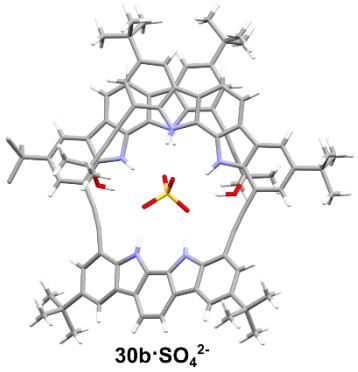

FIGURE 26 Foldamers **30a-b**, the crystal structure of sulfate complex of **30**b and binding constants for **30a** in 4:1 DMSO:MeOH solution.

Expanding the cavity by substituting ethynyl to butadiynyl allows larger anions ($H_2PO_4^-$, $CH_3CO_2^-$ and N_3^-) to be bound to foldamers **31** and **32a-b** (FIGURE 27).[94] Like the triazole foldamer of Meudtner and Hecht[56] (chapter 1.2.1.1), chiral indolocarbazole foldamer **32a** can invert its helicity upon binding to achiral anions (SO_4^{2-}, Cl^-, AcO^-).[95] Foldamer **32b** has selectivity to sulfate ions (K_a = 2.5×10^5 M^{-1}, determined by fluorescence spectroscopy in 10% (v/v) MeOH:acetone) because the urea NHs form hydrogen bonds to the sulfate.[96] Binding constants for **32b·$H_2PO_4^-$** and **32b·AcO^-** complexes were one order of magnitude smaller (determined by ^1H NMR in 10% (v/v) CD_3OH:acetone-d_6).

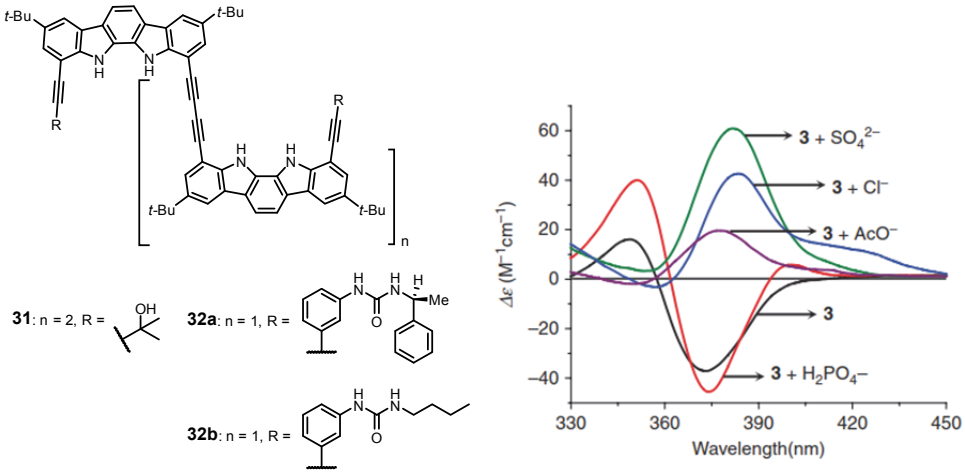

FIGURE 27 Expanded foldamers **31** and **32a-b** (left). The CD spectrum of foldamer **32a** with various anions showing the inversion of chirality with SO_4^{2-}, Cl^- and AcO^- (right). Reprinted with permission from ref. 95. Copyright © 2015 Taylor & Francis Group

Jeong *et al.*[97] made fluorescent indolocarbazole foldamers **33a-b** where the fluorescence is turned off by the π-π staking of the helical conformation present in nonpolar solvents including wet CD_2Cl_2, $CDCl_3$, and toluene-d_8. The fluorescence is turned back on by fluoride and sulfate anions that bind to the foldamer and so disrupt the π - π stacking.

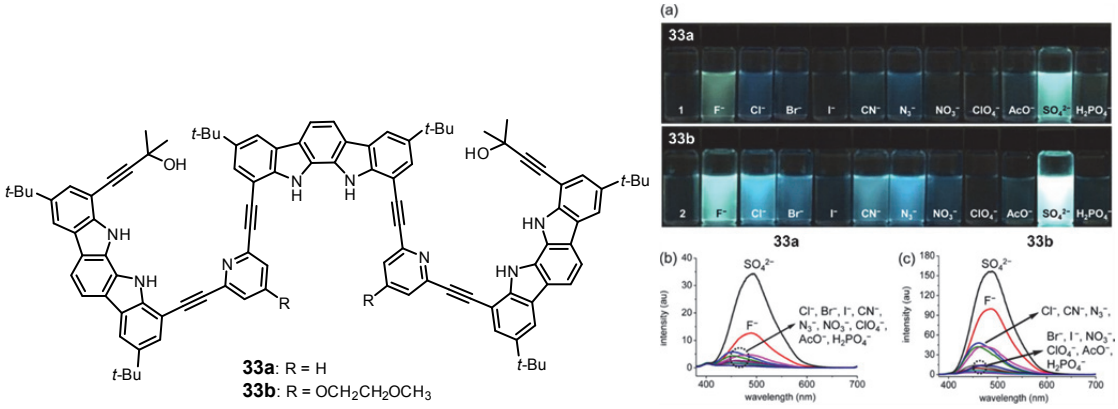

FIGURE 28 Foldamers **33a-b,** photographs of the fluorescent complexes under UV lamp and the fluorescence spectra. Reprinted (adapted) with permission from ref. 97. Copyright (2016) American Chemical Society.

1.2.5 Pyridinium-based foldamers

In pyridinium-based foldamers, either the protonated pyridine acts as a hydrogenbond donor for anion binding or an *N*-alkylpyridium cation facilitates the hydrogen or halogen binding. Johnson *et al.*[98] obtained crystal structures showing that protonated 2,6-bis(anilinoethynyl)pyridine foldamer **34** folds into a helical structure induced by chloride binding in the solid state (FIGURE 29). The chloride is bound by hydrogen bonds from the pyridium NH and from the two

amide NHs. Arylethynyl foldamer **35** (FIGURE 29) self-assembles into a triple helicate when binding to iodides via halogen bonds to iodopyridinium groups.[99] The iodide complex of the triple helicate revealed eight iodine…iodine halogen bonds that bind two iodides inside the tubular helicate. ^{1}H NMR, 2D NOESY, and 2D DOSY experiments indicated the triple helicate is also stable in solution (1:4 v/v [D_7]DMF–CD_3CN) up to 68 °C.

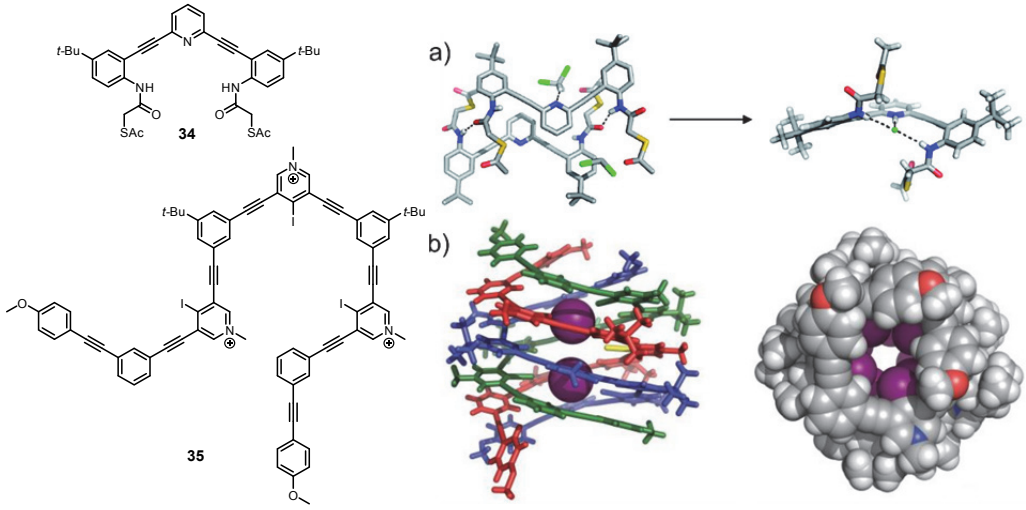

FIGURE 29 Schematic presentation of foldamers **34** and **35** (on the left). a) The crystal structures of 2,6-bis(anilinoethynyl)pyridine foldamer **34** and the chloride complex of the protonated foldamer **34** (Reprinted (adapted) with permission from ref. 98. Copyright (2009) American Chemical Society). b) The crystal structure of **35** triple helicate complex (Used with permission from ref. 99. Copyright (2016) Wiley).

1.2.6 Dipyrrolyldiketone boron complex-based foldamers

Dipyrrolyldiketone boron complex-based foldamers fold into helical structures induced by anion binding.[100] 1:1, 1:2, and 2:2 host to guest binding ratios between the foldamers **36a**, **36b**, and **36c** and chloride anions, respectively, were observed in the solid state (FIGURE 30).[101] ^{1}H NMR studies in CD_2Cl_2 supported 1:1 binding with Cl^- for foldamers **36a** and **36d**. Binding constants for Cl^-, Br^-, and I^- anions with foldamers **36a**, **36b**, **36d**, and **36e** were determined by UV-vis titration in DCM (FIGURE 30).

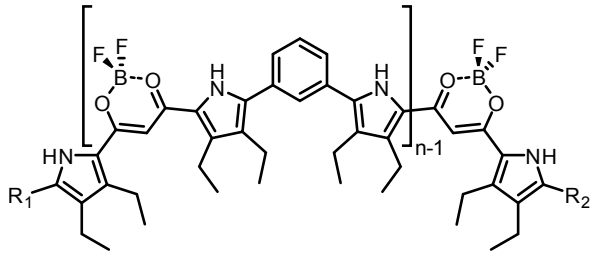

36a: n=2, R_1=R_2=H
36b: n=4, R_1=R_2=H
36c: n=2, R_1=R_2=C_6H_5
36d: n=2, R_1=R_2=I
36e: n=2, R_1=H, R_2=I

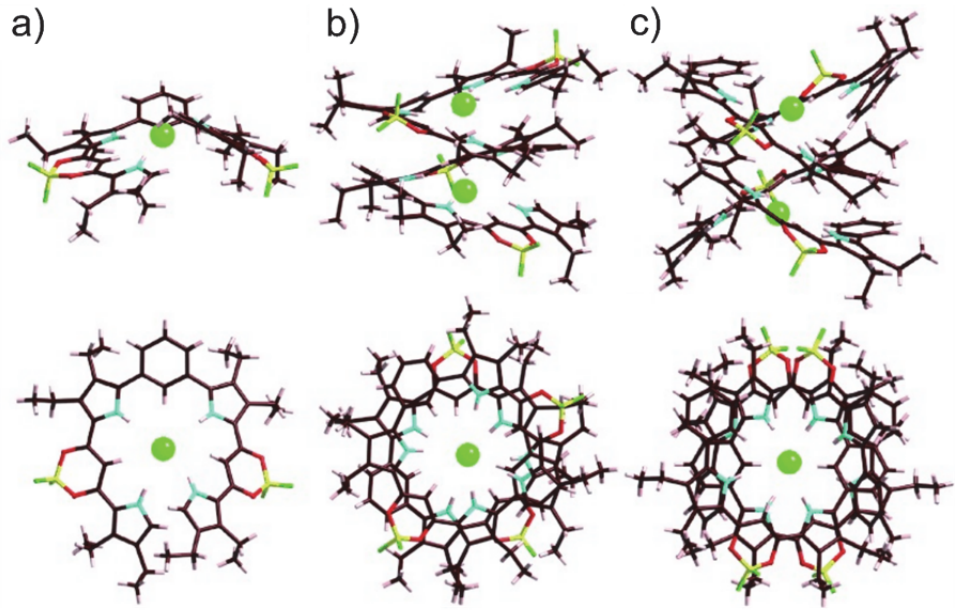

anion	K_a of **36a** [M^{-1}]	K_a of **36b** [M^{-1}]	K_a of **36d** [M^{-1}]	K_a of **36e** [M^{-1}]
Cl^-	59 000 000	K_1: 120 000 000 K_2: 3200	12 000 000	850 000
Br^-	4 800 000	K_1: 23 000 000 K_2: 1600	24 000	38 000
I^-	58 000	K_1: 88 000 K_2: 33	6800	130

FIGURE 30 Foldamers **36a-e** and the crystals structures of a) **36a·Cl⁻**, b) **36b·Cl_2^-** and c) **36c_2·Cl_2^-** complexes. Figure used with permission from ref. 101. Copyright (2010) Wiley. Table below presents the binding constants for **36a-b** and **36d-e** in DCM.

Maeda *et al.*[102] also discovered that the chirality of the dipyrrolyldiketone boron complex-based foldamers **37a-b** is induced by chiral π-conjugated counter cations of the chloride and bromide (**38a-d**) that bind to the foldamers (FIGURE 31). The induction is caused by ion-pair formation between the foldamer-anion complex and the chiral cation in DCM. The asymmetric formation of helical structures was detected in the CD signals and in the increased circularly polarized luminescence (CPL).

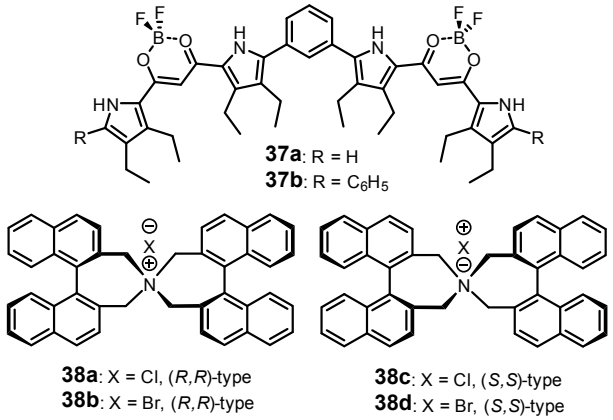

FIGURE 31 Foldamers **37a-b** and the chiral chloride and bromide salts **38a-d**.

In foldamers **39a-d** (FIGURE 32), the chirality of the helix can also be induced by the chirality of the amino acid anion guests (L-Phe$^-$ and D-Phe$^-$).[103] The chirality of L-Phe$^-$ complexes of foldamers **39b-c** was observed with CD spectroscopy and with CPL spectroscopy. The binding constants for L-Phe$^-$, Cl^-, Br^-, and $CH_3CO_2^-$ complexes of **39a-d** were determined by UV-vis spectroscopy in DCM. Binding constant were also determined for complexes (see table in FIGURE 32).

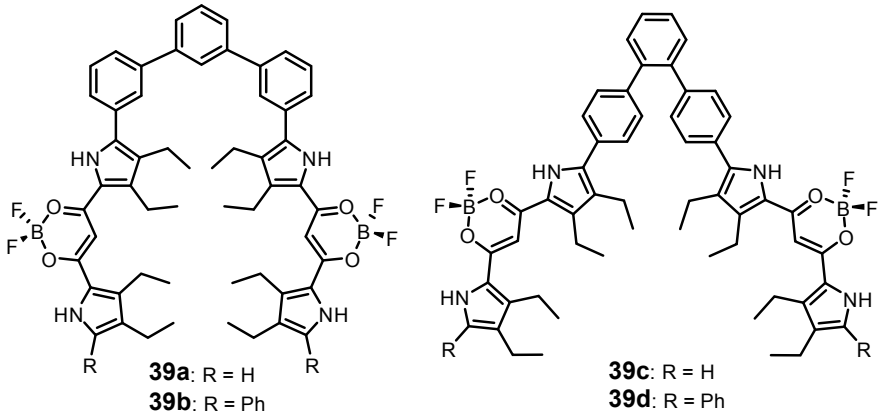

anion	K_a of **39a** [M^{-1}]	K_a of **39b** [M^{-1}]	K_a of **39c** [M^{-1}]	K_a of **39d** [M^{-1}]
Cl^-	7.3×10^6	6.0×10^4	1.4×10^6	4.9×10^5
Br^-	2.7×10^5	-	2.7×10^5	-
$CH_3CO_2^-$	1.3×10^7	-	2.7×10^6	-
L-Phe$^-$	2.4×10^6	8.2×10^4	2.0×10^7	6.0×10^5

FIGURE 32 Foldamers **39a-d** and a table presenting binding constants for Cl^-, Br^-, $CH_3CO_2^-$, and L-Phe$^-$complexes in DCM.

1.2.7 Aromatic amide foldamers

Considering how popular aromatic amide synthons have been in designing foldamers[104] and the fact that the amide NHs are excellent hydrogen bond do-

nors, surprisingly little research has been done on the anion binding of aromatic amide foldamers. The research groups of Light[105] and Feng[106] have both investigated pyridine-2,6-dicarboxamide- and isophthalamide-based receptors for halide binding. The foldamers **40a-b** (FIGURE 33) selectively bind fluoride in DMSO-d_6-water mixtures.[105] The binding constants determined by ^{1}H NMR titration for **40a** complexes were >10^4 M^{-1} for fluoride and <10 M^{-1} for chloride. The crystal structures of fluoride and chloride complexes were also obtained (FIGURE 33). The fluoride and chloride are hydrogen bonded from the amide NH groups and the NHs of the indole end groups. Small size of the fluoride enables it to fit inside the cavity of the foldamers, whereas the chloride is clearly located above the cavity. This might explain the observed selectivity for fluoride.

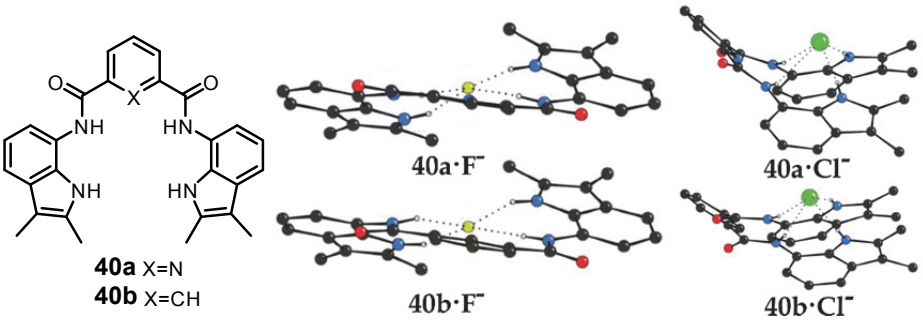

FIGURE 33 The foldamers **40a-b** and the crystals structures of fluoride complexes (middle) and chloride complexes (right) of **40a** (top) and **40b** (bottom). The figures are reproduced from ref. 105 with permission from The Royal Society of Chemistry.

Instead of halides, helical folding of arylamide foldamers **41a-d** (FIGURE 34) is induced by benzene-1,3,5-tricarboxylate anions in DMSO.[107] The helical structure was confirmed by the fluorescent emission from the pyrene interactions at the ends of the foldamers. Similar benzamide foldamers **42a-b** (FIGURE 34) bind helically to di- and tricarboxylate anions in DMSO.[108] Chiral guests D-glutamic acid and L-glutamic acid induce excess of P or M helical chirality, as observed by CD spectroscopy.

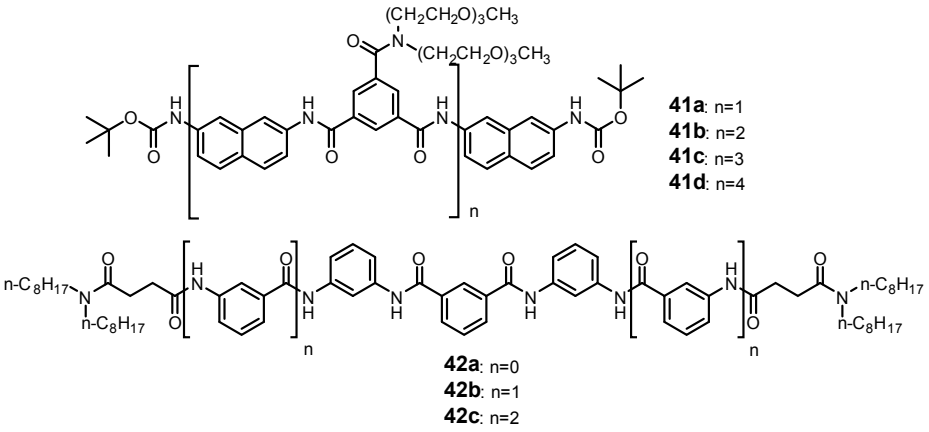

FIGURE 34 Schematic representation of foldamers **41a-d** and **42a-b**.

1.2.8 Aromatic oligourea foldamers

Ureas are effective hydrogen bond donors in anion receptors[109] and typical building blocks of foldamers.[110] The group of Yang[111,112] has studied chloride complexes of *o*-phenyl bridged oligoureas **43a-d** and **44a-e** with varying chain lengths containing four to seven phenyl groups (FIGURE 35). Altogether six crystal structures of the foldamers **43a-d** were obtained. The shortest foldamer **43a** forms two different 1:1 binding crystal structures with chloride, where the foldamer binding conformations are slightly different. The longer foldamers **43b-d** showed helical binding around two chloride anions (1:2 host:guest complexes). Remarkably, the Cl···Cl distance in **43b·Cl$_2$** complex is only 3.613(9) Å, meaning that the strong electrostatic repulsion between the chloride anions is overcome in the structure. It was proposed that the π-π stacking and eight cooperative hydrogen bonds help in overcoming the repulsion. With foldamers **43c-d**, the Cl···Cl distances are longer (3.8 - 4.0 Å). The crystal structures of similar foldamers **44a-e** (FIGURE 35) revealed also 1:2 host-guest ratio with Cl···Cl distances in the range of 3.8 - 4.1 Å. With mass spectrometric studies in $CHCl_3$, the binding ratios of the foldamers **44a-e** seem to be the same as in the solid state, but with NMR titration studies in DMSO-d_6, the binding ratios to Cl^- are 1:1 and the binding constants are at the 10^2 M^{-1} level. It was proposed that the dinuclear complexes form in less polar solvents.

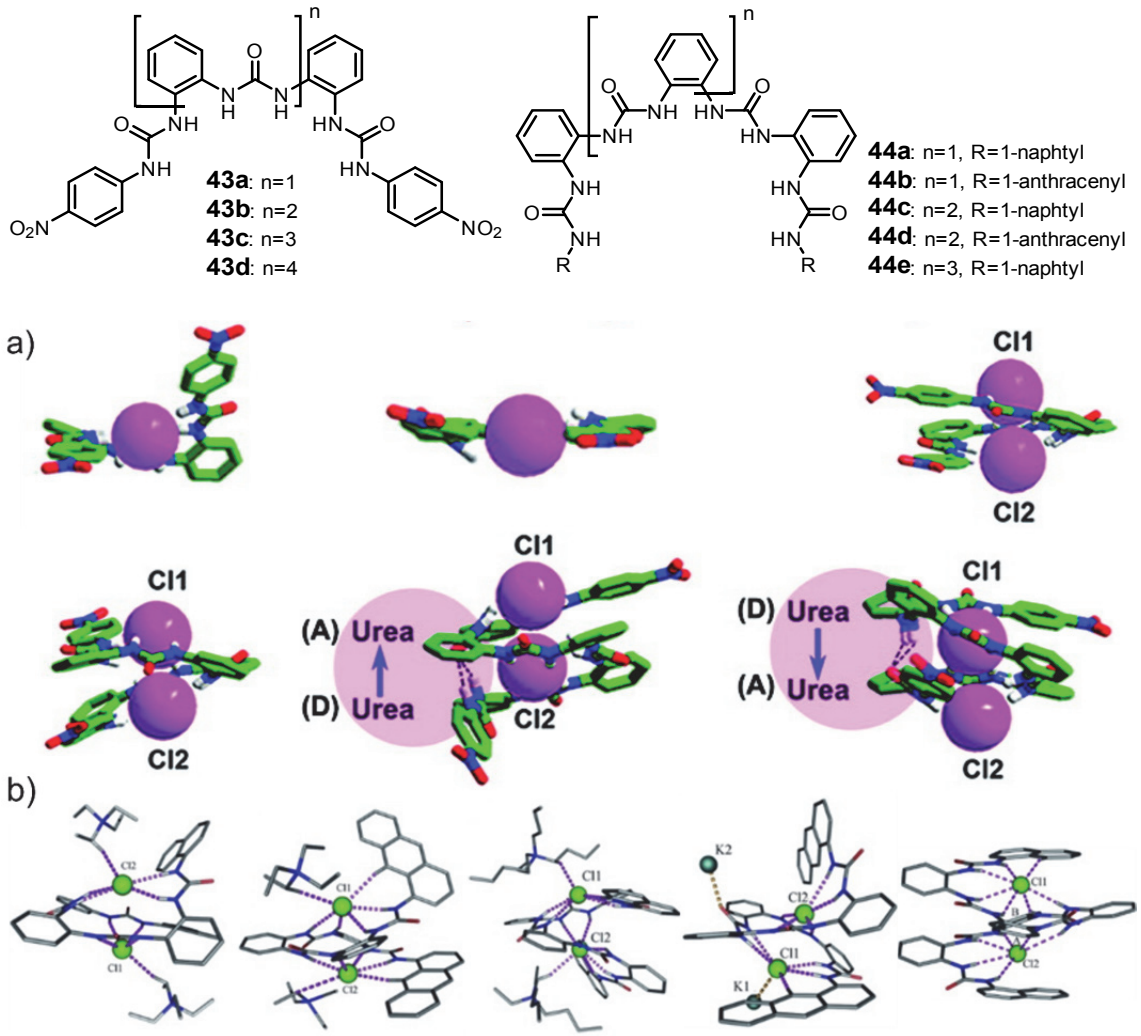

FIGURE 35 Foldamers **43a-d** and **44a-e**. The crystal structures of the chloride complexes of foldamers a) **43a-d** (Reprinted (adapted) with permission from ref. 111. Copyright (2012) American Chemical Society) and b) **44a-e** (Used with permission from ref. 112. Copyright (2013) Wiley).

Increasing the number of urea motifs in sulfate binding foldamers **45a-d** increased the chelate effect and hydrophobic effect, but it was suggested that the shorter urea receptors **45a-b** had better complementarity to sulfate because larger downfield shifts (average of 1.4 ppm for **45a-b** and 0.9 ppm for **45c-d**) of the NHs are seen when 1 eq of sulfate is added in ^{1}H NMR experiments.[113] The urea based foldamer **46** has one of the *ortho*-substituted phenyl groups replaced by a flexible carbohydrate spacer, which enables it to form a triple helicate with phosphate anion coordination (FIGURE 36).[114]

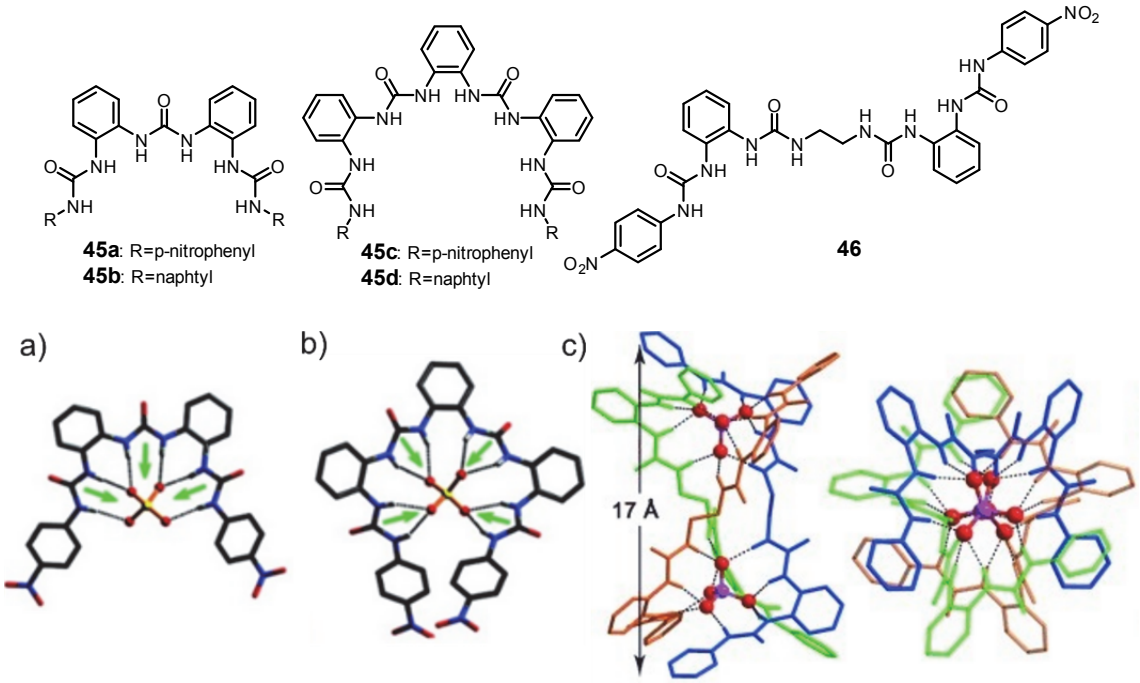

FIGURE 36 Foldamers **45a-d** and **46** (top). a) The calculated and b) the crystal structures the sulfate complexes of foldamers **45a** and **45c**, respectively (bottom left, reprinted (adapted) with permission from ref. 113. Copyright (2010) American Chemical Society). c) Crystal structure of triple helicate phosphate anion complex of foldamer **46** (bottom right, used with permission from ref. 114. Copyright (2011) Wiley).

An interesting example of an ion pair host is an *m*-phenyl bridged oligourea foldamer **47** (FIGURE 37).[115] The foldamer **47** binds chloride (K = 132 M^{-1} in $CDCl_3$) and acetate (K = 251 M^{-1} in $CDCl_3$) outside its cavity and simultaneously also the counter cation Et_4N^+ inside its cavity. The anion is bound by the NHs of one of the two urea groups that are located at the outer ring due to an intramolecular NH···O hydrogen bond to ether oxygen.

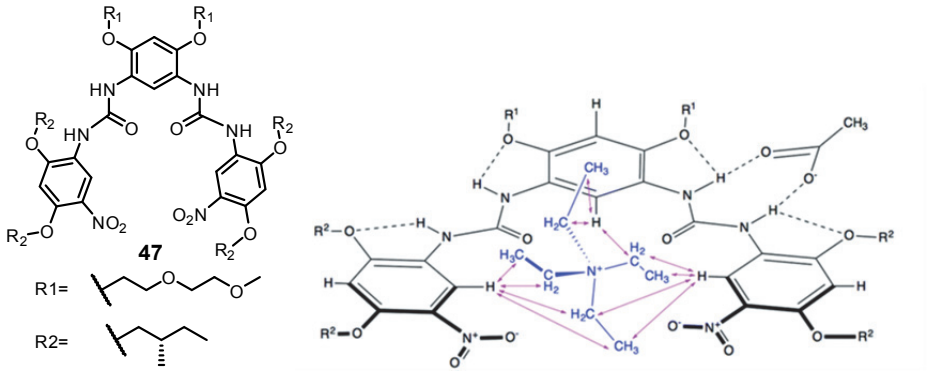

FIGURE 37 Foldamer **47** and a binding model of **47·Et_4N^+·Ac^-** complex based on 2D ROESY correlations (shown with arrows). Reproduced from ref. 115 with permission from The Royal Society of Chemistry.

Jeong et al.[116] investigated the binding affinities of a series of diphenylureas (**48a-e,** FIGURE 38) with chloride and sulfate. For foldamers **48b-e**, the binding affinities were higher for sulfate whereas the foldamer **48a** had better affinity to Cl^-. Overall, the longer foldamers had larger binding constants presumably because of the increased number of urea-groups that can form hydrogen bonds to the anions. A crystal structure of the **48b·SO_4^{2-}** complex showed that the foldamer forms hydrogen bonds to sulfate with the urea NHs and also from the OH groups at the ends of the foldamer.

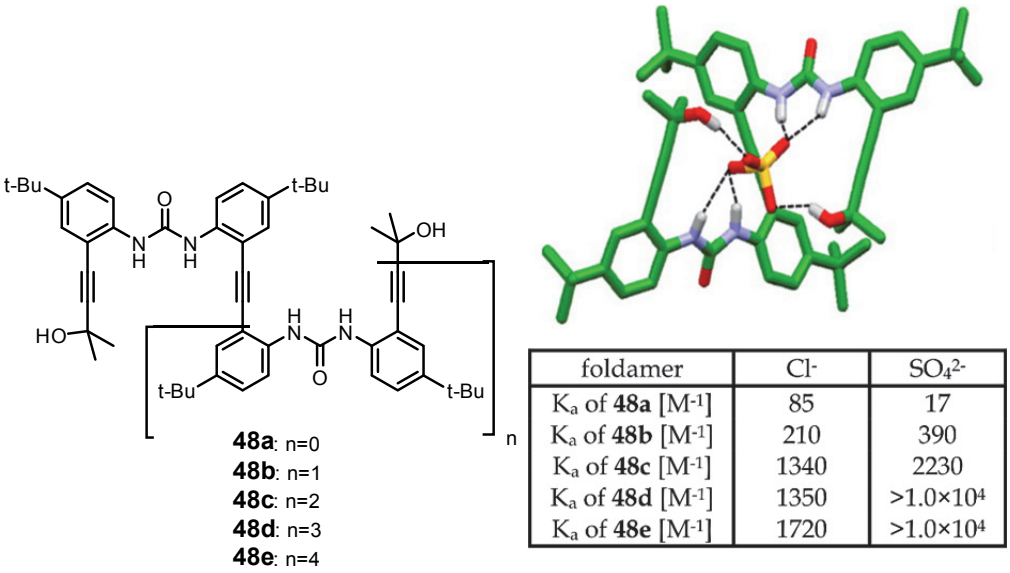

foldamer	Cl^-	SO_4^{2-}
K_a of **48a** [M^{-1}]	85	17
K_a of **48b** [M^{-1}]	210	390
K_a of **48c** [M^{-1}]	1340	2230
K_a of **48d** [M^{-1}]	1350	>1.0×10⁴
K_a of **48e** [M^{-1}]	1720	>1.0×10⁴

FIGURE 38 A scheme of foldamers **48a-e**, the crystal structure of **48b·SO_4^{2-}** complex (Reprinted (adapted) with permission from ref. 116. Copyright (2012) American Chemical Society.) and the binding constants for **48a-e** chloride and sulfate complexes in 15% (v/v) CD_3OH/acetone-d_6 and 20 % (v/v) CD_3OH/DMSO-d_6 solutions, respectively.

Amide-linked bisurea oligomers **49a-e** can function as chloride carriers across POPC (1-palmitoyl-2-oleoyl-2-oleoylphosphatidyl-choline) membranes.[117] The transportation activity depended on the foldamer substituents in order of OCH_3 (**49e**) ~ H (**49d**) < Cl (**49c**) < CO_2CH_3 (**49b**) ≪ CN (**49a**), which was in line with the chloride binding affinities (FIGURE 39). The binding affinities were determined by ^1H NMR in 1:9 (v/v) DMSO-d_6/$CDCl_3$ saturated with water (<0.1%).

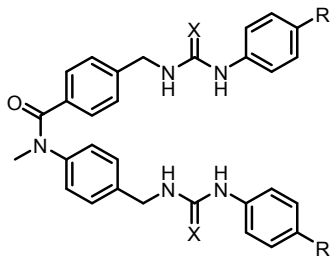

49a: X = O, R = CN $K_a(Cl^-)$ = 3950 M^{-1}
49b: X = O, R = CO_2CH_3 $K_a(Cl^-)$ = 1230 M^{-1}
49c: X = O, R = Cl $K_a(Cl^-)$ = 860 M^{-1}
49d: X = O, R = H $K_a(Cl^-)$ = 370 M^{-1}
49e: X = O, R = OCH_3 $K_a(Cl^-)$ = 250 M^{-1}

FIGURE 39 Foldamers **49a-e** and the binding constants in 1:9 DMSO-d_6/$CDCl_3$.

Dihydrogen phosphate selective foldamer **50a** (FIGURE 40) has potential as a molecular switch, as it has different binding conformations for halides (Cl^-, Br^-, I^-) and oxoanions ($H_2PO_4^-$, HSO_4^-, OAc^-, and NO_3^-).[118] An open structure for halide complexes and an enclosed conformation for oxoanions was interpreted from ^1H NMR shifts and from the crystal structure of **50a·Br$_2$** complex. The conformation of foldamer **50b** is also induced by anion binding, but the enclosed conformation dominates even in the chloride complex.[119] The foldamer **50b** had the highest 1:1 binding for $H_2PO_4^-$. Binding constants for **50a-b** complexes were determined by ^1H NMR titrations in 10% DMSO-d_6:$CDCl_3$ or by UV-vis in 10% DMSO:$CHCl_3$ (FIGURE 40).

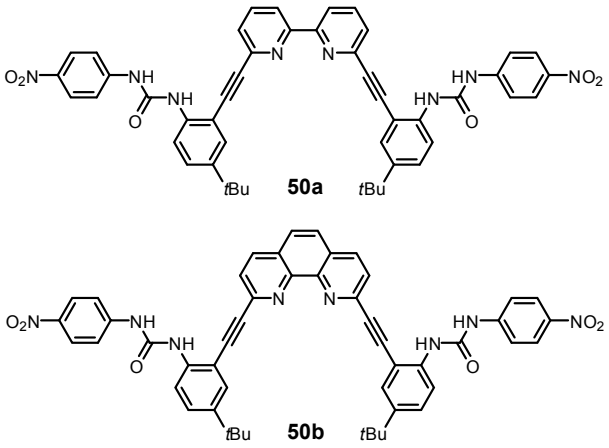

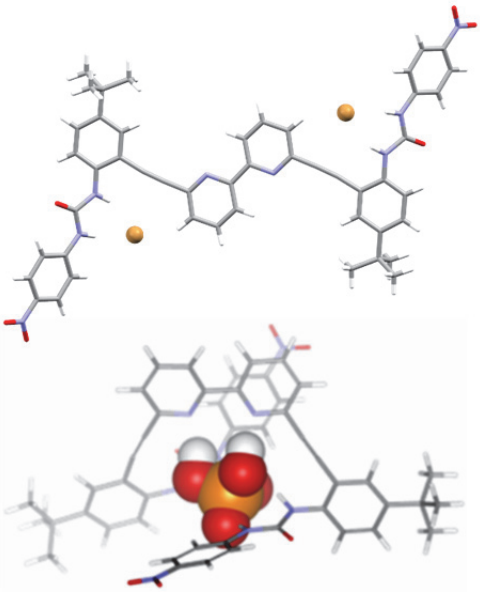

Anion	K_a for **50a** [M^{-1}]	K_a for **50b** [M^{-1}]
Cl^-	$K_{11} = (2.30\pm0.06)\times10^2$ $K_{12} = 1.59\times10^3$	$K_{11} = (2.60\pm0.45)\times10^2$
Br^-	$K_{11} = (1.50\pm0.06)\times10^2$ $K_{12} = 1.59\times10^3$	$K_{11} = (6.0\pm0.1)\times10^1$
I^-	$K_{11} = (4.0\pm1.5)\times10$	-[b]
NO_3^-	$K_{11} = (6.0\pm0.5)\times10$	-
$H_2PO_4^-$[a]	$K_{11} = (7.8\pm0.02)\times10^4$	$K_{11} = (4.60\pm0.0045)\times10^4$
HSO_4^-	$K_{11} = (3.70\pm0.06)\times10^2$ $K_{12} = 1.00\times10^4$	$K_{11} = (3.30\pm0.50)\times10^2$
OAc^-	$K_{11} = (2.11\pm0.002)\times10^4$ $K_{12} = 5.25\times10^6$	$K_{11} = (2.60\pm0.23)\times10^3$

[a] UV-vis titration. [b] Could not be determined.

FIGURE 40 Foldamers **50a-b**, the crystal structure of **50a·Br$_2$** complex showing the open conformation and DFT model of the enclosed conformation of **50a·$H_2PO_4^-$** complex. Figure used with permission from ref. 118. Copyright (2013) Wiley.

Pihko *et al.*[120] have made foldamer organocatalyst **51** for enantioselective Mannich reactions. The crystal structure of hexafluoroacetylacetonate complex has the desired conformation for catalytic activity. When foldamer **51** is bound to a chloride, the folding mode is altered, which inhibits the catalysis (FIGURE 41).

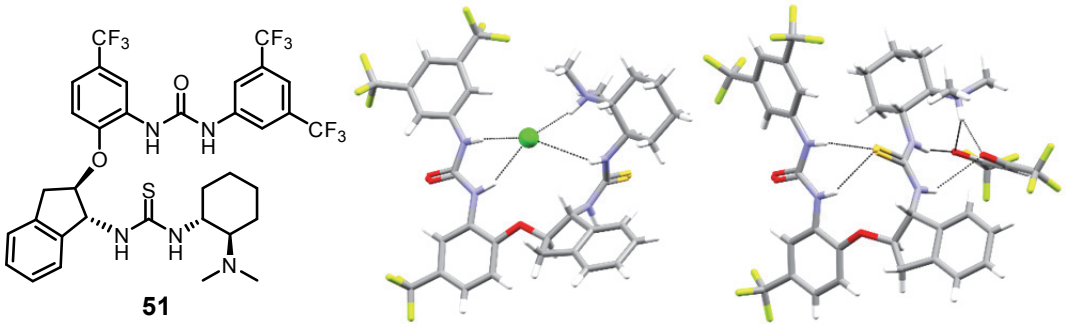

FIGURE 41 Schematic representation of foldamer **51** and the crystal structures of foldamer **51** binding to chloride (middle) and to hexafluoroacetylacetonate (right).

1.2.9 Aliphatic oligoureas and amides

Contrary to aromatic foldamers, the anion binding in aliphatic foldamers often happens at the end of the helix, although crescent wrapping around sulfate anion has also been observed.[121] Guihard *et al.*[122] investigated the anion binding of a series of aliphatic oligoureas **52a-e** with different lengths and end groups (FIGURE 42). The foldamer helix provides preorganization, and the anion is bound to the four urea NHs at the end of helix that do not participate in intramolecular hydrogen bonding. The binding affinity order $PhCO_2^-$ > $CH_3CO_2^-$ > $H_2PO_4^-$ > Cl^- for foldamer **52a** was estimated from an NH signal shift in ^1H NMR spectra. The binding affinity for chloride increased with the length of the foldamer chain (K_a = 89 M^{-1} for **52a** and K_a = 140 M^{-1} for **52b** in DMSO-d_6) and when the terminal group can participate in the binding like the 1*H*□indol□7□yl□urea group of foldamer **52e** (K_a = 212 in DMSO-d_6).

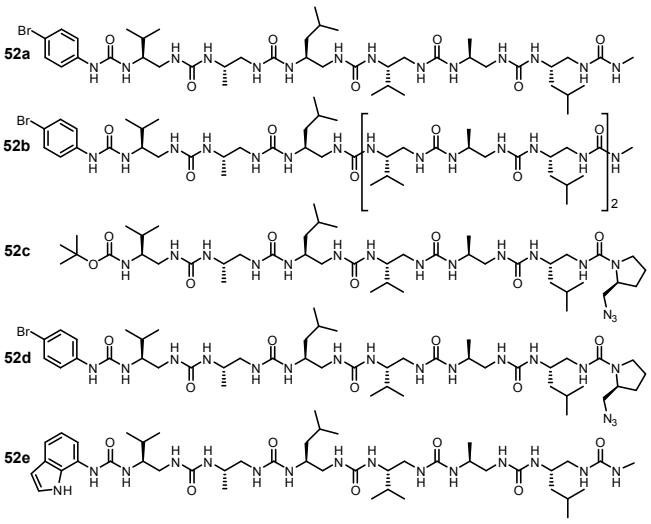

FIGURE 42 Schematic representation of foldamers **52a-e.**

Clayden *et al.*[123] have studied oligourea foldamers composed of meso cyclohexane-1,2-diamines, where the helical folding is caused by the directional hydrogen bonds. The ends of the achiral foldamers are enantiotopic: in the N terminus the urea is in the axial position, and in the C terminus, the urea is in the equatorial position and the termini have different chemical environments according to NMR (FIGURE 43). The helix chirality and the direction of the hydrogen bonds could be controlled by binding a chiral carboxylate anion Boc-D-Proline to the N terminus of the foldamer **53**. The 1:1 complex of foldamer **53** had a binding constant of K= 8500 ± 500 M^{-1}, and approximately 50% helical excess was achieved.

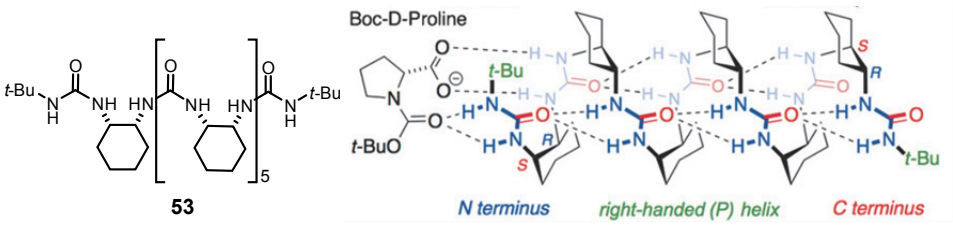

FIGURE 43 Foldamer **53** and the suggested structure of foldamer **53** with Boc-D-Proline, inducing a right-handed helix. Figure used with permission from ref. 123. Copyright (2016) Wiley.

Aliphatic amide foldamers **54a-d** with urea binding sites can also be induced to change their helicity by binding chiral phosphates (FIGURE 44).[124] The foldamers have ^{13}C labeled methyl groups enabling the helicity to be monitored by ^{13}C NMR. The estimates of the binding constants for the phosphate anion complexes of **54a** were determined by adding a base to a 1:3 mixture of **54a** and phosphate acids **55a-c** in THF-d_8 and monitoring the change by ^{13}C NMR.

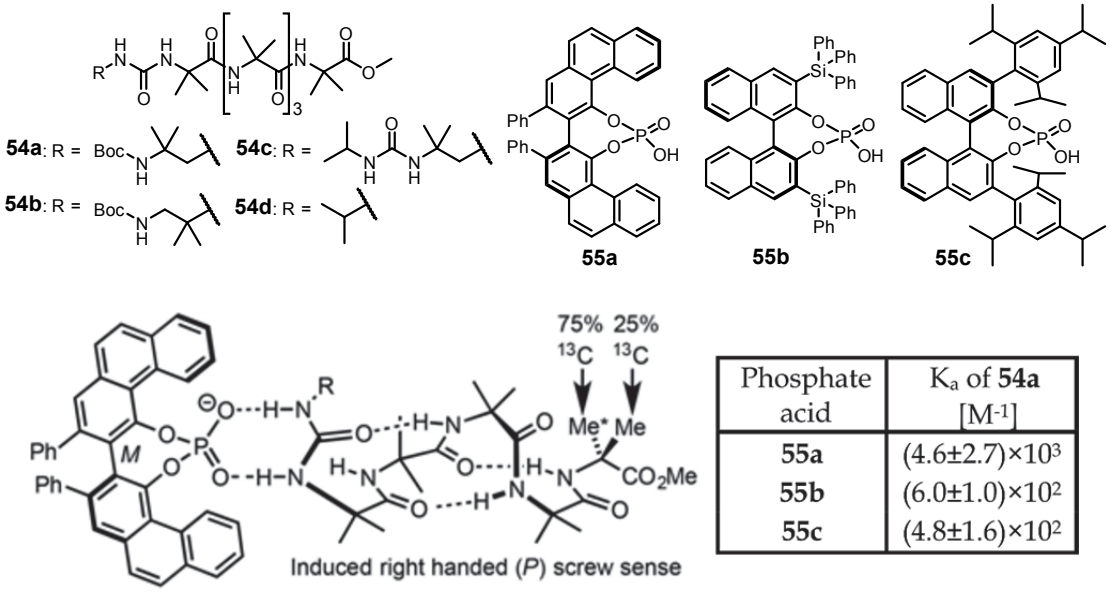

Phosphate acid	K_a of **54a** [M^{-1}]
55a	$(4.6\pm2.7)\times10^3$
55b	$(6.0\pm1.0)\times10^2$
55c	$(4.8\pm1.6)\times10^2$

FIGURE 44 Schematic representation of foldamers **54a-d** and the chiral phospahtes **55a-c** (top). The suggested structure for phosphate anion binding to foldamers (bottom left, Reproduced from ref. 124 with permission from The Royal Society of Chemistry). The estimated binding constants of phosphate anion complexes of foldamer **54a** (table, bottom right).

2 EXPERIMENTAL

2.1 Aims and background of the work

The aim of this work was to study the conformational stability and complexation properties of aromatic oligoamide foldamers **56-65** (FIGURE 45). The main methods used were single crystal X-ray diffraction, nuclear magnetic resonance (NMR) studies and mass spectrometric (MS) studies. Further supporting information was obtained from DFT optimized structures. Using different methods, the properties of the compounds could be determined in each state of mater: solid, in solution, and gas. The work is a continuation of the previous work done in the research group of prof. Nissinen, where the solid state conformations and interactions of aromatic oligoamide foldamers with 4 to 5 aromatic units were studied.[125-128] The previous work started with the study of two different oligomers: one with a central pyridine group and one with a phenyl group instead.[125] The pyridine foldamer showed a preference to form a protohelical conformation, whereas the foldamer with the phenyl ring did not have any obvious folded conformation. The pyridine dicarboxamide motif was selected for further studies because the conformation with three intramoleculer hydrogen bonds from amide NHs to C=O group resembles an oxyanion hole motif of the enzymes.[127] Oxyanion holes are catalytic sites in biomolecules, where hydrogen bonds stabilize negatively charged oxygen atoms of a tetrahedral or enolate intermediates. The similarity comes from the multiple hydrogen bond donors binding to the same hydrogen bond acceptor.

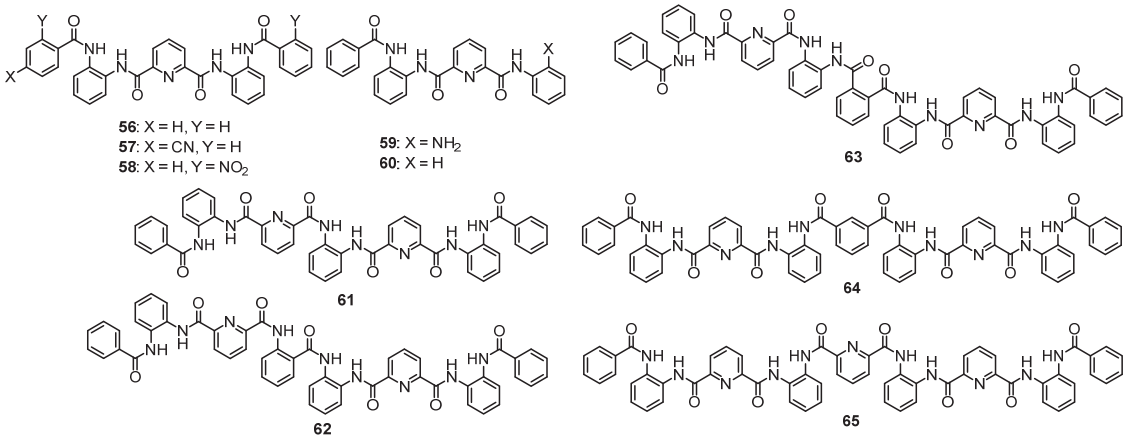

FIGURE 45 The foldamers studied in this work.

The previous studies showed that the modified foldamers folded into essentially two different hydrogen bonded conformations.[127,128] Based on the shape of the conformation, one was noted as the @-fold and the other as the S-fold (FIGURE 46). The compact @-fold has helical conformation, whereas the S-fold is more elongated. Both folds have 2-3 intramolecular hydrogen bonds.

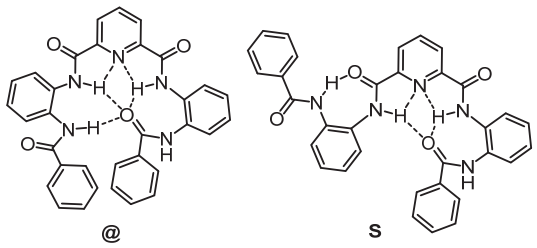

FIGURE 46 The general conformations noted as @-fold and S-fold.

The structural studies indicated that these foldamers may have promizing preorganization for complexation of ions. Thus, in this work, the complexation properties of selected foldamers **56-60** with anions both in the solid state and in solution state have been studied. Additionally, a series of longer foldamers with 7 to 9 aromatic units (**61-65**) was studied in detail to find out how the folding is affected when the foldamer is extended or when different linkers between the pyridine dicarboxamide motifs are added. Finally, the complexation with cations and anions as well as conformational studies were conducted with ion mobility mass spectrometry.

2.2 The synthesis of the foldamers[I,II]

The synthesis of foldamers **56-57**, **59-60** and intermediates **66-72** were reported in previous papers.[127,129] The foldamers **58** and **61-65** were synthetized by modular synthesis, meaning that larger building blocks, such as intermediates **68-72**,

were first synthetized and then connected to create the whole foldamer (FIGURE 47). The amide bonds were formed either by acylation reaction between acid chlorides and amines or by using amide bond cross-linker (EDC) to catalyze the coupling reaction between carboxylic acids and primary amines. A non-protected *o*-phenylenediamine was used for the synthesis of the intermediates **69-71**, but for the synthesis of the intermediate **72,** a mono-*N*-Boc-*o*-phenylenediamine **73** was prepared[130] and used to increase the yield.

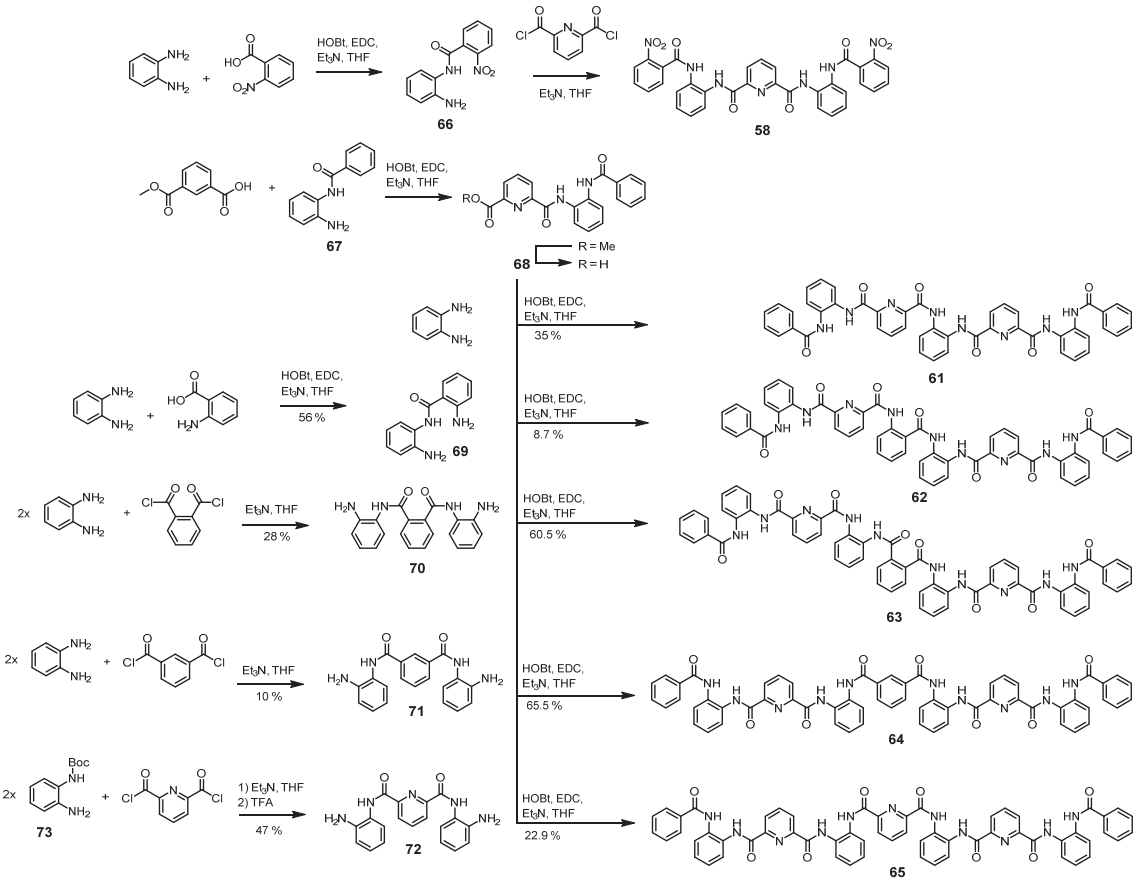

FIGURE 47 The synthesis routes for foldamers **58** and **61-65**.

2.3 Structural studies of extended foldamers[I]

Foldamers **61-65** were synthesized to investigate the stability of the @- and S-fold motifs in longer foldamers. In foldamers **61** and **65**, the number of pyridine groups, when compared to the foldamer **56**, was increased from one to two or three, respectively. In foldamer **62**, the unsymmetrical spacer group between two pyridine rings was used to remove the C_{2v} symmetry present in the other foldamers. Foldamer **63** was made with an *ortho*-substituted rigid spacer group between the pyridine rings, whereas its structural isomer **64** was made flexible with a *meta*-substituted phenyl ring at the center. Overall, 17 solvate crystal

structures were obtained, which indicates that the foldamers have a good ability to crystallize, but they do not pack efficiently together on their own.

2.3.1 Foldamer 61

Foldamer **61** has a single *ortho*-substituted phenyl ring as the linker between two pyridinedicarboxamide units. Two different conformations were observed in the solid state based on six single-crystal structures obtained (FIGURE 49). Helical conformation with both pyridine centers in @-folds was found in five of the crystal structures. A more open conformation where one pyridine center adopts the S-fold and the other the @-fold was found only in the DCM solvate crystal structure.

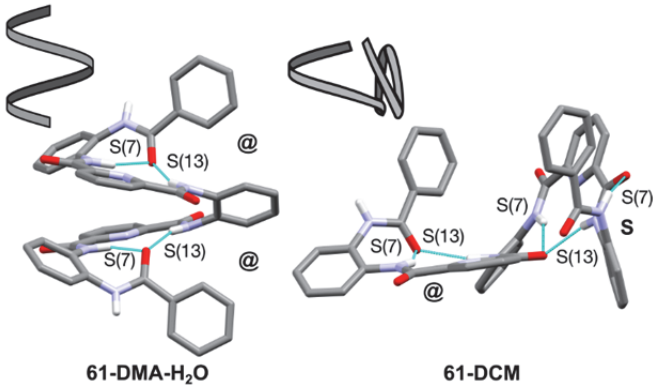

FIGURE 48 Crystal structures of foldamer **61** illustrating the helical conformation where both pyridine centers adopt the @-fold (left) and the open conformation with @- and S-fold (right). Solvents and aromatic protons have been removed for clarity.

Two correlations measured by NOESY ^{1}H NMR in DMSO-d_6 indicate that the foldamer has a folded conformation in solution (FIGURE 49), but the correlations could correspond to either the helical structure or the open structure. Therefore, no conclusion about the conformation in solution could be made.

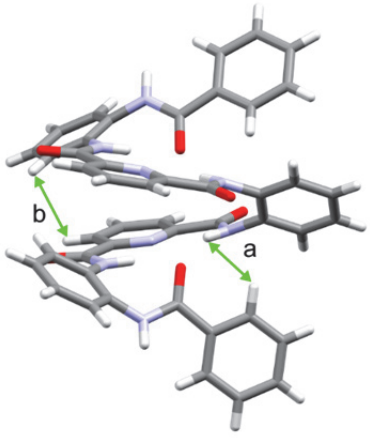

FIGURE 49 The NOESY correlations a and b, showed on the helical crystal structure, are possible in both the helical and in the open conformation. They, however, indicate that the foldamer is somehow folded in solution.

Of the helical structures, the **61**-DMA-H_2O and **61**-MeCN-H_2O structures are isomorphous. In the crystal packing, the foldamers are connected into pairs via $OH_w\cdots O{=}C$ hydrogen bonds by two water molecules (FIGURE 50). The adjacent foldamers also π···π stack between the pyridine centers. The **61**-DMF-H_2O structure has the same pattern in the crystal packing, but the difference to previous structures (**61**-DMA-H_2O and **61**-MeCN-H_2O) comes from the efficiency of the packing. The solvent molecules (DMA, MeCN, DMF) are hydrogen bonded to an outer NH group of the foldamer in all structures, but in **61**-DMF-H_2O, an additional solvent molecule is located between the ends of the foldamers, thus preventing them from π···π stacking conversely to the **61**-DMA-H_2O and **61**-MeCN-H_2O structures.

In **61**-DMSO structure, the foldamers pack into π···π stacked layers and are hydrogen bonded to the DMSO molecules. In **61**-MeOH structure, the foldamers are connected to pairs, and the pairs further connect to chains by intermolecular hydrogen bonds. The foldamers are also directly hydrogen bonded to pairs in the more open **61**-DCM structure and disordered solvent molecules reside in the space created by the non-helical open conformation.

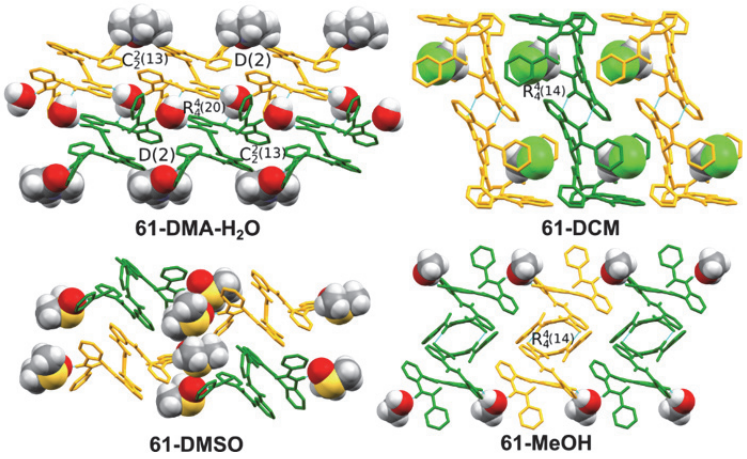

FIGURE 50 The crystal packing of **61**-DMA-H_2O, **61**-DCM, **61**-DMSO, and **61**-MeOH crystal structures and the intermolecular graph set motifs that were observed. Aromatic hydrogens have been removed for clarity.

2.3.2 Foldamer 62

Two very similar solid state conformations from four different crystal structures were obtained for foldamer **62**, which has an unsymmetrical linker unit between the two pyridine units (FIGURE 51). The carbonyl group from the linker prefers to form hydrogen bonds towards the closest pyridine with graph set motifs S(6) and S(12). This results in a compact helical conformation. Aromatic π-π stacking interactions also play a role in the folding. Four NOESY ^1H NMR correlations correspond to the crystal structures (marked in green, FIGURE 51) but five correlations do not correspond to the crystal structures (marked in red). The correlations still indicate that the foldamer is somewhat similarly folded in solution with the difference that the end of the foldamer is in a different position.

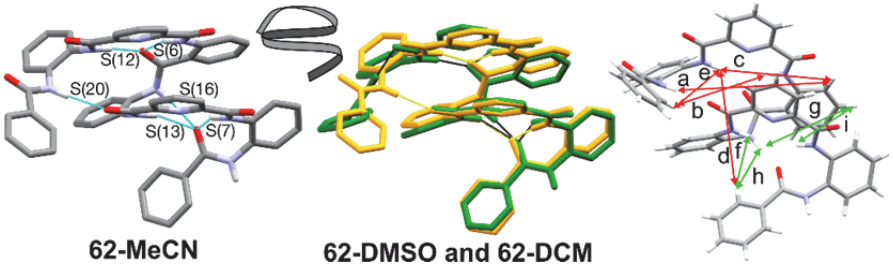

FIGURE 51 The **62**-MeCN crystal structure with intramolecular graph set motifs (left) and overlay of **62**-DMSO (orange) and **62**-DCM (green) structures showing the similarity of the two conformations (middle). The aromatic hydrogens have been removed for clarity. On the right, NOESY correlations a-e (red) that do not correspond to the crystal structures and f-i (green) that correspond to the crystal structures.

In the **62**-DCM structure and in the isomorphous **62**-MeCN and **62**-EtOAc structures, the foldamers form pairs by intermolecular hydrogen bonding (NH···O; $R_2^2(14)$ motif; FIGURE 52). The DCM molecules are located between two foldamer pairs. In the EtOAc and MeCN solvate structures, the foldamer pairs stack with π···π interactions, and the solvents are located in the interstice in the crystal lattice, whereas in the **62**-DMSO structure, the foldamers are hydrogen bonded to two DMSO molecules (D(2) motifs).

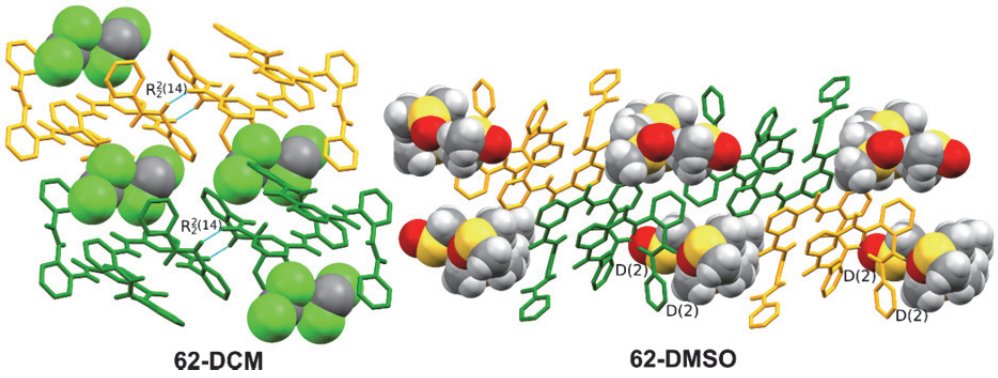

FIGURE 52 The crystal packing of **62**-DCM and **62**-DMSO structures. Aromatic hydrogens have been removed for clarity.

2.3.3 Foldamer 63

Foldamer **63** has three *ortho*-substituted phenyl rings as a rigid spacer between the two pyridine centers. Only two crystal structures were obtained with distinctly different conformations (FIGURE 53). The rigid linker separates the two pyridine-2,6-dicarboxamide units into two independent @-folds, which can orient themselves differently in respect to the linker. In the DMSO solvate structure, the @-folds are at the same side of the linker (so called *cis* conformation), forming a cavity, whereas in the DMA solvate, the @-folds are in different sides

in respect to the linker, making it the *trans* conformation. The seven NOESY ^{1}H NMR correlations (marked in green, FIGURE 53) indicate that the foldamer is in the *cis* conformation in DMSO-d_6 solution.

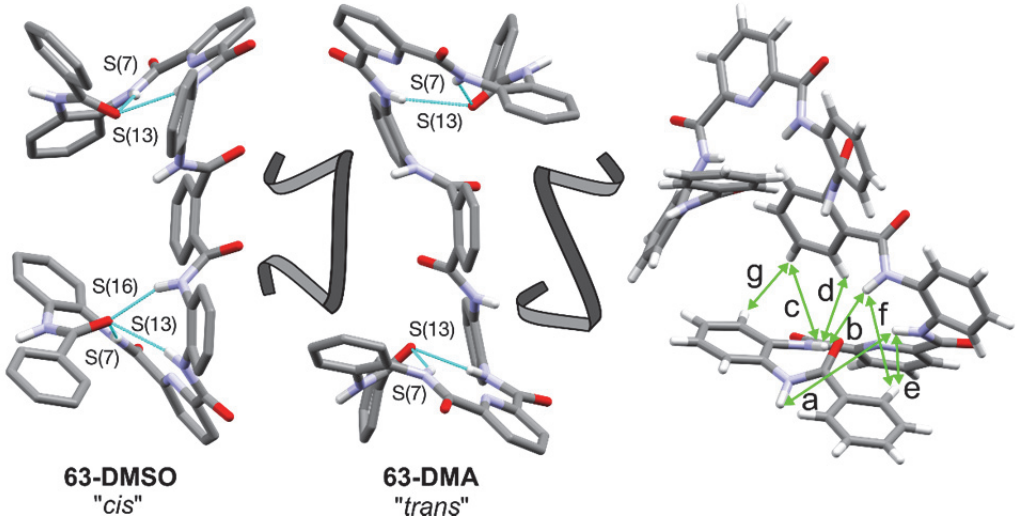

FIGURE 53 The **63**-DMA (left) and **63**-DMSO (middle) crystal structures, where aromatic hydrogens have been removed for clarity. On the right, the seven NOESY correlations a-g (green) that correspond to the *cis* conformation of **63**-DMSO structure.

In the **63**-DMSO crystal packing, the foldamers are connected to chains via intermolecular hydrogen bonds (NH8…O6; C(11) motif and NH1…O4; C(16) motif; FIGURE 54). A disordered DMSO is bound inside the cavity of the foldamer by hydrogen bonds. In the **63**-DMA structure, the solvents are located in between the foldamers that form ladder-like chains by direct intermolecular hydrogen bonds (O3…HN8) and solvent-mediated hydrogen bonds (NH1…Os…HN5; FIGURE 54).

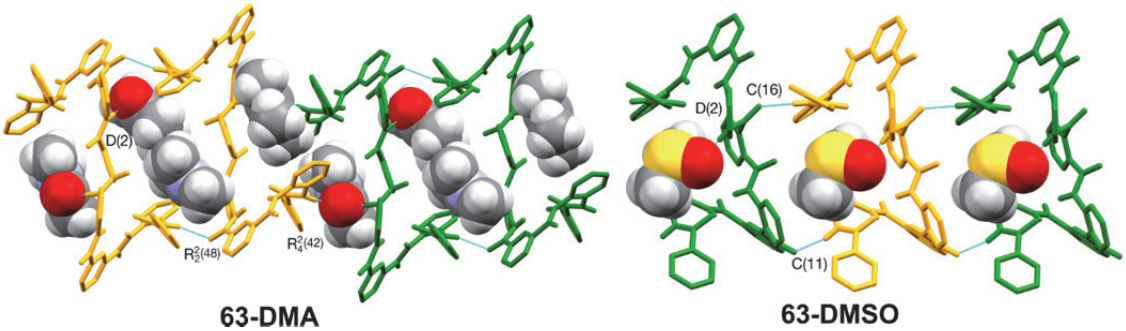

FIGURE 54 Crystal packing of **63**-DMSO and **63**-DCM structures and the intermolecular graph set motifs describing the hydrogen bonding. Aromatic hydrogens have been removed for clarity.

2.3.4 Foldamer 64

Foldamer **64** has also three phenyl rings as a linker between the two pyridine centers, but the central phenyl ring is *meta*-substituted, so the linker is not as rigid as in foldamer **63**. Only one crystal structure, an ethyl acetate solvate, was obtained. The flexibility of the linker allows the pyridine centers to fold in symmetrical S-folds oriented at the opposite sides of the central ring, resulting in an open but still compact conformation. The structure is further stabilized by two additional S(22) hydrogen bonds from the outmost carbonyl (O1 or O8) to the central NH group (NH5 or NH4, respectively), which are not usually part of the S-fold. Many of the ^{1}H NMR peaks of foldamer **64** overlap, so defining interactions from NOESY ^{1}H NMR correlations was difficult. A folded conformation is indicated by correlations a-d (FIGURE 55), but predictions of the structure or comparisons to the solid-state structure are impossible to make.

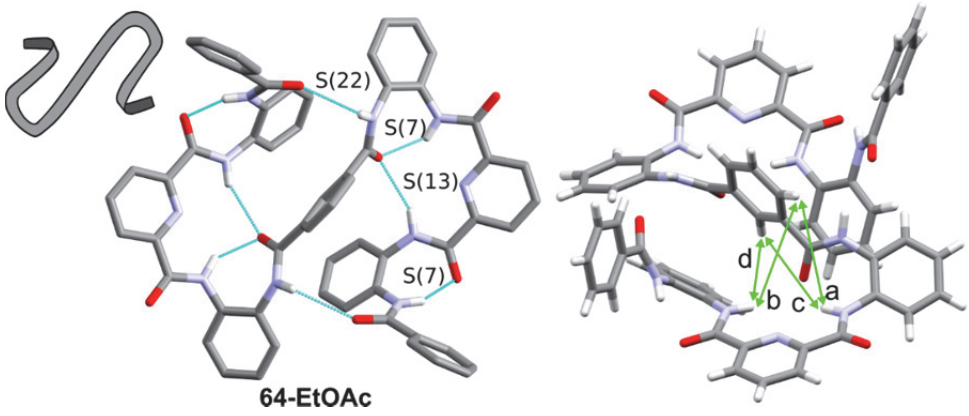

FIGURE 55 The crystal structure of **64**-EtOAc with the solvents and aromatic hydrogens removed for clarity (left). Four NOESY correlations a-d marked to the crystal structure in green (right).

In the crystal packing, the foldamers form continuous chains by intermolecular hydrogen bonds (O3…NH4 and O6…NH5; $R_2^2(14)$ motif; FIGURE 56), and the disordered EtOAc solvents are located between the chains.

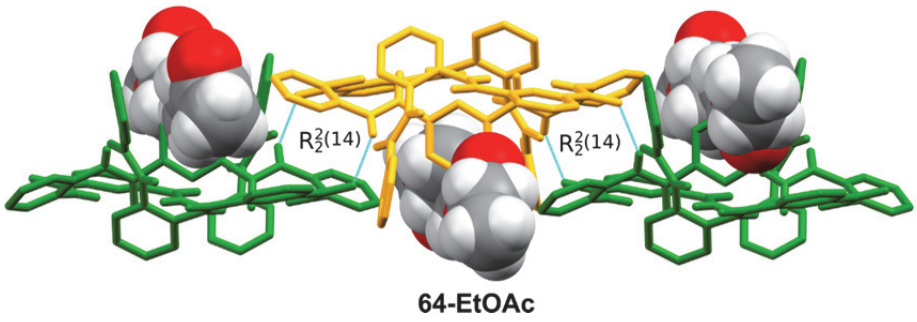

FIGURE 56 The crystal packing of **64**-EtOAc. Aromatic hydrogens have been removed for clarity.

2.3.5 Foldamer 65

Foldamer **65** has a pyridine ring in the linker that enables the linker to contribute to the folding. Two different solid-state conformations were obtained from four crystal structures. The acetone, DCM, and DMF solvate structures are isomorphous with a nearly helical conformation (FIGURE 57). The chloroform solvate has a more open bowl-shaped structure. Two NOESY ^{1}H NMR correlations (g and h, FIGURE 57) indicate that the solution state conformation resembles the helical-type conformation, while most of the correlations (b-f) are viable in both of the crystal structures. One correlation (a) does not fit either of the crystal structures, which implies that the end of the foldamer is orientated slightly differently than in the nearly helical structure.

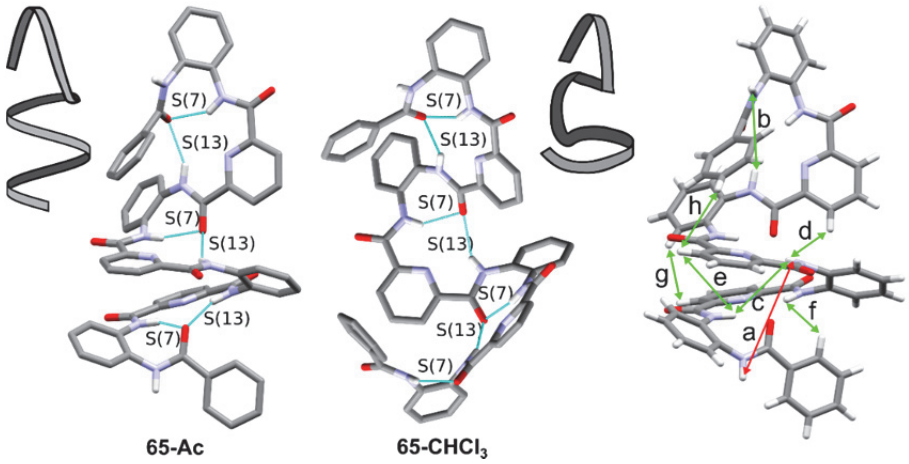

FIGURE 57 The crystal structures of **65**-Ac and **65**-$CHCl_3$. The solvents and aromatic hydrogens were removed for clarity. The NOESY correlations a-g shown on the helical structure.

In the three isomorphs, a complex intermolecular hydrogen-bond network is seen. The foldamers form pairs connected by two hydrogen bonds, and the pairs are connected to chains of pairs (FIGURE 38). The solvents are located inside the interstices in the crystal lattice. In the **65**-$CHCl_3$ crystal structure, the foldamers form pairs via intermolecular hydrogen bonds, and the foldamers also occupy each other's bowl-like cavities together with solvent molecules.

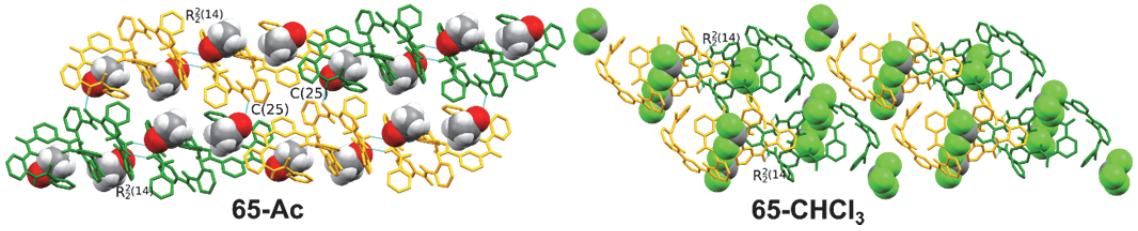

FIGURE 58 The crystal packing of **65**-Ac (left) and **65**-$CHCl_3$ (right) and the intermolecular graph set motifs observed. Aromatic hydrogens have been removed for clarity.

2.3.6 Structural comparison

The folding of foldamers **61-65** is mainly induced by intramolecular hydrogen bonding in a reasonably predictable fashion. When the foldamers are elongated, by adding more pyridinedicarboxamide units separated by an *ortho*-substituted phenyl ring, the folding pattern essentially stays the same as in shorter foldamers, which is illustrated in FIGURE 59. The NMR studies also indicate a helical-type conformation of foldamers **61** and **65** in solution instead of the open conformation. When the spacer between two pyridine rings is longer than one phenyl ring, a greater variety of structures can be obtained. The foldamer **62** with unsymmetrical spacer favors compact conformation with aromatic interactions in solid state. A rigid spacer in foldamer **63** separates the pyridine centers to fold independently, but a more flexible spacer in foldamer **64** allows the spacer to contribute to the folding with additional intramolecular hydrogen bonds.

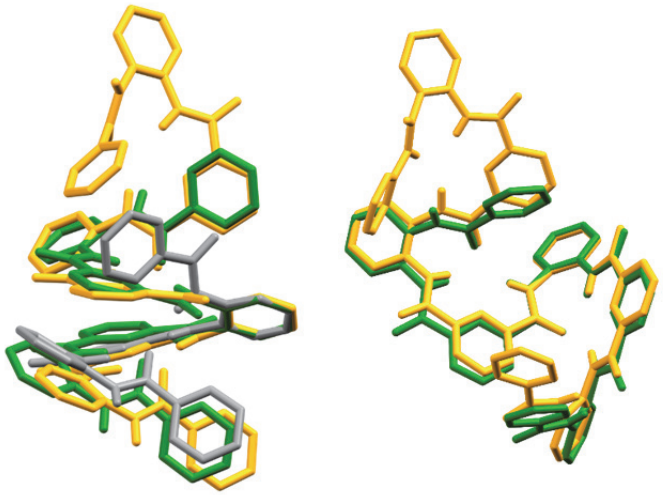

FIGURE 59 The overlay of the crystal structures of foldamers **56** (grey), **61** (green), and **65** (yellow). Aromatic hydrogens have been removed for clarity.

2.4 Complexation studies[II,III]

Anion complexation of foldamers **56-65** was at first attempted by crystallization of foldamers with TBA halide salts. All attempts with larger foldamers **61-65**, however, were unsuccessful. Therefore, the shorter foldamers **56-60** were chosen for further studies. Also in this case, only fluoride complexes formed crystals with foldamers **56-60**, despite several crystallization attempts with halide anions, NO_3^- and HSO_4^-. Preliminary (-)ESI-MS and ^1H NMR experiments for fluoride binding of foldamer **56** were done. In the ESI-MS spectrum the $[M+F]^-$ complex signal was not observed, and only deprotonated foldamer was seen, which indicated that in non-protic organic solvents the F^- tends to deprotonate the foldamer. For this reason, the mass spectra of fluoride salts and of foldamers

57-60 were not measured. The ^{1}H NMR spectrum displayed poor resolution and widening of the signal peaks when fluoride was added to the solution of foldamer **56**, which indicated proton exchange or aggregation.

Based on (-)ESI-MS screening and the competition experiments, the Cl^-, Br^-, I^-, and NO_3^- binding to foldamer **56** was studied with ^{1}H NMR titrations. In order to study the effect of the electron withdrawing substituents, foldamers **57** and **58** were also chosen as comparison for ^{1}H NMR titrations with the most promising anion, namely chloride. The chloride binding of foldamers **56-58** was also studied with ITC titrations.

2.4.1 Foldamer 56

In previous studies the C_{2v} symmetrical achiral foldamer **56** has adopted a protohelical conformation with either right-handed (P) or left handed (M) helicity in centrosymmetric crystal structures.[125,128] When **56** was crystallized with TBAF, the **56·F**-complex surprisingly formed a chiral crystal structure with a space group $P2_12_12_1$. In the crystal structure, all the foldamer molecules have M helicity and are helically wrapped around the F^- (FIGURE 60). The fluoride is bound by four NH···F^- hydrogen bonds and two CH···F^- interactions from the *ortho* protons of the outermost phenyl rings. The anion also forms a CH···F^- interaction with the *para* protons of the outermost phenyl group of the adjacent foldamer complex. The crystallization was repeated several times resulting in the same chiral crystal and structure. The bulk sample of the crystals and three individual crystals were measured with circular dichroism (CD) spectroscopy to investigate the chirality of the crystals (FIGURE 60). The results indicate symmetry breaking during crystallization since all the samples had a negative Cotton effect at 245-380 nm. A computer simulation of the CD spectrum showed a similar Cotton effect.

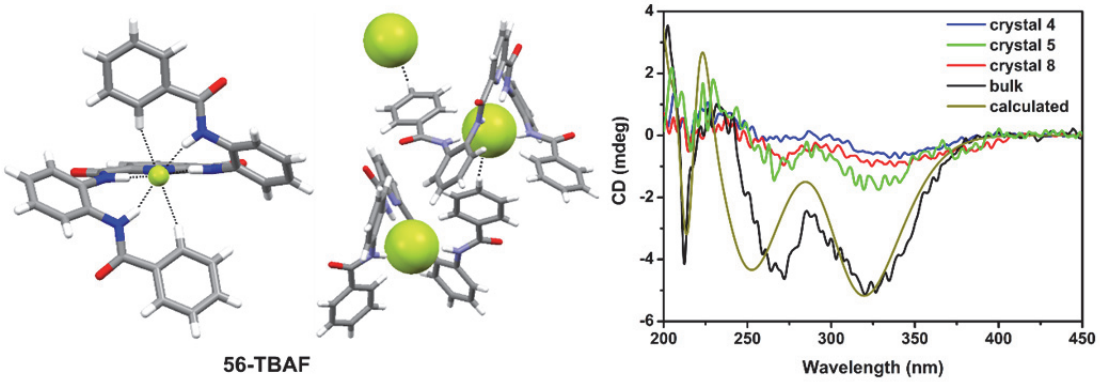

FIGURE 60 The crystal structure of **56·F**−complex (**56**-TBAF) showing the fluoride binding conformation (left) and the crystal packing interactions (middle). The CD spectra of three individual crystals (blue, green, and red), the bulk sample of **56**-TBAF (black), and the simulated CD spectrum (brown).

Preliminary ^{1}H NMR titrations of foldamer **56** with TBAF in acetone-d_6 indicated aggregation and deprotonation, so the fluoride complex could not be

studied further in solution. (-)ESI-MS screenings with ammonium salts of F^-, Cl^-, Br^-, I^-, NO_3^-, $H_2PO_4^-$, SO_4^{2-}, HSO_4^- or CO_3^{2-} resulted in peaks corresponding to Cl^-, Br^-, NO_3^-, I^-, and HSO_4^- 1:1 complexes. A binding order of Cl^- > Br^- > I^- was observed in the competition experiments for the halides. Based on these results Cl^-, Br^-, NO_3^-, and I^- were chosen for titration experiments.

^{1}H NMR titrations were executed in acetone-d_6 with tetrabutylammonium salts of the anions. Efficient 1:1 binding enabled by the suitable cavity size was only observed with the smallest chloride anion with binding constant over 10^4 M^{-1}. Titration with TBABr, TBAI, and $TBANO_3$ showed smaller chemical shifts for NH protons and smaller binding constants than with TBACl, indicating that chloride has the best fit in terms of size and shape. Based on the shifts in the ^{1}H NMR spectra and supporting DFT calculations the foldamer **56** assumes a helical conformation around the chloride with NH···Cl^- and C-H···Cl^- interactions (FIGURE 61). A binding constant of (2.3 ± 0.4)×10^4 M^{-1} was measured by isothermal titration calorimetry (ITC) for the **56·Cl⁻**-complex. The ITC experiments also provided the enthalpy and entropic parameters of ΔH = -2.5 ± 0.2 kcal/mol, TΔS = 3.4 ± 0.3 kcal/mol and ΔG = -5.9 Δ ± 0.1 kcal/mol. The favorable entropy increase was the main driving force for the chloride binding and was probably due to the desolvation/solvation processes during the complexation.

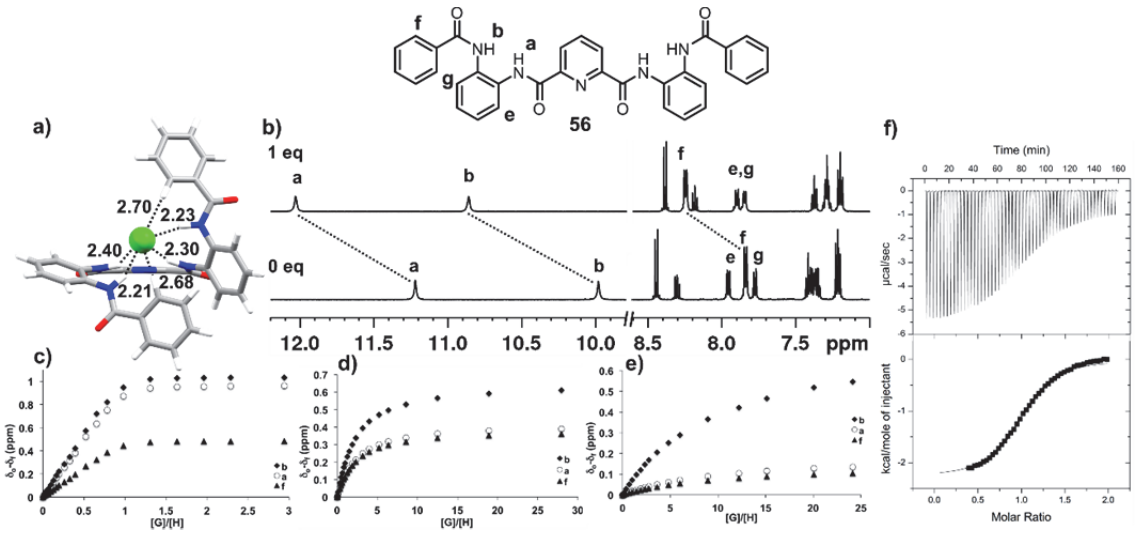

FIGURE 61 a) The solution state DFT structure showing the distances of hydrogen bonding interactions (Å). b) ^{1}H NMR spectra of foldamer **56** with 0 and 1 equivalent of TBACl in acetone-d_6. Chemical shift changes of the NH protons (**a**,**b**) and *ortho* protons of the outermost phenyl rings (**f**) in c) TBACl titration, d) TBABr titration, and e) $TBANO_3$ titration of foldamer **56**. f) The spectrum of one of the ITC titration experiments.

2.4.2 Foldamer 57

Foldamer **57** has a cyano substituent at the *para* position of the outmost phenyl group. Therefore, the foldamer does not have C_{2v} mirror symmetry. The **57·F⁻** complex forms centrosymmetric crystal structure, where the foldamer wraps

around the fluoride with similar interactions as in **56**·F^- complex (FIGURE 62). Two complexes (P and M helical) pack together with π···π stacking interactions from a p-cyanophenyl ring and a phenyl ring. In addition to this, the electron deficient p-cyanophenyl ring from one complex has 3.90 Å anion···π interaction with the fluoride of the other complex.

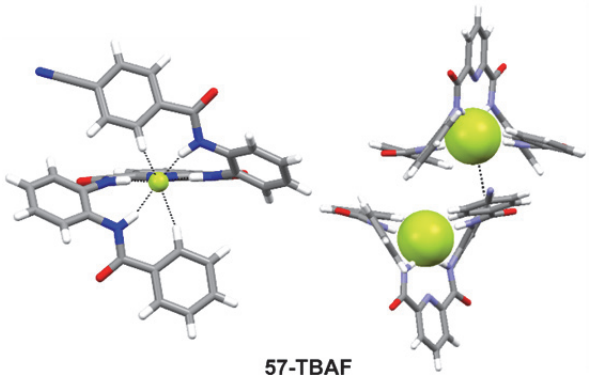

FIGURE 62 The crystal structure of **57**·F^- complex (**57**-TBAF) showing the fluoride binding conformation (left) and the crystal packing (right) and anion···π interactions with dashed lines.

In the (-)ESI-MS experiments, the chloride, iodide, and bromide complexes were studied, and the peaks for the 1:1 complexes of all three halides were observed. ^{1}H NMR titration studies for foldamer **57** were done with TBACl in acetone-d_6. The foldamer had very similar chemical shifts to foldamer **56**, and the equilibrium was also reached at 1 eq (FIGURE 63). This suggests that the chloride binding conformation of foldamer **57** is similar to foldamer **56**. The DFT minimized structure of **57**·Cl^--complex also had a very similar binding mode to chloride. The ITC measurements indicated a 1:1 binding with K_a = (4.6 ± 0.9) 10^4 M^{-1}. The **57**·Cl^--complex formation has the enthalpy and entropic parameters of ΔH = -2.5 ± 0.2 kcal/mol, TΔS = 3.9 ± 0.3 kcal/mol and ΔG = -6.4 Δ ± 0.1 kcal/mol. Similarly to foldamer **56**, the favorable entropy increase was the main driving force for the chloride binding to foldamer **57**.

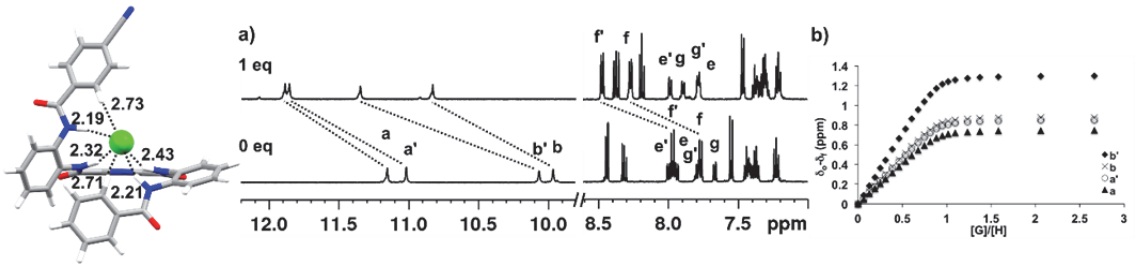

FIGURE 63 The solution state DFT optimized structure showing the distances of hydrogen bonding interactions (Å). a) ^{1}H NMR spectra of foldamer **57** with 0 and 1 equivalent of TBACl in acetone-d_6. b) Chemical shift changes of the NH protons (a, a', b and b') in TBACl titration.

2.4.3 Foldamer 58

The foldamer **58** crystallizes in a flatter and more open conformation than **56** and **57**. Foldamer **58** has only two intramolecular hydrogen bonds, but the 1,2-diamino ring and the nitrophenyl ring interact with intramolecular π···π stacking, which is uncommon for these foldamers. Moreover, the crystal packing is stabilized by intermolecular π···π interactions.

The fluoride binding significantly affects the solid-state conformation by inducing a helical conformation instead of the flatter conformation (FIGURE 64). In the solid state, the **58·F⁻**-complex forms a polar crystal structure with a space group $Pca2_1$. In the structure, the nitro groups orient along the crystallographic c-axis, and the foldamer wraps around the fluoride into P and M helical complexes. The fluoride is bound by four NH···F⁻ hydrogen bonds and only one CH···F⁻ interaction, since one of the nitrophenyl rings is rotated perpendicular to the anion. Additionally, the anion forms a CH···F⁻ interaction with the pyridine ring of the adjacent complex causing the complexes pack into chains. Contrary to **57·F⁻** complex, no anion···π interaction was observed in the packing of the **58·F⁻**complex, although both have electron deficient aromatic rings suitable for the interaction.

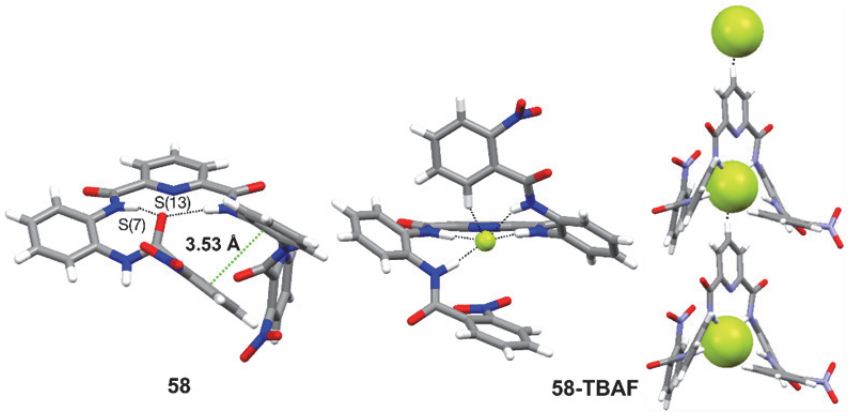

FIGURE 64 The crystal structure of foldamer **58** (left) without anion. The crystal structure of **58·F⁻** complex (**58**-TBAF) showing the fluoride binding conformation (middle) and the crystal packing (right).

In the (-)ESI-MS experiments the chloride, iodide, and bromide complexes were studied and peaks for the 1:1 complexes of all three halides were observed. Titration studies for foldamer **58** were done with TBACl in acetone-d_6. The internal NH_a protons and the terminal *ortho*-aryl proton H_f do not shift as much as the respective protons of the **56·Cl⁻** and **57·Cl⁻** complexes (FIGURE 65). The foldamer **58** may change its conformation more than foldamer **56** and **57** upon binding to chloride, since the *ortho*-aryl protons H_g and H_e in the ring B experienced downfield shifts.

Two pieces of evidence suggest that the binding stoichiometry could be higher than 1:1; in the titration, the chemical shifts reaches the saturation at 2 equiv of the guest and the binding constant for 1:1 complex (5800 M^{-1}) is lower

than expected considering that the foldamer has two electron withdrawing groups and it is one order of magnitude smaller than the binding constants of **56** and **57**. A 1:2 (H:G) model resulted in a better fit for the titration data and a binding constant of $K_{11} > 10^4$ M^{-1}, which fits the expectations. The K_{12} value for the 1:2 complex is 10^8 M^{-1}.

The DFT minimized structures for both the 1:1 and 1:2 complexes were calculated (FIGURE 65). In the 1:1 complex, the anion resides inside the helically folded foldamer bound by four NH hydrogen bonds and by CH···F^- and π···F^- interactions. In the 1:2 complex, the fluorides are bound outside the foldamer helix by one NH hydrogen bond and a π···F^- interaction from the nitrophenyl rings.

The ITC measurements indicated the 1:1 binding with $K_a = (3.0 \pm 0.3)\ 10^4$ M^{-1}, but the 1:2 binding could not be disregarded because the enthalpy loss from the disassembly of 1:1 complex could be compensating for the enthalpy gain from the assembly of the 1:2 complex.

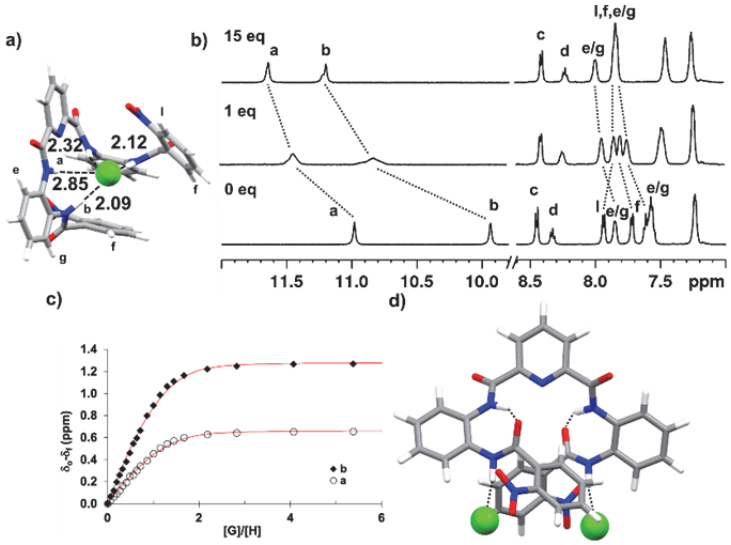

FIGURE 65 a) The solution state DFT structure showing the distances of hydrogen binding interactions (Å). a) ^{1}H NMR spectra of foldamer **58** with 0, 1 and 15 equivalent of TBACl in acetone-d_6. b) Chemical shift changes of the NH protons (a and b) in TBACl titration. c) The DFT calculated structures for the 1:2 complex.

2.4.4 Foldamers 59 and 60

Additional solid-state fluoride complexes were crystallized with the shorter foldamers **59** and **60** that wrap around the fluoride anion only partially due to their shortness. Therefore, the packing in **59** and **60** structures is affected by the countercation TBA^+ located between the complexes in TBA-complex chains. For complex **59·F$^-$**, the P and M helices alternate in the chain. For **60·F$^-$** -complex, however, the P or M handedness cannot be determined because the foldamer **60** is severely disordered in the structure.

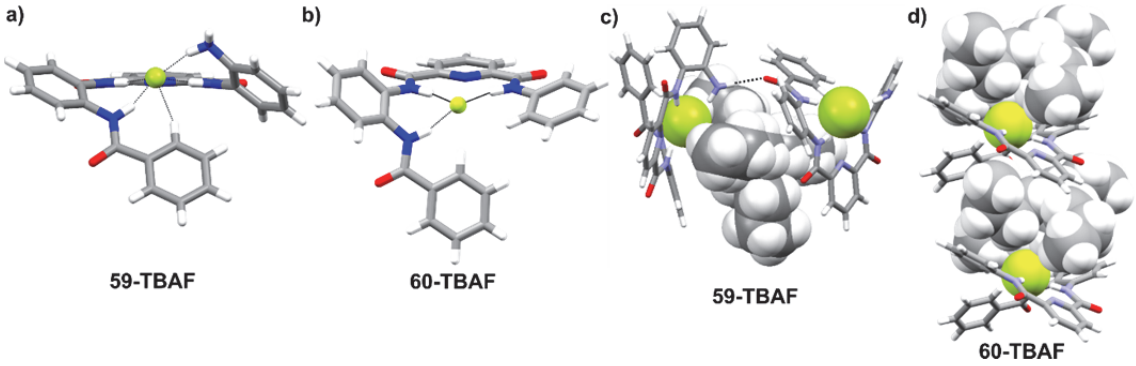

FIGURE 66 The crystal structure of a) **59**·F^--complex (**59**-TBAF) and b) **60**·F^--complex (**60**-TBAF) showing the fluoride binding conformation. The crystal packing of the structures c) **59**-TBAF and d) **60**-TBAF.

2.5 IM-MS studies of foldamers 56 and 61-65*

2.5.1 Introduction to IM-MS

Ion mobility mass spectrometry (IM-MS) combines ion mobility spectrometry (IM) and mass spectrometry (MS). IM-MS is an experimental technique that enables the gas phase study of the conformations of ions and ionic complexes. The method has been widely used in the conformational analysis of biological molecules and complexes and recently has been applied to the study of supramolecular complexes.[131]

With IM-MS, ions can be separated based on their shape and size. In drift-tube (DT) IM spectroscopy the separation is achieved with a uniform electric field that drives ions through a buffer gas filled tube.[132] The collisions with the gas and the ions determine the drift time (t_d) of the ions. Small and compact ions have a smaller t_d than large and elongated ions. From the measurements, a collision cross section value (^{DT}CCS) can be calculated and compared with CCS values obtained from other experiments, such as crystal structures, DOSY NMR, or from calculated structures. IM-MS has been used to determine the tertiary structures of foldamers[133], conformational properties of β-peptides[134], and the folding behavior of oligorotaxanes[135]. The purpose of this work was to study the complexation and conformations of six different aromatic oligoamide foldamers **56** and **61-65** (FIGURE 67) with ion mobility mass spectrometry and test the suitability of the method to this type of foldamers.

* These results have not been previously published. Detailed methods and parameter are presented in Appendix I.

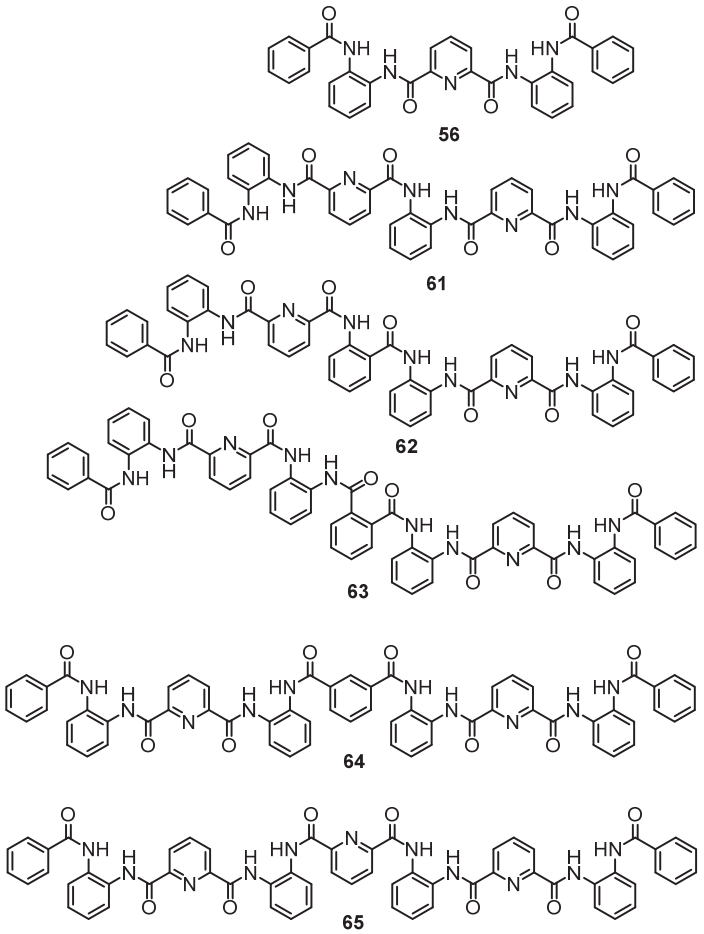

FIGURE 67 Foldamers **56** and **61-65** were studied with IM-MS.

2.5.2 Negative polarity results

Except for foldamer **63**, all the foldamers had only a single peak in the ion mobility spectra (FIGURE 68) meaning that they have only one major conformation in the gas phase. Foldamer **63** revealed two peaks indicating two possible conformations. The second peak at higher drift time, however, is likely due to the Cl^-complex dissociating in the drift tube on the way to the detector. Foldamers **63** and **64** have the same mass, but foldamer **64** moved slower in the drift tube, indicating a larger conformation. The mass of foldamer **65** differs from foldamer **63** and **64** by 1 Da, but the drift time is similar to foldamer **63**, indicating that foldamer **65** has a similar surface area in its conformation as foldamer **63**.

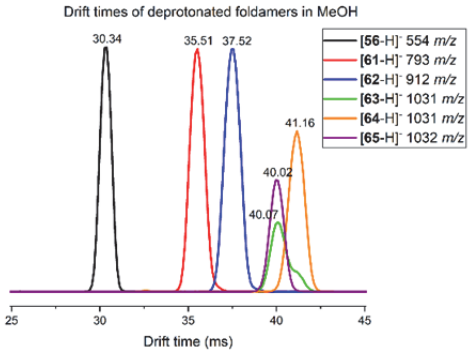

FIGURE 68 The drift times of the deprotonated foldamers **56** and **61-65**.

The $^{DT}CCS_{N2}$ results for the deprotonated foldamers are presented in TABLE 2. The $^{DT}CCS_{N2}$ value of 231.6 (± 0.16) Å^2 for **56** was compared with the CCS values calculated from the helical crystal structure of foldamer **56** and a crystal structure with an S-fold, modified from foldamer **57** since foldamer **56** has not crystallized in the S-fold conformation (FIGURE 69). The CCS value of 234.3 Å^2 from the helical crystal structure was the closest to the experimental value, whereas the CCS value of the S-fold was much larger (245.4 Å^2). On the other hand, CCS values calculated from the DFT structures[127] had only a small difference between the helical **56**-@1 (231.5 Å^2) and S-folded **56-S** (234.1 Å^2). Two other, previously simulated conformations had much smaller CCS values (**56-**@2: 223.3 Å^2 and **56-h**: 214.6 Å^2), and one conformation had a significantly larger CCS value (**56**-w: 266.4 Å^2, FIGURE 69). It can be concluded that in the gas phase, deprotonated foldamer **56** has a similar surface area to the @-fold crystal structure and a folded conformation between the non-folded and the most compact conformations.

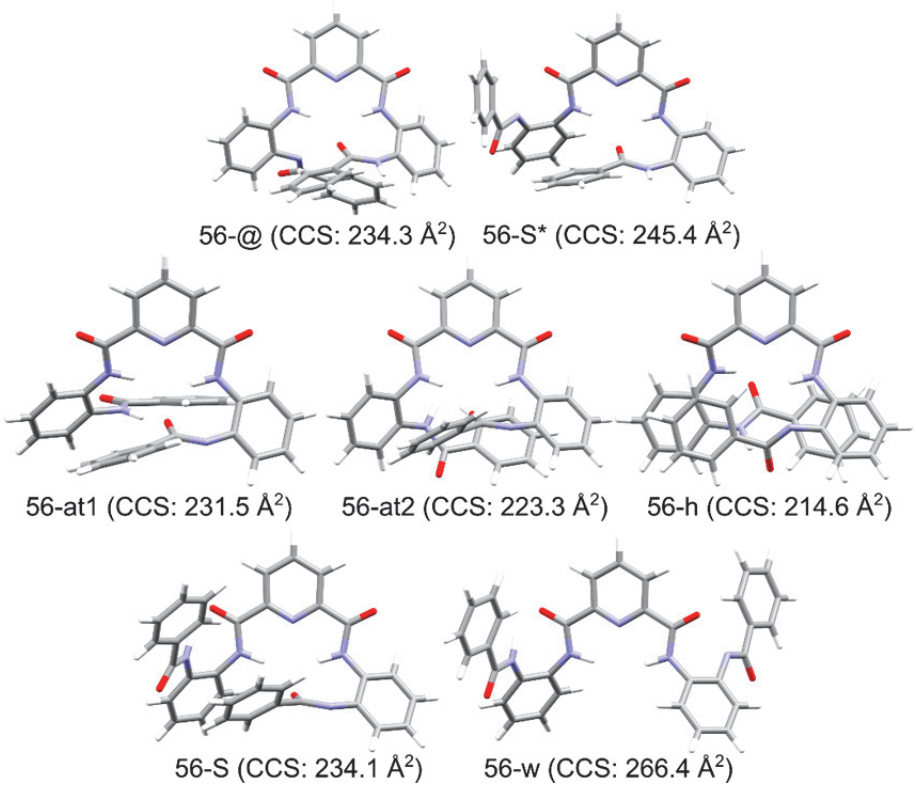

FIGURE 69 CCS values were calculated from crystal structures (**56**-@ and **56**-S*) and from previously simulated DFT conformations (**56**-@1, **56**-@2, **56**-h, **56**-S and **56**-w).[127] One NH proton was removed, and negative charge was placed on the nitrogen atom in the crystal structures and the molecular models of foldamer **56**. From these deprotonated models, the CCS values were calculated. (*The deprotonated S-fold was modified from the crystal structure of foldamer **57** by removing the cyano group and replacing it with a proton.)

Foldamer **61** has a $^{DT}CCS_{N2}$ value of 268.2 (± 0.34) Å², and the CCS values from the helical (280.0 Å²) and the more open crystal structure (311.4 Å²) are significantly higher. The experimental $^{DT}CCS_{N2}$ values are also significantly lower than the values obtained from crystal structures (TABLE 2) in the case of other foldamers **62-65**. This means that the deprotonated foldamer is in a more compact conformation in the gas phase than the foldamers are in any of the crystal structures.

A CCS value of 251.4 Å² for the **56**·$\mathbf{Cl^-}$ complex was calculated from the gas phase DFT structure, and it is 11.7 Å² larger than the experimental value (239.7 ± 0.21; TABLE 2). This implies that the chloride is bound to the foldamer in a compact way, possibly in a helical conformation. Compared with deprotonated foldamers, foldamer-chloride complexes have 5.0-8.3 Å² larger $^{DT}CCS_{N2}$ values. For foldamer **64**, however, the $^{DT}CCS_{N2}$ value of the chloride complex is 2 Å² smaller than that of the deprotonated foldamer. This means that the flexible foldamer **64** wraps around the chloride and makes the conformation of the complex more compact.

TABLE 2 The $^{DT}CCS_{N2}$ values (Å²) from IM-MS experiments and calculated CCS values for the deprotonated foldamers **56** and **61-65** and foldamer-chloride complexes.

deprotonated	[**56**-H]⁻	[**61**-H]⁻	[**62**-H]⁻	[**63**-H]⁻	[**64**-H]⁻	[**65**-H]⁻
$^{DT}CCS_{N2}$/Å²	231.6 (± 0.16)	268.2 (± 0.34)	282.3 (± 0.38)	301.6 (± 0.42)	309.6 (± 0.43)	301.0 (± 0.34)
CCS-1*/Å²	234.8	280.0	311.8	352.8	357.4	341.5
CCS-2**/Å²	245.4	311.4	312.6	366.7	-	367.3

chloride complex	[**56**+Cl]⁻	[**61**+Cl]⁻	[**62**+Cl]⁻	[**63**+Cl]⁻	[**64**+Cl]⁻	[**65**+Cl]⁻
$^{DT}CCS_{N2}$/Å²	239.7 (± 0.21)	274.5 (± 0.34)	290.6 (± 0.45)	309.4 (± 0.41)	307.6 (± 0.40)	306.0 (± 0.42)
CCS-DFT/Å²	251.4	-	-	-	-	-

* CCS values calculated from **56**-MeOH, **61**-DMA-H2O, **62**-EtOAc, **63**-DMSO, **64**-EtOAc and **65**-Ac crystal structures.
** CCS values calculated from **57**-EtOAc, **61**-DCM, **62**-DMSO, **63**-DMA and **65**-$CHCl_3$ crystal structures.

2.5.3 Positive polarity results

All the foldamers had only a single peak in the ion mobility spectra (FIGURE 70), meaning that they only have one major conformation in the gas phase. The minor peak of protonated **61** at t_d~27 is probably a measurement artifact/impurity. The $^{DT}CCS_{N2}$ values of the protonated foldamers are in the same order as the deprotonated foldamers, meaning that the protonated foldamer **64** has larger conformation than foldamers **63** and **65**, which have the same drift times.

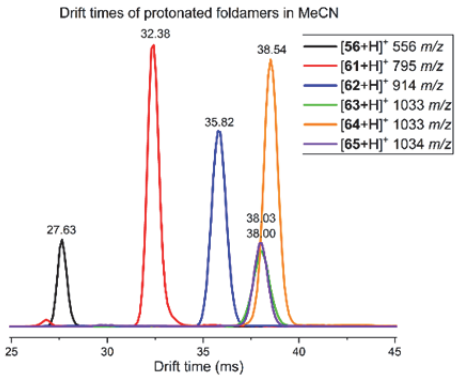

FIGURE 70 The drift times of the protonated foldamers **56** and **61-65**.

The $^{DT}CCS_{N2}$ values of alkali metal complexes of **56** and **61-65** are all larger than those of the protonated foldamer. The $^{DT}CCS_{N2}$ value of [**56**+K]⁺ is slightly smaller than [**56**+Na]⁺, suggesting that [**56**+K]⁺ has a smaller surface area despite its larger mass (TABLE 3). This indicates that foldamer **56** has a different mode to binding K⁺ than Na⁺, enabling more compact conformation for [**56**+K]⁺.

Alternatively, the binding modes of Na^+ to **56** vary more, resulting in larger distribution of different sizes, but the resolutions of the peaks do not support this conclusion (see Appendix I).

The $^{DT}CCS_{N2}$ values of [**61**+K]$^+$ and [**61**+Cs]$^+$ are also smaller than those of [**61**+Na]$^+$, indicating different and more compact binding modes for [**61**+K]$^+$ and [**61**+Cs]$^+$ (FIGURE 71). The $^{DT}CCS_{N2}$ values for [**61**+K]$^+$ and [**61**+Cs]$^+$ differ slightly, suggesting that the binding of these cations are in a position where the size of the cation does not affect the overall size of the complex.

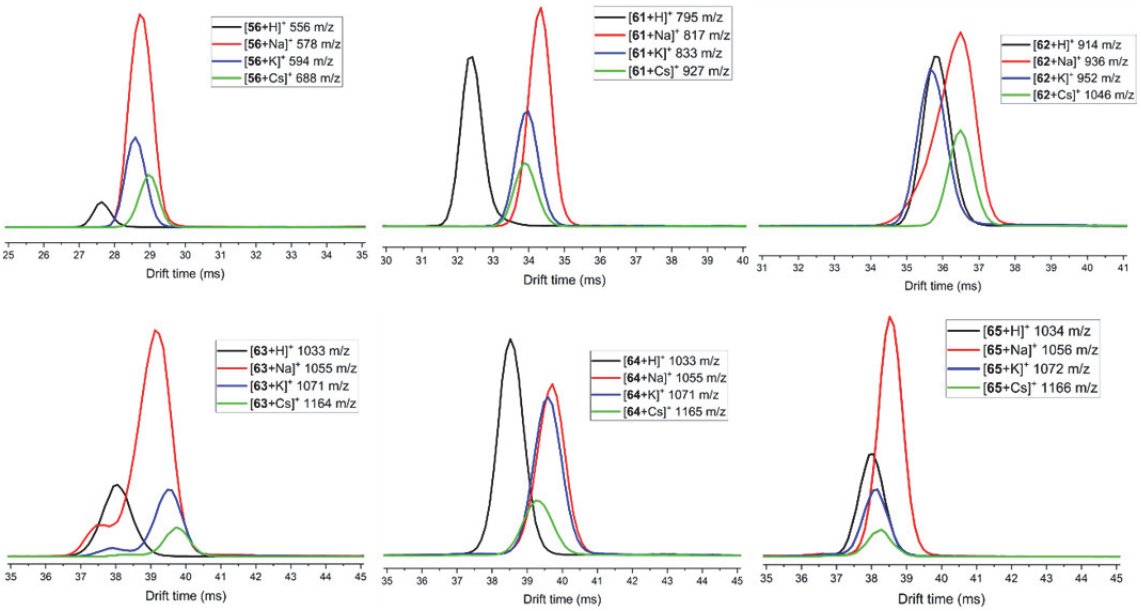

FIGURE 71 Drift spectrums for the protonated foldamers and their Na^+, K^+, and Cs^+ complexes.

The [**62**+K]$^+$ complex has the similar $^{DT}CCS_{N2}$ value as the protonated foldamer **62** ([**62**+H]$^+$). Thus, they have a conformation in which the size of the cation does not affect the size of the conformation. Furthermore, in this case K^+ and Cs^+ complexes had smaller $^{DT}CCS_{N2}$ values, indicating a more compact conformation. The $^{DT}CCS_{N2}$ values of the cation complexes of **63** are in the predicted order ($H^+ < Na^+ < K^+ < Cs^+$) based on the differences in the masses of the complexes.

TABLE 3 The $^{DT}CCS_{N2}$ values (Å^2) from experiments for the protonated foldamers **56** and **61-65** and for their Na, K, and Cs complexes.

	[**56**+H]$^+$	[**61**+H]$^+$	[**62**+H]$^+$	[**63**+H]$^+$	[**64**+H]$^+$	[**65**+H]$^+$
$^{DT}CCS_{N2}$ / Å^2	223.5 (± 0.19)	259.9 (± 0.20)	285.7 (± 1.3)	304.0 ± 0.41	307.9 ± 0.35	303.9 ± 0.38
	[**56**+Na]$^+$	[**61**+Na]$^+$	[**62**+Na]$^+$	[**63**+Na]$^+$	[**64**+Na]$^+$	[**65**+Na]$^+$
$^{DT}CCS_{N2}$ / Å^2	232.1 (± 0.15)	275.1 (± 0.20)	291.8 (± 0.31)	312.1 (± 0.50)	315.8 (± 0.42)	307.8 (± 0.41)
	[**56**+K]$^+$	[**61**+K]$^+$	[**62**+K]$^+$	[**63**+K]$^+$	[**64**+K]$^+$	[**65**+K]$^+$
$^{DT}CCS_{N2}$ / Å^2	231.1 (± 0.16)	272.2 (± 0.24)	287.8 (± 0.32)	315.2 (± 0.40)	314.9 (± 0.40)	304.6 (± 0.38)
	[**56**+Cs]$^+$	[**61**+Cs]$^+$	[**62**+Cs]$^+$	[**63**+Cs]$^+$	[**64**+Cs]$^+$	[**65**+Cs]$^+$
$^{DT}CCS_{N2}$/ Å^2	233.0 (± 0.14)	271.2 (± 0.18)	294.8 (± 0.30)	317.1 (± 0.41)	312.5 (± 0.41)	305.1 (± 0.35)

The Na^+, K^+, and Cs^+ cation complexes of foldamer **64** all have similar $^{DT}CCS_{N2}$ values, indicating that they also have similar conformations in which the size of the cation does not affect the size of the conformation. [**64**+Cs]$^+$ has slightly more compact conformation, which may indicate that the flexible foldamer **64** can more easily wrap around bigger cations. The protonated foldamer **64** [**64**+H]$^+$, however, still has the smallest $^{DT}CCS_{N2}$ and thus the most compact conformation.

The drift spectra suggest that [**65**+H]$^+$, [**65**+K]$^+$, and [**65**+Cs]$^+$ have similar binding modes, where the size of the cation has little effect to the size of the complex (FIGURE 71). [**65**+Na]$^+$, on the other hand, has a larger conformation or wider variety of different conformations.

Unfortunately, within the timeframe of the Ph.D. project, we did not have time and possibility to simulate the protonated foldamers or cation complexes nor did we have any respective crystal structures available. Therefore, these results can be considered as preliminary, and they still require confirmation and comparison to other methods to fully support the conclusions.

SUMMARY

In this work, the conformational properties and complexation of aromatic oligoamide foldamers **56-65** were studied. Single crystal x-ray diffraction was used to study the conformations of foldamers **61-65** and the fluoride complexes of foldamer **56-60** in the solid state. CD spectroscopy was used to study the chirality of the crystals. NMR experiments revealed the intramolecular interactions of foldamers **61-65**. ^{1}H NMR and ITC titrations were used to elucidate the binding of anions to foldamers, and DFT calculations of the chloride complexes provided further information of the possible binding modes.

The conformational properties of foldamers **61-56** are remarkably predictable and stable, which is seen, among other things, by the number of solvated crystal structures they produce. The folding motifs (@-fold and S-fold) of shorter foldamers are retained in the longer foldamers. By tuning the structure of the spacer groups between the pyridine rings, a variety of conformations can be obtained. Foldamers **61** and **65** both exhibited either a helical conformation or a more open conformation. The unsymmetrical spacer group in foldamer **62** enabled a compact conformation with π-π interactions of the aromatic rings. Foldamer **63** has two distinct conformations based on which side of the rigid spacer the two pyridine centers fold with the @-fold motif in relation to each other. Because the structural isomer foldamer **64** has a flexible spacer group, the foldamer can adopt a flatter conformation in crystal structure, but NOESY NMR correlations were inconclusive.

As expected, the preorganization of foldamers **56-60** facilitated the binding of small halides, such as fluoride and chloride, but only fluoride complexes crystallized. The fluoride is located at the center of the helix bound by three to four amide NHs and CH···anion, π···anion, or NH_2···anion interactions depending on the foldamer. The crystal packing of the fluoride complexes resulted in chiral, noncentrosymmetrical, and centrosymmetrical space groups. The formation of chiral crystal structure from achiral compounds is in itself really rare, but astonishingly the chiral complex **56·F$^-$** also exhibited exceptional symmetry breaking in the bulk sample.

Foldamer **56** binds chloride selectively and with high affinity ($K_a = 10^4$ M^{-1}) in solution. Comparison to foldamers **57** and **58** with electron withdrawing groups revealed a slight increase in chloride binding affinity. The 1:1 complexes most likely have a helicoid structure, but for foldamer **58** a 1:2 host:guest complex was also observed. The chloride complexes showed positive entropies, and the largest entropy term was for the **58·Cl$^-$** complex.

The IM-MS studies indicated that the deprotonated and protonated foldamers **56** and **61-65** and their anion and cation complexes have only one preferential conformation in the gas phase. The $^{DF}CCS_{N2}$ values also indicated that **63** and **65** have a more compact conformation than foldamer **64**. Many of the cation complexes had a conformation in which the size of the cation did not affect the size of the conformation. These results are in line with the conformational stability and folding properties seen in solid state and in solution. Further

comparisons to molecular models are needed to make further conclusions about the gas phase complexation conformations.

This work provides important information on the conformation properties and anion complexation of pyridine-2,6-dicarboxamide based oligoamide foldamers. The unexpected symmetry breaking of complex **56**·$\mathbf{F}^-$ shines light on how the homochirality in biomolecules could have originated from achiral organic compounds. In future, the predictability and stability of the conformations and the fluoride and chloride complexation properties of the foldamers could be exploited in a number of applications ranging from molecular switches to anion catalysts.

REFERENCES

1. Gellman, S.H., *Acc. Chem. Res.* **1998**, *31,* 173-180.

2. Shi, Y.; Teng, P.; Sang, P.; She, F.; Wei, L. and Cai, J., *Acc. Chem. Res.* **2016**, *49,* 428-441.

3. Gopalan, R.; Del Borgo, M.; Mechler, A.; Perlmutter, P. and Aguilar, M., *Chemistry & Biology.* **2015**, *22,* 1417-1423.

4. Zhang, D.; Zhao, X.; Hou, J. and Li, Z., *Chem. Rev.* **2012**, *112,* 5271-5316.

5. Horne, W.S. and Gellman, S.H., *Acc. Chem. Res.* **2008**, *41,* 1399-1408.

6. Nair, R.V.; Vijayadas, K.N.; Roy, A. and Sanjayan, G.J., *Eur. J. Org. Chem.* **2014**, 7763-7780.

7. Yashima, E.; Ousaka, N.; Taura, D.; Shimomura, K.; Ikai, T. and Maeda, K., *Chem. Rev.* **2016**, *116,* 13752-13990.

8. Yashima, E.; Maeda, K.; Iida, H.; Furusho, Y. and Nagai, K., *Chem. Rev.* **2009**, *109,* 6102-6211.

9. Hill, D.J.; Mio, M.J.; Prince, R.B.; Hughes, T.S. and Moore, J.S., *Chem. Rev.* **2001**, *101,* 3893-4012.

10. Hecht, S. and Huc, I., *Foldamers: Structure, Properties, and Applications,* WILEY-VCH Verlag GmbH & Co. KGaA, Weinheim, 2007.

11. Hartley, C.S., *Acc. Chem. Res.* **2016**, *49,* 646-654.

12. Martinek, T.A. and Fülöp, F., *Chem. Soc. Rev.* **2012**, *41,* 687-702.

13. Saraogi, I. and Hamilton, A.D., *Chem. Soc. Rev.* **2009**, *38,* 1726-1743.

14. Haldar, D. and Schmuck, C., *Chem. Soc. Rev.* **2009**, *38,* 363-371.

15. Maayan, G., *Eur. J. Org. Chem.* **2009**, 5699-5710.

16. Yashima, E. and Maeda, K., *Macromolecules.* **2008**, *41,* 3-12.

17. Liu, S.; Zavalij, P.Y.; Lam, Y. and Isaacs, L., *J. Am. Chem. Soc.* **2007**, *129,* 11232-11241.

18. Ferrand, Y. and Huc, I., *Acc. Chem. Res.* **2018**, *51,* 970-977.

19. Zhu, Y.; Wang, G. and Li, Z., *Curr. Org. Chem.* **2011**, *15,* 1266-1292.

20. Mateus, P.; Wicher, B.; Ferrand, Y. and Huc, I., *Chem. Commun.* **2018**, *54,* 5078-5081.

21. Zhang, D.; Zhao, X. and Li, Z., *Acc. Chem. Res.* **2014**, *47,* 1961-1970.

22. Juwarker, H. and Jeong, K., *Chem. Soc. Rev.* **2010**, *39,* 3664-3674.

23. Kakuchi, R.; Nagata, S.; Sakai, R.; Otsuka, I.; Nakade, H.; Satoh, T. and Kakuchi, T., *Chem. Eur. J.*, **2008**, *14,* 10259-10266.

24. Sánchez-Quesada, J.; Seel, C.; Prados, P.; de Mendoza, J.; Dalcol, I. and Giralt, E., *J. Am. Chem. Soc.* **1996**, *118,* 277-278.

25. Fernández-Carneado, J.; Van Gool, M.; Martos, V.; Castel, S.; Prados, P.; de Mendoza, J. and Giralt, E., *J. Am. Chem. Soc.* **2005**, *127,* 869-874.

26. Juwarker, H.; Suk, J. and Jeong, K., *Chem. Soc. Rev.* **2009**, *38,* 3316-3325.

27. Saha, S.; Kauffmann, B.; Ferrand, Y. and Huc, I., *Angew. Chem. Int. Ed.* **2018**, *57,* 13542-13546.

28. Chandramouli, N.; Ferrand, Y.; Lautrette, G.; Kauffmann, B.; Mackereth, C.D.; Laguerre, M.; Dubreuil, D. and Huc, I., *Nature Chem.* **2015**, *7,* 334.

29. Horeau, M.; Lautrette, G.; Wicher, B.; Blot, V.; Lebreton, J.; Pipelier, M.; Dubreuil, D.; Ferrand, Y. and Huc, I., *Angew. Chem. Int. Ed.* **2017**, *56,* 6823-6827.

30. Wang, W.; Zhang, C.; Qi, S.; Deng, X.; Yang, B.; Liu, J. and Dong, Z., *J. Org. Chem.* **2018**, *83,* 1898-1902.

31. Ferrand, Y.; Chandramouli, N.; Kendhale, A.M.; Aube, C.; Kauffmann, B.; Grélard, A.; Laguerre, M.; Dubreuil, D. and Huc, I., *J. Am. Chem. Soc.* **2012**, *134,* 11282-11288.

32. Abramyan, A.M.; Liu, Z. and Pophristic, V., *Phys. Chem. Chem. Phys.* **2014**, *16,* 20406-20410.

33. Hayashi, T.; Ohishi, Y.; Hee-Soo, S.; Abe, H.; Matsumoto, S. and Inouye, M., *J. Org. Chem.* **2018**, *83,* 8724-8730.

34. Xiong, J.; Feng, H.; Wang, J.; Zhang, C.; Li, B. and Zheng, Y., *Chem. Eur. J.* **2018**, *24,* 2004-2012.

35. Yi, H.; Shao, X.; Hou, J.; Li, C.; Jiang, X. and Li, Z., *New J. Chem.* **2005**, *29,* 1213-1218.

36. Morcillo, S.P.; Miguel, D.; Álvarez, d.C.; Justicia, J.; Abbate, S.; Castiglioni, E.; Bour, C.; Ribagorda, M.; Cárdenas, D.J.; Paredes, J.M.; Crovetto, L.; Choquesillo-Lazarte, D.; Mota, A.J.; Carreño, M.C.; Longhi, G. and Cuerva, J.M., *Chem. Sci.* **2016**, *7,* 5663-5670.

37. Wang, G.; Zhu, H.; Lin, Y.; Chen, Y. and Fu, N., *Sens Actuators B Chem.* **2015**, *206,* 624-629.

38. Beer, P.D. and Gale, P.A., *Angew. Chem. Int. Ed.* **2001**, *40,* 486-516.

39. Molina, P.; Zapata, F. and Caballero, A., *Chem. Rev.* **2017**, *117,* 9907-9972.

40. Evans, N.H. and Beer, P.D., *Angew. Chem. Int. Ed.* **2014**, *53,* 11716-11754.

41. Yang, D.; Zhao, J.; Yang, X. and Wu, B., *Org. Chem. Front.* **2018**, *5,* 662-690.

42. Busschaert, N.; Caltagirone, C.; Van Rossom, W. and Gale, P.A., *Chem. Rev.* **2015**, *115,* 8038-8155.

43. Gale, P.A. and Caltagirone, C., *Chem. Soc. Rev.* **2015**, *44,* 4212-4227.

44. Schindler, D.W., *Science.* **1974**, *184,* 897-899.

45. Teresa Albelda, M.; Frías, J.C.; García-España, E. and Schneider, H., *Chem. Soc. Rev.* **2012**, *41,* 3859-3877.

46. Gale, P.; Howe, E.W. and Wu, X., *Chem.* **2016**, *1,* 351-422.

47. Welsh, M.J. and Smith, A.E., *Cell.* **1993**, *73,* 1251-1254.

48. Rodríguez-Lucena, D.; Benito, J.M.; Mellet, C.O. and García Fernández, J.M., *Chem. Commun.* **2007** 831-833.

49. Shang, J.; Si, W.; Zhao, W.; Che, Y.; Hou, J. and Jiang, H., *Org. Lett.* **2014**, *16,* 4008-4011.

50. Cai, J. and Sessler, J.L., *Chem. Soc. Rev.* **2014**, *43,* 6198-6213.

51. Kumler, W.D., *J. Am. Chem. Soc.* **1935**, *57,* 600-605.

52. Sutor, D.J., *J. Chem. Soc.* **1963** 1105-1110.

53. Taylor, R. and Kennard, O., *J. Am. Chem. Soc.* **1982**, *104,* 5063-5070.

54. Rostovtsev, V.V.; Green, L.G.; Fokin, V.V. and Sharpless, K.B., *Angew. Chem. Int. Ed.* **2002**, *41,* 2596-2599.

55. Meudtner, R.; Ostermeier, M.; Goddard, R.; Limberg, C. and Hecht, S., *Chem. Eur. J.* **2007**, *13,* 9834-9840.

56. Meudtner, R. and Hecht, S., *Angew. Chem. Int. Ed.* **2008**, *47,* 4926-4930.

57. Lee, S.; Hua, Y.; Park, H. and Flood, A.H., *Org. Lett.* **2010**, *12,* 2100-2102.

58. Hua, Y.; Liu, Y.; Chen, C. and Flood, A.H., *J. Am. Chem. Soc.* **2013**, *135,* 14401-14412.

59. Wang, Y.; Zhao, W.; Bie, F.; Wu, L.; Li, X. and Jiang, H., *Chem. Eur. J.* **2016**, *22,* 5233-5242.

60. Wang, Y.; Li, F.; Han, Y.; Wang, F. and Jiang, H., *Chem. Eur. J.* **2009**, *15,* 9424-9433.

61. Shang, J.; Zhao, W.; Li, X.; Wang, Y. and Jiang, H., *Chem. Commun.* **2016**, *52,* 4505-4508.

62. Wang, Y.; Bie, F. and Jiang, H., *Org. Lett.* **2010**, *12,* 3630-3633.

63. Hua, Y. and Flood, A.H., *J. Am. Chem. Soc.* **2010**, *132,* 12838-12840.

64. Lee, S.; Hua, Y. and Flood, A.H., *J. Org. Chem.* **2014**, *79,* 8383-8396.

65. Zhao, W.; Wang, Y.; Shang, J.; Che, Y. and Jiang, H., *Chem. Eur. J.* **2015**, *21,* 7731-7735.

66. Liu, Y.; Zhang, L.; Xu, X.; Li, Z.; Zhang, D.; Zhao, X. and Li, Z., *Org. Chem. Front.* **2014**, *1,* 494-500.

67. Juwarker, H.; Lenhardt, J.; Pham, D. and Craig, S., *Angew. Chem. Int. Ed.* **2008**, *47,* 3740-3743.

68. Juwarker, H.; Lenhardt, J.M.; Castillo, J.C.; Zhao, E.; Krishnamurthy, S.; Jamiolkowski, R.M.; Kim, K. and Craig, S.L., *J. Org. Chem.* **2009**, *74,* 8924-8934.

69. Li, Y. and Flood, A.H., *J. Am. Chem. Soc.* **2008**, *130,* 12111-12122.

70. Hua, Y.; Ramabhadran, R.O.; Karty, J.A.; Raghavachari, K. and Flood, A.H., *Chem. Commun.* **2011**, *47,* 5979-5981.

71. Wang, Y.; Xiang, J. and Jiang, H., *Chem. Eur. J.* **2011**, *17,* 613-619.

72. Yang, L.; Wang, Y.; Che, Y. and Jiang, H., *Org. Biomol. Chem.* **2017**, *15*, 7747-7752.

73. Yang, L.; Zhao, W.; Che, Y.; Wang, Y. and Jiang, H., *Chin. Chem. Lett.* **2017**, *28*, 1659-1662.

74. Zhao, W.; Huang, F.; Wang, Y.; Li, Q.; Shang, J.; Che, Y. and Jiang, H., *Tetrahedron Letters*. **2016**, *57*, 1691-1694.

75. Cao, L.; Jiang, R.; Zhu, Y.; Wang, X.; Li, Y. and Li, Y., *Eur. J. Org. Chem.* **2014**, 2687-2693.

76. Borissov, A.; Lim, J.Y.C.; Brown, A.; Christensen, K.E.; Thompson, A.L.; Smith, M.D. and Beer, P.D., *Chem. Commun.* **2017**, *53*, 2483-2486.

77. Zurro, M.; Asmus, S.; Beckendorf, S.; Mück-Lichtenfeld, C. and Mancheño, O.G., *J. Am. Chem. Soc.* **2014**, *136*, 13999-14002.

78. Ohmatsu, K.; Kiyokawa, M. and Ooi, T., *J. Am. Chem. Soc.* **2011**, *133*, 1307-1309.

79. Cai, W.; Wang, G.; Du, P.; Wang, R.; Jiang, X. and Li, Z., *J. Am. Chem. Soc.* **2008**, *130*, 13450-13459.

80. Li, C.; Wang, G.; Yi, H.; Jiang, X.; Li, Z. and Wang, R., *Org. Lett.* **2007**, *9*, 1797-1800.

81. Hou, J.; Shao, X.; Chen, G.; Zhou, Y.; Jiang, X. and Li, Z., *J. Am. Chem. Soc.* **2004**, *126*, 12386-12394.

82. Bie, F.; Wang, Y.; Shang, J.; Gallagher, N.M. and Jiang, H., *Eur. J. Org. Chem.* **2013**, *2013*, 8135-8144.

83. Suk Jae-min; Chae, M.K.; Kim Nam-Kyun; Kim Uk-Il and Jeong Kyu-Sung,*Pure and App. Chem.* **2008**, *80*, 599-608.

84. Chang, K.; Kang, B.; Lee, M. and Jeong, K., *J. Am. Chem. Soc.* **2005**, *127*, 12214-12215.

85. Kim, U.; Suk, J.; Naidu, V. and Jeong, K., *Chem. Eur. J.* **2008**, *14*, 11406-11414.

86. Naidu, V.R.; Kim, M.C.; Suk, J.; Kim, H.; Lee, M.; Sim, E. and Jeong, K., *Org. Lett.* **2008**, *10*, 5373-5376.

87. Naidu, V.R.; Suk, J.; Lee, G.W. and Jeong, K., *Bull. Korean Chem. Soc.* **2009**, *30*, 482-485.

88. Lee, C.; Yoon, H. and Jang, W., *Chem. Eur. J.* **2009**, *15,* 9972-9976.

89. Dydio, P.; Zieliński, T. and Jurczak, J., *Org. Lett.* **2010**, *12,* 1076-1078.

90. Suk, J.; Chae, M.K. and Jeong, K., *Pure Appl. Chem.* **2012**, *84,* 953-964.

91. Suk, J. and Jeong, K., *Bull. Korean. Chem. Soc.* **2011**, *32,* 2891-2892.

92. Suk, J. and Jeong, K., *J. Am. Chem. Soc.* **2008**, *130,* 11868-11869.

93. Kim, J.; Juwarker, H.; Liu, X.; Lah, M.S. and Jeong, K., *Chem. Commun.* **2010**, *46,* 764-766.

94. Suk, J.; Kim, J. and Jeong, K., *Chem. Asian J.* **2011**, *6,* 1992-1995.

95. Lee, H.J.; Jeon, H. and Jeong, K., *Supramolecular Chemistry.* **2015**, *27,* 378-385.

96. Kim, H.J.; Suk, J. and Jeong, K., *Supramolecular Chemistry.* **2013**, *25,* 46-53.

97. Jeon, H.; Jang, H.B.; Kang, P.; Choi, Y.R.; Kim, J.; Lee, J.H.; Choi, M. and Jeong, K., *Org. Lett.* **2016**, *18,* 4404-4407.

98. Johnson, C.A.; Berryman, O.B.; Sather, A.C.; Zakharov, L.N.; Haley, M.M. and Johnson, D.W., *Cryst. Growth Des.* **2009**, *9,* 4247-4249.

99. Massena, C.J.; Wageling, N.B.; Decato, D.A.; Martin Rodriguez, E.; Rose, A.M. and Berryman, O.B., *Angew. Chem. Int. Ed.* **2016**, *55,* 12398-12402.

100. Maeda, H. and Haketa, Y., *Pure Appl. Chem.* **2011**, *83,* 189-199.

101. Haketa, Y. and Maeda, H., *Chem. Eur. J.* **2011**, *17,* 1485-1492.

102. Haketa, Y.; Bando, Y.; Takaishi, K.; Uchiyama, M.; Muranaka, A.; Naito, M.; Shibaguchi, H.; Kawai, T. and Maeda, H., *Angew. Chem. Int. Ed.* **2012**, *51,* 7967-7971.

103. Maeda, H.; Shirai, T.; Bando, Y.; Takaishi, K.; Uchiyama, M.; Muranaka, A.; Kawai, T. and Naito, M., *Org. Lett.* **2013**, *15,* 6006-6009.

104. Huc, I., *Eur. J. Org. Chem.* **2004**, 17-29.

105. Bates, G.W.; Gale, P.A. and Light, M.E., *Chem. Commun.* **2007,** 2121-2123.

106. Du, J.; Kang, K.; Hu, J.; Mao, L.; Yuan, L. and Feng, W., *Chin. J. Chem.* **2016**, *34,* 866-872.

107. Xu, Y.; Wang, G.; Zhao, X.; Jiang, X. and Li, Z., *J. Org. Chem.* **2009**, *74,* 7267-7273.

108. Shi, Z.; Chen, S.; Zhao, X.; Jiang, X. and Li, Z., *Org. Biomol. Chem.* **2011**, *9,* 8122-8129.

109. Cholewiak, A.; Stepniak, P. and Jurczak, J., *Synthesis.* **2018**, *50,* 4555-4568.

110. Fischer, L. and Guichard, G., *Org. Biomol. Chem.* **2010**, *8,* 3101-3117.

111. Wu, B.; Jia, C.; Wang, X.; Li, S.; Huang, X. and Yang, X., *Org. Lett.* **2012**, *14,* 684-687.

112. Yang, P.; Wang, J.; Jia, C.; Yang, X. and Wu, B., *Eur. J. Org. Chem.* **2013**, 3446-3454.

113. Jia, C.; Wu, B.; Li, S.; Huang, X. and Yang, X., *Org. Lett.* **2010**, *12,* 5612-5615.

114. Li, S.; Jia, C.; Wu, B.; Luo, Q.; Huang, X.; Yang, Z.; Li, Q. and Yang, X., *Angew. Chem. Int. Ed.* **2011**, *50,* 5721-5724.

115. Connor, A.L.; Hu, T.; Detchou, C.S.F.; Liu, R.; Pulavarti, S.V.S.R.K.; Szyperski, T.; Lu, Z. and Gong, B., *Chem. Commun.* **2016**, *52,* 9905-9908.

116. Kim, M.J.; Lee, H.; Moon, D. and Jeong, K., *Org. Lett.* **2012**, *14,* 5042-5045.

117. Park, E.B. and Jeong, K., *Chem. Commun.* **2015**, *51,* 9197-9200.

118. Gavette, J.V.; Mills, N.S.; Zakharov, L.N.; Johnson II, C.A.; Johnson, D.W. and Haley, M.M., *Angew. Chem. Int. Ed.* **2013**, *52,* 10270-10274.

119. Gavette, J.V.; Evoniuk, C.J.; Zakharov, L.N.; Carnes, M.E.; Haley, M.M. and Johnson, D.W., *Chem. Sci.* **2014**, *5,* 2899-2905.

120. Probst, N.; Madarász, Á; Valkonen, A.; Pápai, I.; Rissanen, K.; Neuvonen, A. and Pihko, P.M., *Angew. Chem. Int. Ed.* **2012**, *51,* 8495-8499.

121. Jia, C.; Wang, Q.; Begum, R.A.; Day, V.W. and Bowman-James, K., *Org. Biomol. Chem.* **2015**, *13,* 6953-6957.

122. Diemer, V.; Fischer, L.; Kauffmann, B. and Guichard, G., *Chem. Eur. J.* **2016**, *22,* 15684-15692.

123. Wechsel, R.; Raftery, J.; Cavagnat, D.; Guichard, G. and Clayden, J., *Angew. Chem. Int. Ed.* **2016**, *55,* 9657-9661.

124. Gratzer, K.; Diemer, V. and Clayden, J., *Org. Biomol. Chem.* **2017**, *15,* 3585-3589.

125. Suhonen, A.; Nauha, E.; Salorinne, K.; Helttunen, K. and Nissinen, M., *CrystEngComm.* **2012**, *14,* 7398-7407.

126. Suhonen, A.; Morgan, I.S.; Nauha, E.; Helttunen, K.; Tuononen, H.M. and Nissinen, M., *Cryst. Growth Des.* **2015**, *15,* 2602-2608.

127. Kortelainen, M.; Suhonen, A.; Hamza, A.; Pápai, I.; Nauha, E.; Yliniemelä-Sipari, S.; Nissinen, M. and Pihko, P.M., *Chem. Eur. J.* **2015**, *21,* 9493-9504.

128. Suhonen, A.; Kortelainen, M.; Nauha, E.; Yliniemela-Sipari, S.; Pihko, P.M. and Nissinen, M., *CrystEngComm.* **2016**, *18,* 2005-2013.

129. Suhonen, A.; Nauha, E.; Salorinne, K.; Helttunen, K. and Nissinen, M., *CrystEngComm.* **2012**, *14,* 7398-7407.

130. Wong, J.C.; Tang, G.; Wu, X.; Liang, C.; Zhang, Z.; Guo, L.; Peng, Z.; Zhang, W.; Lin, X.; Wang, Z.; Mei, J.; Chen, J.; Pan, S.; Zhang, N.; Liu, Y.; Zhou, M.; Feng, L.; Zhao, W.; Li, S.; Zhang, C.; Zhang, M.; Rong, Y.; Jin, T.; Zhang, X.; Ren, S.; Ji, Y.; Zhao, R.; She, J.; Ren, Y.; Xu, C.; Chen, D.; Cai, J.; Shan, S.; Pan, D.; Ning, Z.; Lu, X.; Chen, T.; He, Y. and Chen, L., *J. Med. Chem.* **2012**, *55,* 8903-8925.

131. Kalenius, E.; Groessl, M. and Rissanen, K., *Nature Rev. Chem.* **2019**, *3,* 4-14.

132. Lanucara, F.; Holman, S.W.; Gray, C.J. and Eyers, C.E., *Nature Chem.* **2014**, *6,* 281.

133. De, S.; Chi, B.; Granier, T.; Qi, T.; Maurizot, V. and Huc, I., *Nature Chem.,* **2017**, *10,* 51-57.

134. Schubert, F.; Pagel, K.; Rossi, M.; Warnke, S.; Salwiczek, M.; Koksch, B.; von Helden, G.; Blum, V.; Baldauf, C. and Scheffler, M., *Phys. Chem. Chem. Phys.* **2015**, *17,* 5376-5385.

135. Hanozin, E.; Mignolet, B.; Morsa, D.; Sluysmans, D.; Duwez, A.; Stoddart, J.F.; Remacle, F. and De Pauw, E., *ACS Nano.* **2017**, *11,* 10253-10263.

APPENDIX I

IM-MS methods

The mass spectra and the ion mobility spectra were measured by an Agilent 6560 TOF mass spectrometer. Dual ESI ion source was used, and high purity N_2 gas was utilized in the drift tube. 5 μM samples of the foldamers in MeOH, MeCN, DMSO or 9:1 mixture of DCM:MeCN were prepared. One equivalent of NH_4Cl, NH_4Br, or NH_4I were added to the samples to measure the complexes at negative polarity. NaI, KI, and CsI salts were added to form Na, K, and Cs complexes, and 0.1 % of formic acid was used to protonate the foldamers at positive polarity. All samples were injected with a syringe pump at a 5 μl/min flow rate. The parameters for stepped field measurements are in Tables A1 and A2. MeCN was used as solvent in the positive polarity measurements and MeOH in the negative polarity measurements.

The $^{DT}CCS_{N2}$ values of ESI tuning mix calibrant were measured in both polarity and compared to the literature values (Table A3)[11]. The results were acceptable, since the CCS values deviated approximately only ±3 Å^2. The resolution of the peaks was in the range of 38-49, which indicates that a peak represents only one conformation.

---

1 Gabelica, V.; Afonso, C.; Barran, P.E.; Justin, L.P.B.; Bleiholder, C.; Bowers, M.T.; Bilbao, A.; Bush, M.F.; Larry Campbell, J.; Iain, D.G.C.; Causon, T.J.; Clowers, B.H.; Creaser, C.; Pauw, E.D.; Far, J.; Francisco Fernandez-Lima; Fjeldsted, J.C.; Giles, K.; Groessl, M.; Hogan, C.J.; Hann, S.; Kim, H.I.; Kurulugama, R.T.; May, J.C.; McLean, J.A.; Pagel, K.; Richardson, K.; Mark. E. Ridgeway; Frédéric Rosu; Sobott, F.; Shvartsburg, A.A.; Thalassinos, K.; Valentine, S.J. and Wyttenbach, T., *chemrxiv preprint*, **2018**, 10.26434/chemrxiv.7072070.v2.

Table A1. IM-MS stepped field parameters for negative polarity measurements

General		**Source**	
ion polarity	negative	gas temp	325 °C
stop time	3.5 min	drying gas	1 l/min
		nebulizer	2 psig
abs. threshold	200	VCap	5190 V
rel. threshold	0.01	fragmentor	380 V
time segments	8#, 0.5 min	oct 1 RF Vpp	800 V
Acquisition		**Advanced Parameters**	
mass range	100-1700 m/z	high pressure funnel RF	-150 V
frame rate	0.5 frames/s	trap funnel RF	-150 V
IM transient rate	32 IM transients/frame	trap entrance grid delta	-10 V
max drift time	70 ms	trap exit grid 2 delta	-10 V
TOF transient rate	503 transients/IM transients	drift tube entrance voltage	-1074 V − -1674 V
IM trap fill time	10000 µs	drift tube exit voltage	-224 V
IM trap release time	150 µs	rear funnel entrance	-217.5 V
		rear funnel RF	-150 V
		rear funnel exit	-45 V
		IM hex delta	8 V
		IM hex entrance	-41 V
		collision cell delta delta	0 V
		IBC delta delta	0 V

Table A2. IM-MS stepped field parameters for positive polarity measurements

General		**Source**	
ion polarity	positive	gas temp	250 °C
stop time	3.5 min	drying gas	10 l/min
		nebulizer	8 psig
abs. threshold	200	VCap	5250 V
rel. threshold	0.01	fragmentor	400 V
time segments	7#, 0.5 min	oct 1 RF Vpp	790 V
Acquisition		**Advanced Parameters**	
mass range	100-1700 m/z	high pressure funnel RF	150 V
frame rate	0.5 frames/s	trap funnel RF	150 V
IM transient rate	32 IM transients/frame	trap entrance grid delta	10 V
max drift time	70 ms	trap exit grid 2 delta	10 V
TOF transient rate	503 transients/IM transients	drift tube entrance voltage	1074 V − 1674 V
IM trap fill time	10000 µs	drift tube exit voltage	224 V
IM trap release time	150 µs	rear funnel entrance	217.5 V
		rear funnel RF	150 V
		rear funnel exit	45 V
		IM hex delta	-8 V
		IM hex entrance	41 V
		collision cell delta delta	0 V
		IBC delta delta	0 V

Table A3. The measured $^{DT}CCS_{N2}$ values of calibrant (ESI Tune mix) and the literature values.

ESI tune mix positive polarity	$^{DT}CCS_{N2}$ (Å²)	literature CCS values (Å²)
m/z 322	155.2 ± 0.16	153.67 ± 0.20
m/z 622	204.6 ± 0.23	202.67 ± 0.24
m/z 1222	283.3 ± 0.38	281.25 ± 0.55
m/z 1522	318.0 ± 0.42	315.79 ± 0.81
ESI tune mix negative polarity	$^{DT}CCS_{N2}$ (Å²)	literature CCS values (Å²)
m/z 302	141.6 ± 0.20	140.66 ± 0.32
m/z 602	183.0 ± 0.18	180.94 ± 0.31
m/z 1034	258.0 ± 0.32	255.59 ± 0.53
m/z 1334	287.4 ± 0.38	285.29 ± 0.78
m/z 1634	321.7 ± 0.42	319.53 ± 1.34

CCS calculation methods

The calculations were performed with the Ion Mobility Spectrometry Suite (IMoS v1.08) program. Parameters for CCS value calculations are in Table A4.

Table A4. The IMoS v1.08 program calculation parameters

Is it simplified?	no
Total Charge	-1
Method used	trajectory method
Number of rotations	3
Gas molecules per rotation	300000
Lennard-Jones?	yes
Reduction Coef.	1.000
Molecular mass of Gas	28.00 Da
Alpha polarization	1.70 A^3
Radius of gas	1.50 A
Accommodation coefficient	0
Diffuse Scattering?	yes
Reemission vel. (mean)	521.68 m/s 92% Maxwell
Timestep	150
Boxdomain (one charge)	16 A

ORIGINAL PAPERS

I

STRUCTURAL TUNING AND CONFORMATIONAL STABILITY OF AROMATIC OLIGOAMIDE FOLDAMERS

by

Riia Annala, Aku Suhonen, Heikki Laakkonen, Perttu Permi & Maija Nissinen, 2017

Chem. Eur. J., **2017**, *23*, 16671-16680

DOI : 10.1002/chem.201703985

Structural tuning and conformational stability of aromatic oligoamide foldamers

Riia Annala,[a] Aku Suhonen,[a] Heikki Laakkonen,[a] Perttu Permi[a,b] and Maija Nissinen*[a]

Abstract: A series of aromatic oligoamide foldamers with two or three pyridine-2,6-dicarboxamide units as their main folding motifs and varying aromatic building blocks as linkers have been synthetized to study the effects of the structural variation on the folding properties and conformational stability. Crystallographic studies showed that in the solid state the central linker unit either elongates the helices and more open S-shaped conformations, compresses the helices to more compact conformations or acts as a rigid spacer separating the pyridine-2,6-dicarboxamide units, which for their part add the predictability of the conformational properties. Multidimensional NMR studies showed that, even in solution, foldamers show conformational stability and folded conformations comparable to the solid state structures.

Introduction

During the last decades our understanding about biological processes, such as the catalytic activity and selectivity of enzymes, has greatly increased. This understanding has brought numerous new opportunities for chemists to learn from and adapt towards chemical applications. Synthetic biomimetic oligomers known as foldamers aim to combine the advantages of biological polymers to the favourable properties of synthetic oligomers, such as endurance of varying temperatures, pH and salt concentrations, and possibility to function in organic solvents.[1,2] Their structural rigidity obtained by, for example, repeating aromatic moieties connected by amide or urea bonds allows smaller size and a simpler design of the molecules and adds predictability and stability to their folding and secondary structures, which is the basis for potential applications of foldamers.[3]

A number of different types of aromatic oligoamides have been studied both in solution and in the solid state giving indication on how structural features and interactions affect the folding and conformational properties.[4] In solution the folding properties are greatly affected by competitive interactions with solvent, thus diminishing the predictability of the folding in solution.[5] In the solid state, on the other hand, the requirement of the closest packing and possibility of small molecule inclusion either in the interstice between the foldamers or inside the fold, may alter the folding and conformational properties.[6,7] The properties of aromatic foldamers, such as the flexibility[8], water solubility[9] and overall conformation[10] as well as diameter[11] and chirality[12] of the helix, have been tuned by the addition of different types of monomers. The most common trend has been the addition of aliphatic monomers to make heterogeneous foldamers[13,14] but also foldamers with different aromatic sequences have been made to create, for example, foldamer capsules[15] and selective receptors[16].

The pyridine-2,6-dicarboxamide unit is one of the structural motifs used as a turn unit to impose helical conformations on oligomers.[17] Our previous studies with a series of aromatic oligoamides (4-5 aromatic rings) with a pyridine-2,6-dicarboxamide center have shown that this type of short foldamers reliably adopt two, almost equally stabile folded conformers with only small variances in their hydrogen bonding and structural features.[18-20] Which conformer, denoted as @ or S according to their overall shape (Scheme 1),[21] prevails depends on the chemical structure of the foldamer as well as environment, such as crystallization conditions and solvent. The conformers and folding of these molecules are based on intramolecular hydrogen bonding between the amide groups and the pyridine-2,6-dicarboxamide unit, which forms a suitable niche for multiple interactions, whereas aromatic interactions seem to play a minor role in the folding preferences of the oligoamides. Interestingly, the @ conformer with three intramolecular hydrogen bonds forming to a single carbonyl oxygen, resembles closely an oxyanion hole motif found in the active sites of certain enzymes.[22] Artificial, non-peptidic models for oxyanion hole are not common, as only a few examples of amide and ester carbonyls motifs as acceptors for multiple hydrogen bonds have been described.[23] Thus, aromatic oligoamide foldamers possess great potential as structural and functional mimics of enzyme catalysts.

In our current study, we show that the oxyanion hole motif and the folding patterns are preserved, when the size of the foldamer increases and the number of pyridine-2,6-dicarboxamide units is doubled or tripled (Scheme 1). The spacer unit separating the pyridine-2,6-dicarboxamide units affects the overall folding of the foldamer by preventing certain geometries and/or inducing helicity or compact conformations by participating in intramolecular hydrogen bonding. This indicates that conformational adaptability of foldamers can be controlled with suitable spacers without losing the essential folding motifs and potential binding sites, such as oxyanion hole motif.

Results and Discussion

A series of five oligoamide foldamers (7-9 aromatic rings) were synthetized applying the procedures described in our previous

[a] R. Annala, Dr. Aku Suhonen, H. Laakkonen, Prof. Dr. M. Nissinen
Department of Chemistry, Nanoscience Center
University of Jyvaskyla
P.O. Box 35
40014 University of Jyvaskyla (Finland)
E-mail: maija.nissinen@jyu.fi
[b] Prof. Dr. P. Permi
Department of Chemistry and Department of Biological and Environmental Sciences, Nanoscience Center
University of Jyvaskyla
P.O. Box 35
40014 University of Jyvaskyla (Finland)

Supporting information for this article is available on the WWW under http://

papers[18-20] (see SI for details). The conformational features and the stability of the fold and oxyanion hole motif were studied in the solid state by X-ray crystallography and compared with the solution state information obtained by multidimensional NMR spectroscopy. In foldamers **1**-**3** two pyridine-2,6-dicarboxamide units are separated by 1-3 ortho-substituted phenyl rings and 0-2 amide bonds, whereas in foldamers **4** and **5** either a third pyridine-2,6-dicarboxamide center or its phenyl analogue are used as a spacer. The ortho substituted phenyl rings of foldamers **1**-**3**, especially three consequent rings, act as a linear type of spacer, whereas meta substituted centers of **4** and **5** automatically cause a different type of overall fold, which in the case of the pyridine-2,6-dicarboxamide center of **5** leads to a helical fold stabilized by intramolecular hydrogen bonding to pyridine.

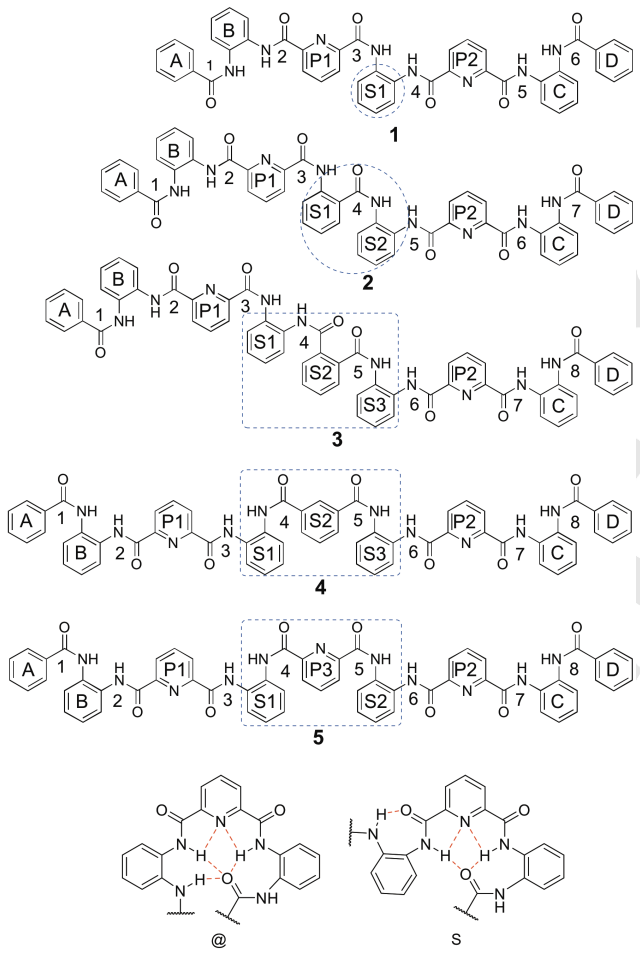

Scheme 1. Chemical structures of the foldamers **1**-**5** including notifications of benzene and pyridine rings and numbering of C=O and NH groups. The spacer groups are circled with dotted lines. A schematic presentation of two observed folding patterns around pyridine-2,6-dicarboxamide center (bottom row).

Solid state conformations

The crystallization studies of the foldamers resulted in 17 different crystal structures. All of the crystal structures obtained for **1**-**5** were solvates, which indicates that folded molecules cannot pack very efficiently due to their complex and awkward shape. In the structures of foldamers **1**-**3** and **5** at least one of the pyridine-2,6-carboxamide units adopts the predicted folded @ conformation (Scheme 1; Table 1; Table S-3 in SI) by 2-3 hydrogen bonds from adjacent C=O group to NH groups next to pyridine ring, thus retaining the desired oxyanion hole motif. Foldamer **4** is the only exception to this as both pyridine-2,6-dicarboxamide centers are in a more open S conformation.

Table 1. 17 solvate structures of the foldamers **1**-**5** and the conformations of the pyridine centers

Structure	Center P1	Center P2	Notes
1-DMA-H_2O	@	@	isomorphous
1-MeCN-H_2O			
1-DMF-H_2O	@	@	
1-MeOH	@	@	
1-DMSO	@	@	
1-DCM	S	@	
2-MeCN	@	S	isomorphous
2-EtOAc			
2-DCM	@	S	
2-DMSO	@	S	
3-DMA	@	@	*trans*
3-DMSO	@	@	*cis*
4-EtOAc	S	S	
5-Ac	@	@	isomorphous
5-DCM			
5-DMF			
5-$CHCl_3$	S	@	

Foldamer 1

Altogether six single crystal structures of the foldamer **1** were obtained (see SI for crystallization details), but only two variations of overall conformation were observed. The isomorphous structures of **1**-DMA-H_2O and **1**-MeCN-H_2O adopt an overall tight helical conformation with both pyridine centers in an @ fold (@/@; Figure 1). The conformations of **1**-DMSO, **1**-MeOH and **1**-DMF-H_2O solvates are also similar with both pyridine centers in @ fold (see ESI Figure S-1 for an overlay of all @/@ structures). In these structures either one (**1**-MeOH) or both (**1**-DMA-H_2O, **1**-MeCN-H_2O, **1**-DMF-H_2O and **1**-DMSO) of the outmost phenyl rings have a CH-π interaction with the spacer phenyl ring. **1**-DCM solvate has a less folded structure, as one of the pyridine-2,6-dicarboxamide centers adopts an open S fold whereas the other one is in an @ fold (@/S; Figure 1). The outmost phenyl ring of the @ folded part of the molecule interacts with the spacer phenyl ring via CH-π interaction (3.041 Å) like in the other structures.

The crystal packing in all structures of foldamer **1** is based on intermolecular hydrogen bonding. In isomorphous @/@-

structures (**1**-DMA-H_2O and **1**-MeCN-H_2O) and in **1**-DMF-H_2O structure two water molecules connect two foldamers into pairs via bifurcated hydrogen bonds (OH_w…O=C; graph set $R_4^4(20)$) and further to chains formed by these pairs (NH1…O_w, graph sets $C_2^2(13)$ and $R_4^4(20)$; Figure 1). The pairing is enhanced by π-π stacking between the pyridine centers P1 of the adjacent molecules. The solvent (DMA, MeCN or DMF) is hydrogen bonded to the outer groove of the fold (NH6…Solvent; D(2) motif). The difference of the crystal structures of isomorphous structures and **1**-DMF-H_2O comes from the efficiency of packing. In **1**-DMA-H_2O and **1**-MeCN-H_2O there is π-π stacking between the end phenyl rings (D), which is prevented in **1**-DMF-H_2O structure by the inclusion of one extra solvent molecule between the rings (See SI Figure S-2). In **1**-DMSO solvate the intermolecular hydrogen bonds orient to two DMSOs, which fill the interstice between the foldamers. The foldamers still pack into layers: the grooves of the folds assemble parallel to each other and interact via π-π interactions (See SI; Figure S-2).

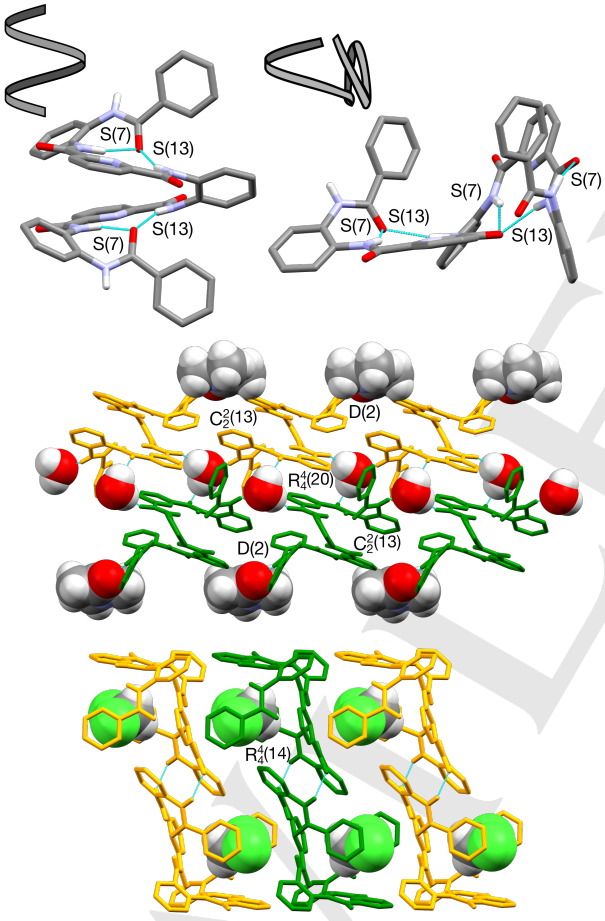

Figure 1 The conformations and schematic presentations of folding of **1**-DMA-H_2O (top left) and **1**-DCM (top right). Crystal packing of **1**-DMA-H_2O (middle) and **1**-DCM structures (below) showing the inclusion of solvents and intermolecular hydrogen bonding motifs (turquoise lines and graph set notifications). Nonbonding hydrogens and disorder have been omitted for clarity and solvents are shown with space fill model.

In **1**-DCM and **1**-MeOH solvates there are direct hydrogen bonds between the foldamers as two intermolecular hydrogen bonds between NH1 and C=O2 groups ($R_4^4(14)$ motif) connect the foldamers into pairs. In case of the more open @/S conformation of **1**-DCM structure, this leads to a niche for a disordered solvent molecule inside the pair of the awkwardly shaped molecules (Figure 1). In **1**-MeOH solvate the pairs are further connected to chains via solvent mediated hydrogen bonds from MeOH to NH6 of one foldamer and C=O4 of the next pair (see SI Figure S-2).

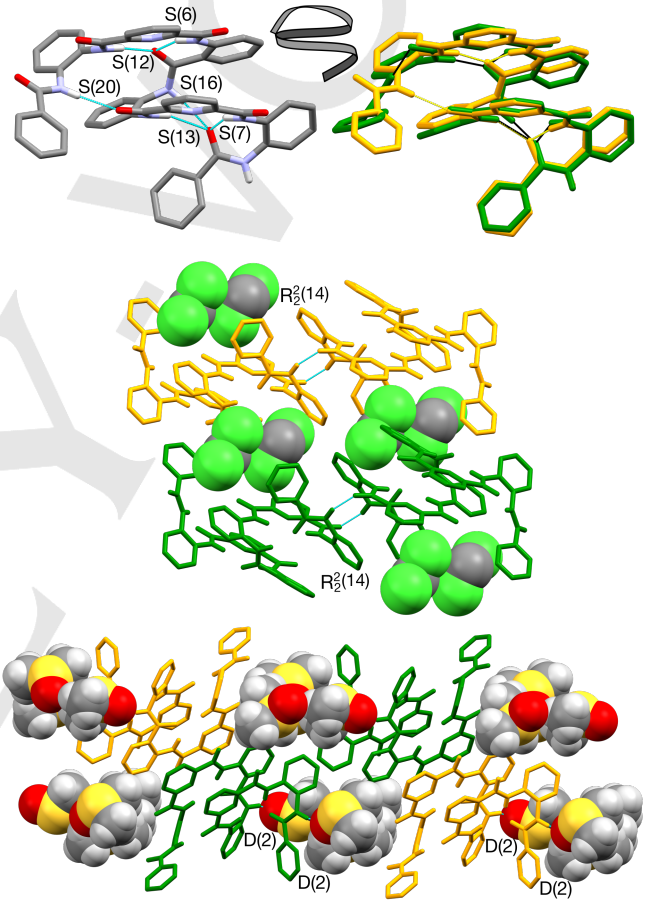

Figure 2 The conformations of **2**-MeCN (top left) and an overlay presentation of the structures of **2**-DMSO (orange) and **2**-DCM (green; top right). The crystal packing of **2**-DCM (middle) and **2**-DMSO (below). Solvents are shown with space filling model and hydrogen bonds with turquoise bonds. Nonbonding hydrogens and disorder have been omitted for clarity.

Foldamer 2

Four different single crystal structures of foldamer **2** were obtained from acetonitrile, ethyl acetate, dichloromethane and DMSO solutions. Two of these structures, the MeCN and the EtOAc solvates (**2**-MeCN and **2**-EtOAc), are isomorphous and the differences between all four structures are minor. In all four structures the P2 pyridine-2,6-dicarboxamide center adopts an @-fold, whereas the P1 center is in S-fold (Figure 3). The overall

conformation is compact, almost helical structure where two pyridines have parallel displaced π-interactions with each other and the end of the S-fold surrounds the helical part. The similarities are facilitated by the unsymmetrical linker unit, where the C=O4 group prefers to form the S-fold by hydrogen bonds to the NH groups of the pyridine-2,6-dicarboxamide unit P1 (graph set motifs S(6) and S(12)). The outmost NH1 finishes the S-fold by a hydrogen bond to O2 (S(7) motif; **2**-DCM) or to O5 of the pyridine-2,6-dicarboxamide center P2 (S(20) motif; other solvates), which leads to slight difference in the orientation of the outmost phenyl ring. The @ folds around pyridine center P2 in isomorphous **2**-MeCN and **2**-EtOAc structures and in **2**-DCM solvate are based on typical three hydrogen bonds between the outmost C=O group (O7) and NH groups of the P2 unit (S(7) and S(13) motifs) and to the next NH group (NH4) in the linker (S(16) motif). In **2**-DMSO, however, the third hydrogen bond is missing as the amide NH4 is hydrogen bonded to solvent (D(2) motif).

Also in the case of foldamer **2** the crystal packing is based on the pairing of molecules via direct intermolecular hydrogen bonding (NH7…O6; $R_2^2(14)$ motif; Figure 2). The solvents are located inside the cleft formed by two hydrogen bonded pairs of foldamers (DCM) or interstice in the crystal lattice (EtOAc and MeCN) (See SI Figure S-4). The exception to pairwise hydrogen bonding is the DMSO solvate, as DMSO disrupts this pattern and the intermolecular hydrogen bonds to two DMSO molecules (from NH7 and NH4 to O10A and O30A; D(2) motifs).

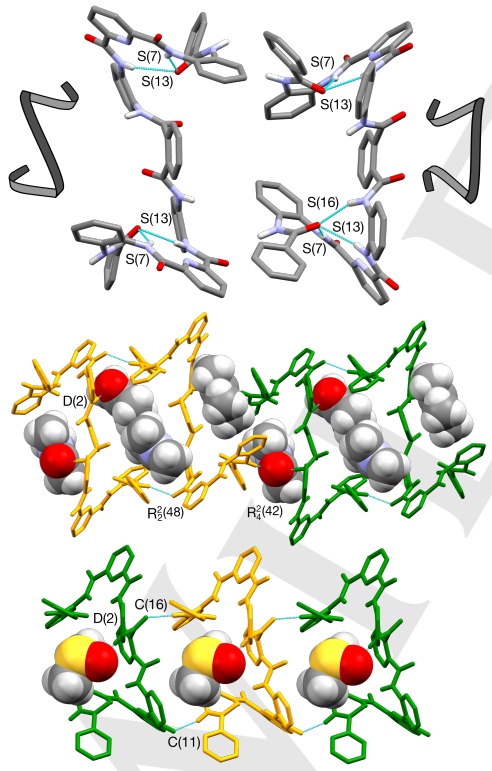

Figure 3 The solid state conformations and crystal packing of **3**-DMA (top left and middle) and **3**-DMSO (top right and below) showing the *trans* and *cis* orientations of pyridine-2,6-dicarboxamide centers in respect to spacer unit. Non-bonding hydrogens and disorder have been omitted for clarity and the solvents are shown with space fill model.

Foldamer 3

Two single crystal structures of the foldamer **3** were obtained from crystallizations in DMA and DMSO solution. Both structures have two @-folded pyridine-2,6-dicarboxamide units with typical hydrogen bonding patterns (S(7) and S(13) motifs), but the foldamer **3** does not have an overall helical conformation because the linker group constituting of three ortho-substituted phenyl rings is fairly rigid, thus separating the ends of the foldamer as independent folds, which can orient differently in respect to the spacer unit. The two conformers observed in the crystal structures are indeed distinctly different (Figure 3). In **3**-DMSO solvate the pyridine-2,6-dicarboxamide units of the molecule turn on the same side of the spacer (*cis*) giving a foldamer a bowl-like overall conformation with a solvent accessible cavity occupied by a disordered DMSO which is hydrogen bonded to NH4. The foldamer molecules are connected head-to-tail manner into continuous chains (NH8…O6; C(11) motif and NH1…O4; C(16) motif; Figure 3). In **3**-DMA solvate the pyridine-2,6-dicarboxamide units are oriented on the different sides of the linker group (*trans*), which leaves the center of the foldamer open for interaction with solvents and enables the packing into ladder-like chains via direct intermolecular hydrogen bonding (O3…HN8) on one side and via solvent mediated hydrogen bonds on the other side (NH1…O_s…HN5; Figure 5). Two DMA molecules are nested in between the directly hydrogen bonded foldamer pair and have intermolecular hydrogen bonds to the NH4 of the foldamers (NH4…O_s). The conformational difference between the two solvates may be caused by the efficiency of packing, as nearly planar DMA enables denser packing than DMSO, as well as the hydrogen bonding preferences in each case.

Foldamer 4

The only crystal structure of foldamer **4** was obtained from ethyl acetate. The conformation is symmetrical with two S folds oriented on the opposite sides of the central phenyl ring. The meta-substituted spacer of foldamer **4** is not as planar and rigid as the ortho-substituted analogue of the foldamer **3**, which might be a reason for the preference of S folds. The conformation is stabilized to a compact entity by an additional intramolecular hydrogen bond from outmost carbonyl C=O (O1 and O8) to central NH groups (NH5 and NH4, respectively). The packing of **4**-EtOAc is based on continuous chains formed by intermolecular hydrogen bond from O3 and O6 to NH4 and NH5 of the neighboring foldamers. Two disordered EtOAc molecules fill the interstice between the chains.

Foldamer 5

Four single crystal structures of the foldamer **5** were obtained, three of which (**5**-Ac, **5**-DCM and **5**-DMF) are isomorphous and nearly helical structures with the outmost pyridine-2,6-dicarboxamide units adopting an @ fold. In this case, the fold is stabilized by only two hydrogen bonds (S(7) and S(13) motifs) as additional hydrogen bonds are prevented because of hydrogen bonds to the pyridine-2,6-dicarboxamide center P3 at the spacer unit. This center facilitates significantly helical-type of folding by forming a third center for intramolecular hydrogen

bonds. The helical folding of the foldamer leaves several hydrogen bonding groups exposed at the outer surface of the fold, which enables the formation of a complex intermolecular hydrogen bond network. The foldamers form pairs with two hydrogen bonds (NH8…O7) and these pairs are further connected to the chains of pairs via hydrogen bonds (NH1…O6) which connects each foldamer to three other foldamers; to one with two hydrogen bonds, to two with one hydrogen bond.

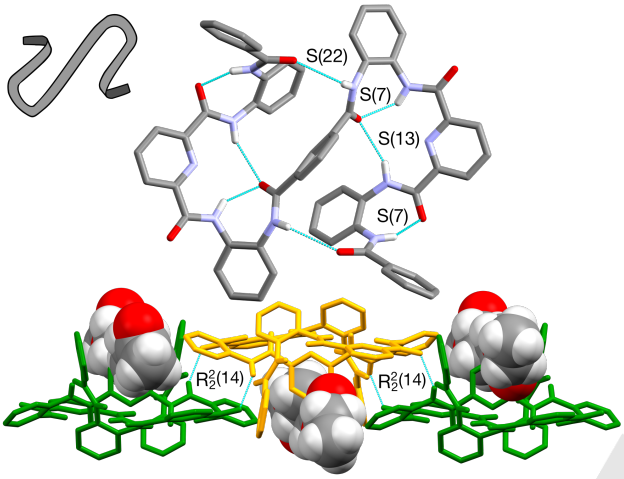

Figure 4 Conformation and crystal packing of **4**-EtOAc. The conformation of the foldamer **4** is very compactly folded and the solvents fill the interstice between the chains of foldamers. Non-bonding hydrogens and solvent disorder have been omitted for clarity. Solvents are shown with space fill model and hydrogen bonds with turquoise.

In **5**-$CHCl_3$ solvate, however, the overall conformation is less folded and bowl-like, as pyridine-2,6-dicarboxamide center P1 adopts an S fold. The bowl-shaped molecule is occupied by the ends of the neighboring foldamers and solvents. The mutually included assembly is further strengthened by intermolecular hydrogen bonds between a pair of foldamers occupying each other's cavities (H8N…O7; $R_2^2(14)$ motif). The hydrogen bonded pairs pack together in a 2D plane by π-stacking from the sides of the bowls. The gaps between the 2D planes are filled with disordered solvents.

Structural comparison of the compounds

The solid state structures of a series of foldamers **1**-**5** show that the hydrogen bonding and the folding patterns of the pyridine-2,6-dicarboxamide units are reliably the same as observed with shorter oligoamide foldamers with only one pyridine-2,6-dicarboxamide unit.[18-20] The role of the spacer unit for the overall conformation becomes evident, when comparing foldamers **1**-**3**. In foldamer **3** the rigidity of the spacer separates the pyridine centers to act like individual folding centers and hinder the formation of S folds in the solid state. The position of individual centers in respect to relatively long, linear and rigid spacer may be either *cis* or *trans*, which induces either Z-shaped or bowl-shaped overall conformation, respectively. Both these conformations have an intrinsic niche or cavity for binding small guests, which is seen as solvent inclusion. In foldamers **1** and **2** the spacer is shorter and such individual behaviour of pyridine-2,6-dicarboxamide units is not possible. In foldamer **1** the short phenyl spacer plays only a minor role in conformational preferences and four different crystal forms with two distinctly different overall conformers are hence likely caused by packing effects. The foldamer **2**, on the other hand, has unsymmetrical spacer which exclusively favors @/S conformation in the solid state and the differences in overall conformations of different crystal structures are only minor.

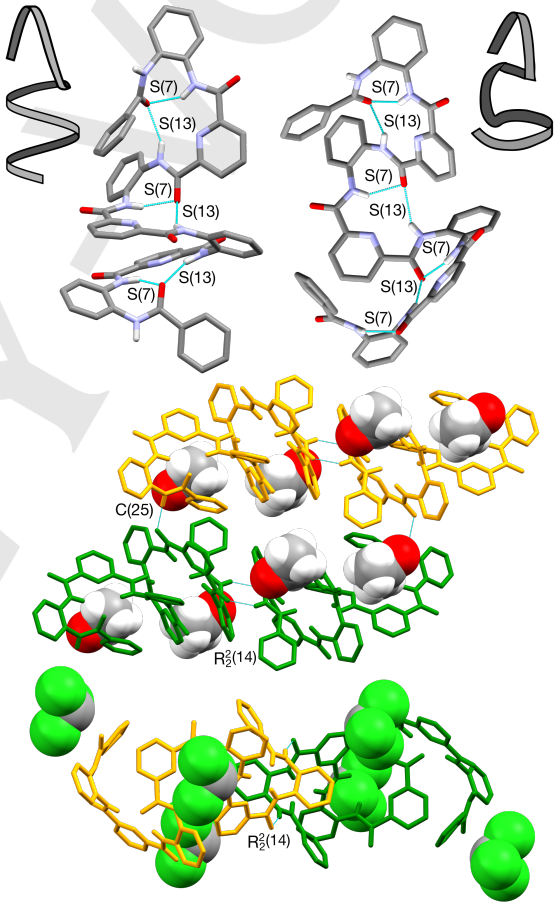

Figure 5 The conformations and packing of **5**-Ac (top left and middle) and **5**-$CHCl_3$ (top right and below). Aromatic hydrogens have been removed for clarity.

Changing the substitution positions of the central phenyl ring from ortho to meta in foldamer **4** increases the flexibility of the molecule which changes both the overall conformation and behaviour of pyridine-2,6-dicarboxamide units. More flexible linker part enables the formation and stabilization of S folds by additional intramolecular hydrogen bonds. The overall conformation, however, is relatively compact. It is not possible to make any definite conclusions about the conformational stability

and prevalence as only one crystal structure of foldamer **4** was obtained.

Introducing a third pyridine-2,6-dicarboxamide unit as a spacer in foldamer **5** changes the intramolecular hydrogen bonding significantly, which is seen as a reduction of number of hydrogen bonds from three to two in @ folded conformations of pyridine centers P1 and P2. The foldamer **5** can be seen as an extended version of foldamer **1** and they indeed share similar types of conformations (Figure 6). The foldamer **1** and **5** both have helical solvate structures and one more open structure. The difference between the two conformations observed is probably due to solvent interactions and packing.

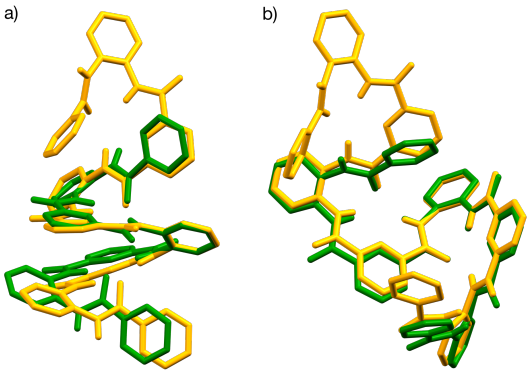

Figure 6 Comparison of the different conformations of foldamer **1** (green) and foldamer **5** (orange): a) comparison between the helical structures of **1**-DMA-H_2O and **5**-Ac. b) Comparison between the open structures of **1**-DCM and **5**-$CHCl_3$.

Solution state studies

Solution state studies were performed for foldamers **1**-**5** to compare their solution state conformations with their solid state structures and to see, if the solid state motifs are observed in solution. To this end, a suite of 2D of homo- and heteronuclear correlation experiments was employed in addition to 1D ^{1}H NMR and ^{13}C NMR experiments to yield a complete resonance assignment to all foldamers (see SI for details). 2D NOESY spectra were measured to obtain through space internuclear connectivities for conformational analysis. DMSO-d_6 was used as solvent in all samples. The 2D NOESY spectra show that the foldamers adopt folded conformations in the solution and in the case of foldamers **3**-**5** the data is fairly consistent with conformations seen in the crystal structures.

In the case of foldamer **1** the correlations show that the compound has a folded structure, but the correlations fit both solid state conformations equally well (see ESI Table S-3 for a detailed list of correlations). Two of the correlations, however, support the conclusion that the foldamer is folded also in solution (Figure 7a). The correlation *a* shows an interaction between the hydrogens of aromatic ring A or D and the amide NH3 or 4. This correlation is possible in both @/@- and S/@-conformations although based on the crystal structures **1**-DMSO and **1**-DCM the correlation is stronger in the @/@-conformation. Another observation supporting the conclusion about a folded conformation is the correlation *b*, which is an interaction between the hydrogens of aromatic ring B or C and pyridine ring P2 or P1. This correlation is also possible in both @/@- and S/@-conformations.

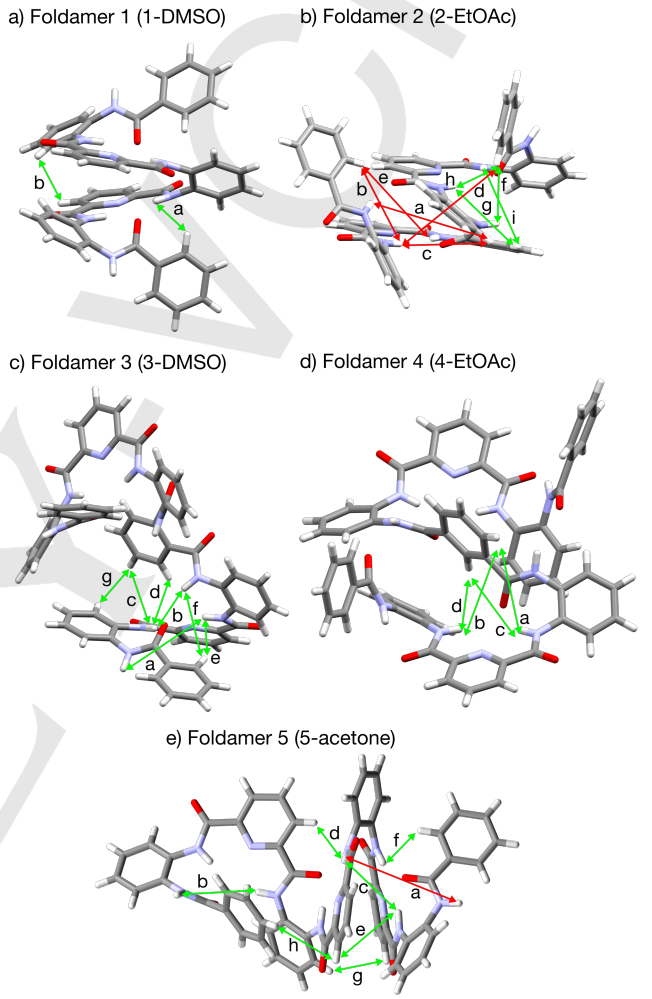

Figure 7 Selected NOE correlations of foldamers **1**-**5** shown in relation to relevant crystal structures. In symmetric foldamers only one set of correlations is shown. Correlations are marked with green if they are seen in the crystal structure and with red if they are not seen in the crystal structure

The solution state conformation of foldamer **2** is likely to deviate from the one observed in the solid state. The correlations of the one half of the foldamer match the solid state conformation, while the other end does not correspond to any of the interactions seen in the crystal structures. The deviating correlations *a*-*e* are all located at the pyridine center adopting the S-conformation in the crystal structure (Figure 7b; left side of the molecule, red lines). If the solution state conformation corresponded to the crystal structures, the correlation *a* should be found between NH1 and hydrogens on the opposite side of

the aromatic ring S2 (para position to NH4 and NH5). Instead, the correlation is seen between NH1 and S2 hydrogens next to the amide groups. The same difference is observed with the correlation *c* (NH2) with respect to the orientation of ring S2. Correlation *b* between NH2 and aromatic ring A hydrogens is not possible in the crystalline state conformation, which indicates different orientation towards the end of the molecule compared with the crystal structures. Correlation *d* between NH2 and aromatic ring D hydrogens and correlation e between NH3 and aromatic ring A hydrogens further confirm the tighter and more folded orientation of the molecule end in solution. Correlations *f*-*i* (*f* = NH4 - D; *g* = NH5 - S1; *h* = NH5 – D; *i* = NH6 - S1) correspond well to the @-folded pyridine-2,6-dicarboxamide center of the crystal structures (Figure 7b; the right side of the molecule, green lines). These results indicate that the conformation of foldamer **2** in solution is probably @/@ instead of @/S that is exclusively seen in all crystal structures.

The NOE correlations *a*-*f* of foldamer **3** agree well with the @ folds of the crystal structures (Figure 7c, Table 2). Additionally, a strong correlation (*g*) between the aromatic hydrogens of rings B and S2 suggests that the structure resembles the crystal structure **3**-DMSO where the pyridine centers are in *cis* orientation with respect to the spacer. Given that DMSO was used as a solvent both in the solution and solid state studies, the observed similarities between the crystal structure and the NMR data are somewhat expected. Based on the roughly similar correlations of symmetrically equivalent bonds (see ESI Table S-3), the conformation is nearly symmetrical in solution like in the solid state structure of **3**-DMSO. The correlation *f*, however, differs from the distances of the crystal structures. This can be explained by permanent hydrogen bonding to solvent DMSO in the crystal structure. Another minor difference between the solution and solid state structures is the stronger correlation *a* between NH1 and NH3 in solution. The NMR spectra also show some peaks, which could be identified as an additional solution state conformation. No clear NOE correlations, however, that could be used to determine the features of this conformation were identified.

The characterization of the solution state conformation of foldamer **4** was difficult because of many overlapping interactions and the presence of a second minor conformation in solution. Correlations *a*-*d* from NH2/7 and NH3/6 protons to aromatic hydrogens still indicate a folded conformation (Figure 7d, Table S-3 in SI). Due to overlapping peaks of S2 and P1/P2 hydrogens and S2 and A/D hydrogens, however, it is not possible to unambiguously determine the conformations or how well they correspond to the solid state structure.

NOESY spectra of foldamer **5** show several correlations that confirm a folded solution state conformation (Figure 7e, Table S-3 in ESI). Most of these correlations (*b*-*f*) are in agreement with both conformations observed in the crystal structures, while two correlations (*g* = *P1-S2* and *h* = *P3-D*) narrow the conformation to resemble the @/@ structure, which is also more prevalent in the solid state. Correlation *a*, however, does not correspond to any of the interactions seen in the crystal structures. This suggests that although the solution state conformation resembles the helical @/@ conformation, it is still slightly different with respect to the orientation of the end of the molecule in the solid state. Alternatively, fast conformational exchange on the NMR timescale may take place between different structures.

Conclusions

Foldamers **1**-**5** with two or three pyridine-2,6-dicarboxamide centers and varying linker groups as their structural components show reliable folding patterns and stability of the desired oxyanion hole motif in respect to pyridine-2,6-dicarboxamide centers both in solution and in the solid state. Additionally, the number of pyridine-2,6-dicarboxamide centers can be multiplied without losing the essential structural features. The overall conformation of the foldamer varies depending on the linker unit. Foldamer **1** and foldamer **5,** which is an extended version of **1**, have similar ubiquitous helical conformations (@/@), but also alternative, more open structure in the solid state (@/S), probably caused by solvent effects during the crystallization. In the case of foldamer **1**, no conclusive information about the solution conformation could be obtained, whereas in case foldamer **5** the prevalent conformation in solution appears to be @/@. The unsymmetrical linker unit of foldamer **2** directs the foldamers to have similar compact helical conformations in the solid state, whereas NOESY spectra indicate more folded @/@ type of conformer in solution. The flexibility of the *meta*-substituted linker group in foldamer **4** enables compact S-shaped folded conformation with additional intramolecular hydrogen bonds in contrast to the rigid ortho substituted spacer of foldamer **3** which enables the @-folded pyridine-2,6-dicarboxamide units to orient in either *trans* or *cis* in relation to the center. The flexibility of foldamer **4** was also seen in solution, as no conclusive conformational information could be obtained and a possibility of alternative conformers was observed in NMR spectra.

Our future studies will orient toward utilizing extended foldamers as anion hosts utilizing their conformational predictability, and on the other hand, conformational adaptability without losing the binding site structure, which creates a suitable binding site for, for example, halogen anions.[24] Additionally, anion binding capacity together with the resemblance to oxyanion hole motifs of enzymes provides excellent basis for future studies as enzyme-mimicking organocatalysts.

Experimental Section

Materials and methods

The synthesis and characterization details of foldamers **1**-**5** are presented in ESI. All starting materials were commercially available and used as such unless otherwise noted. Analytical grade solvents and Millipore water were used for crystallizations and slurries. NMR spectra were measured with Bruker Avance DPX250 MHz, Bruker Avance DRX 500 MHz or with Bruker Avance III HD 800 MHz spectrometer and the chemical shifts were calibrated to the residual proton and carbon resonance of the deuterated solvent. Melting points were measured in an

Table 3. Crystal data and data collection parameters. The data of the isomorphous structures and the data of the structures **1**-DMF-H_2O and **1**-MeOH are presented in ESI.

	1-DMA-H_2O	**1**-DMSO	**1**-DCM	**2**-MeCN	**2**-DCM
Formula	$C_{46}H_{34}N_8O_6$• C_4H_9NO•H_2O	$C_{46}H_{34}N_8O_6$• $2(C_2H_6OS)$	$C_{46}H_{34}N_8O_6$• CH_2Cl_2	$C_{53}H_{39}N_9O_7$• $1.5(C_2H_3N)$	$C_{53}H_{39}N_9O_7$• CH_2Cl_2
M/gmol^{-1}	899.95	951.07	879.74	975.51	998.86
Crystal system	Triclinic	Monoclinic	Monoclinic	Triclinic	Triclinic
Space group	P-1	$P2_1/c$	$P2_1/c$	P-1	P-1
a/Å	11.7500(4)	16.1850(4)	21.4224(4)	9.6033(3)	11.7016(3)
b/Å	12.2120(6)	20.8963(3)	8.59628(14)	14.7566(6)	12.8693(3)
c/Å	17.0988(6)	15.4316(4)	23.4432(5)	18.3628(10)	17.0721(5)
α/°	105.575(4)	90	90	66.954(4)	70.042(2)
β/°	99.439(3)	117.981(3)	98.435(2)	83.106(4)	86.966(2)
γ/°	100.534(4)	90	90	82.514(3)	76.8250(10)
V/Å^3	2263.99(17)	4609.0(2)	4270.44(14)	2367.33(19)	2352.04(11)
Z	2	4	4	2	2
ρ_{calc}/g cm^{-3}	1.320	1.371	1.368	1.369	1.410
μ/mm^{-1}	0.092	1.587	0.213	0.761	0.205
F(000)	944	1992	1824	1018	1036
Crystal size/mm	0.18x0.10x0.10	0.22x0.10x0.02	0.26x0.08x0.08	0.28x0.12x0.02	0.32x0.14x0.14
$2\theta_{max}$/°	58.412	148.778	50.698	153.886	57.28
T/K	173	123	173	123	173
Radiation	Mo-Kα	Cu-Kα	Mo-Kα	Cu-Kα	Mo-Kα
λ/Å	0.7107	1.5418	0.7107	1.5418	0.71073
Monochromation	mirror	mirror	mirror	mirror	graphite
Absorption correction	Multi-scan	Multi-scan	Multi-scan	Multi-scan	Multi-scan
Abs. cor. program	CrysAlisPro	CrysAlisPro	CrysAlisPro	CrysAlisPro	Denzo-SMN 1997
Refinement programs	ShelXle	ShelXle	ShelXle	ShelXle	SHELXL-97
Meas. reflns	30246	27685	13910	15013	23446
Indep. reflns	10756	9190	7760	9464	12030
Parameters	650	635	614	683	670
R_{int}	0.0269	0.0331	0.0236	0.0265	0.0449
R_1 [I> 2σ(I)]	0.0487	0.0379	0.0495	0.0430	0.0648
wR_2 [I> 2σ(I)]	0.1071	0.0956	0.1006	0.1065	0.1454
GooF on F^2	1.033	1.032	1.020	1.037	1.070
d. peak/ hole/eÅ^{-3}	0.217 and -0.242	0.499 and -0.375	0.487 and -0.468	0.255 and -0.407	0.463 and -0.732

	3-DMA	**3-DMSO**	**4-EtOAc**	**5-Ac**	**5-$CHCl_3$**
Formula	$C_{60}H_{44}N_{10}O_8$• $2(C_4H_9NO)$	$C_{60}H_{44}N_{10}O_8$• C_2H_6OS	0.5 $C_{60}H_{44}N_{10}O_8$• $0.5(C_4H_8O_2)$	$C_{59}H_{43}N_{11}O_8$• $0.16(C_3H_6O)$	$C_{59}H_{43}N_{11}O_8$• $CHCl_3$
M/gmol^{-1}	1207.29	1111.18	1121.15	1043.57	1153.41
Crystal system	Triclinic	Triclinic	Monoclinic	Triclinic	Triclinic
Space group	P-1	P-1	C2/c	P-1	P-1
a/Å	13.4719(11)	9.4954(3)	30.8937(6)	11.8122(4)	13.0605(2)
b/Å	16.0247(8)	14.7041(5)	8.3612(2)	12.4913(4)	13.21636(19)
c/Å	16.1687(13)	20.5624(5)	22.6973(4)	18.8041(6)	22.8823(3)
α/°	115.068(6)	80.211(2)	90	91.549(3)	79.6980(12)
β/°	104.451(7)	77.542(2)	108.423(2)	108.190(3)	82.4084(12)
γ/°	93.334(5)	75.175(3)	90	102.989(3)	63.0169(16)
V/Å^3	3007.8(4)	2689.91(15)	5562.4(2)	2554.26(14)	3357.19(10)
Z	2	2	4	2	2
ρ_{calc}/g cm^{-3}	1.333	1.372	1.339	1.357	1.108
μ/mm^{-1}	0.749	1.119	0.093	0.764	1.647
F(000)	1268	1160	2344	1086	1192
Crystal size/mm	0.227x0.145x0.44	0.216x0.176x0.100	0.360x0.222x0.134	0.20x0.10x0.08	0.343x0.168x0.138
$2\theta_{max}$/°	152.686	154.112	28.950	153.988	153.984
T/K	123	123	123	123	123
Radiation	Cu-Kα	Cu-Kα	Mo-K_α	Cu-Kα	Cu-Kα
λ/Å	1.5418	1.5418	0.71073	1.5418	1.5418
Monochromation	mirror	mirror	mirror	mirror	mirror
Absorption correction	Analytical	Analytical	Multi-scan	Multi-scan	Analytical
Abs. cor. Program	CrysAlisPro	CrysAlisPro	CrysAlisPro	CrysAlisPro	CrysAlisPro
Refinement programs	ShelXle	ShelXle	ShelXle	ShelXle	ShelXle
Meas. reflns	17709	20331	18883	40504	69781
Indep. reflns	11797	11025	6458	10625	14337
Parameters	877	810	477	765	791
R_{int}	0.0306	0.0249	0.0138	0.0266	0.0305
R_1 [I> 2σ(I)]	0.0513	0.0491	0.0435	0.394	0.0751
wR_2 [I> 2σ(I)]	0.1323	0.1311	0.1149	0.1007	21.63
GooF	1.047	1.019	1.062	1.025	1.045
d. peak/ hole/eÅ^{-3}	0.322 and -0.348	1.021 and -0.314	0.514 and -0.230	0.260 and -0.257	0.489 and -0.509

open capillary using a Stuart SMP30 melting point apparatus and are uncorrected. ESI-TOF mass spectra were measured with a LCT Micromass spectrometer.

X-Ray Crystallography

The crystal data and data collection parameters are presented in Table 3 and in ESI (isomorphous structures and the structures **1**-DMF-H_2O and **1**-MeOH). General procedure for crystallization: 5-50 mg of foldamers were dissolved in 0.1-6 ml of solvent. Heating and stirring were used to help the dissolving process. After the compounds had dissolved the solutions were allowed to evaporate at room temperature until the crystals formed. The details of crystallization and refinement are presented in ESI. Single crystal X-ray diffraction data of structures **1**-MeCN-H_2O and **2**-DCM were measured with a Bruker Nonius KappaCCD diffractometer using a Bruker AXS APEX II CCD detector. Single crystal structures **1**-MeOH, **1**-DMSO, **2**-MeCN, **2**-EtOAc, **2**-DMSO, **3**-DMA, **3**-DMSO, **5**-DCM, **5**-Ac, **5**-DMF and **5**-$CHCl_3$ were measured with an Agilent Supernova Dualsource diffractometer and an Agilent Atlas CCD detector. Single crystal structures **1**-DMF-H_2O, **1**-DMA-H_2O, **1**-DCM and **4**-EtOAc were measured with an Agilent Supernova diffractometer using an Agilent Eos CCD detector. All structures were solved with direct methods and refined using Fourier techniques. All non-hydrogen atoms were refined unisotropically, except for one acetonitrile in the structure **2**-MeCN, which was refined isotropically due to disorder. The hydrogen atoms were placed in idealized positions except for the N-H and H_2O hydrogen atoms which were found from the electron density map. N-H hydrogen H5NB of structure 3-DMSO was placed in an ideal position, and included in the structure factor calculations. SQUEEZE was used on structure **5**-$CHCl_3$ to remove severely disordered $CHCl_3$ molecules that could not be modelled. Details of the crystal data and the refinement are presented Supporting information. Graph set symbols[25] for hydrogen bonding were assigned and used to compare the hydrogen bonding between the different crystal structures. CCDC 1555244-1555260 contain the supplementary crystallographic data for this paper. These data can be obtained free of charge from The Cambridge Crystallographic Data Centre through www.ccdc.cam.ac.uk/data_request/cif.

Acknowledgements

The financial support of Academy of Finland (proj. no. 257246 and 288235) is gratefully acknowledged. We thank B.Sc. Anniina Aho, M.Sc. Minna Kortelainen and M.Sc. Jussi Ollikka for the help in the synthesis, Spec. Lab. Technician Elina Hautakangas for the elemental analysis and Spec. Lab. Technician Esa Haapaniemi for the part of the NMR measurements.

Keywords: foldamers • hydrogen bonding • X-ray crystallography • NMR spectroscopy • molecular folding • supramolecular chemistry

[1] S. H. Gellman, *Acc. Chem. Res.* **1998**, *31*, 173-180.
[2] D. J. Hill, M. J. Mio, R. B. Prince, T. S. Hughes, J. S. Moore, *Chem. Rev.* **2001**, *101*, 3893-4012.
[3] I. Huc, *Eur. J. Org. Chem.* **2004**, 2004, 17-29.
[4] See for example: a) J. F. Galan, C. N. Tang, S. Chakrabarty, Z. Liu, G. Moyna, V. Pophristic, *Phys. Chem. Chem. Phys.* **2013**, 15, 11883-11892; b) Y. Yan, B. Qin, C. Ren, X. Chen, Y. K. Yip, R. Ye, D. Zhang, H. Su, H. Zeng, *J. Am. Chem. Soc.* **2010**, 132, 5869-5879; c) H. Jiang, J. Léger, C. Dolain, P. Guionneau, I. Huc, *Tetrahedron* **2003**, 59, 8365-8374; d) X. Hu, S. J. Dawson, Y. Nagaoka, A. Tanatani, I. Huc, *J. Org. Chem.* **2016**, 81, 1137-1150.
[5] a) N. Delsuc, L. Poniman, J. Léger, I. Huc, *Tetrahedron* **2012**, *68*, 4464-4469; b) Z. Hu, H. Hu, C. Chen, *J. Org. Chem.* **2006**, *71*, 1131-1138; b) C. Dolain, J. Léger, N. Delsuc, H. Gornitzka, I. Huc, *Proc. Nat. Acad. Sci.* **2005**, *102*, 16146-16151.
[6] A. Suhonen, I. Morgan, E. Nauha, K. Helttunen, H. Tuononen and M. Nissinen, *Cryst. Growth & Des.* **2015**, *15*, 2602-2608.
[7] H. Goto, H. Katagiri, Y. Furusho, E. Yashima, *J. Am. Chem. Soc.* **2006**, *128*, 7176-7178.
[8] D. Sánchez-García, B. Kauffmann, T. Kawanami, H. Ihara, M. Takafuji, M. Delville, I. Huc, *J. Am. Chem. Soc.* **2009**, *131*, 8642-8648.
[9] E. Gillies, F. Deiss, C. Staedel, J. Schmitter, I. Huc, *Angew. Chem. Int. Ed.* **2007**, *46*, 4081-4084.
[10] a) M. Kudo, D. Carbajo López, V. Maurizot, H. Masu, A. Tanatani, I. Huc, *Eur. J. Org. Chem.* **2016**, *2016*, 2457-2466; b) N. Delsuc, F. Godde, B. Kauffmann, J. Léger, I. Huc, *J. Am. Chem. Soc.* **2007**, *129*, 11348-11349; c) J. Brüggemann, S. Bitter, S. Müller, W. Müller, U. Müller, N. Maier, W. Lindner, F. Vögtle, *Angew. Chem. Int. Ed.* **2007**, *46*, 254-259; d) C. A. Hunter, A. Spitaleri, S. Tomas, *Chem. Commun.* **2005**, 3691-3693.
[11] B. Gong, *Acc. Chem. Res.* **2008**, *41*, 1376-1386.
[12] a) E. Kolomiets, V. Berl, J. Lehn, *Chem. - Eur. J.* **2007**, *13*, 5466-5479; b) M. Kudo, V. Maurizot, B. Kauffmann, A. Tanatani, I. Huc, *J. Am. Chem. Soc.* **2013**, *135*, 9628-9631.
[13] R. V. Nair, K. N. Vijayadas, A. Roy, G. J. Sanjayan, *Eur. J. Org. Chem.* **2014**, *2014*, 7763-7780.
[14] A. Roy, P. Prabhakaran, P. K. Baruah, G. J. Sanjayan, *Chem. Commun.* **2011**, *47*, 11593-11611.
[15] C. Bao, Q. Gan, B. Kauffmann, H. Jiang, I. Huc, *Chem. - Eur. J.* **2009**, *15*, 11530-11536.
[16] G. Lautrette, B. Wicher, B. Kauffmann, Y. Ferrand, I. Huc, *J. Am. Chem. Soc.* **2016**, *138*, 10314-10322.
[17] a) Y. Hamuro, S. J. Geib, A. D. Hamilton, *Angew. Chem. Int. Ed.* **1994**, *33*, 446-448; b) Y. Hamuro, S. J. Geib, A. D. Hamilton, *J. Am. Chem. Soc.* **1996**, *118*, 7529-7541; c) Y. Hamuro, S. J. Geib, A. D. Hamilton, *J. Am. Chem. Soc.* 1997, 119, 10587-10593; d) V. Berl, I. Huc, R. G. Khoury, J. Lehn, *Chem. –Eur. J.* **2001**, *7*, 2798-2809; e) V. Berl, I. Huc, R. G. Khoury, J. Lehn, *Chem. –Eur. J.* **2001**, *7*, 2810-2820.
[18] A. Suhonen, E. Nauha, K. Salorinne, K. Helttunen, M. Nissinen, *CrystEngComm* **2012**, *14*, 7398–7407.
[19] M. Kortelainen, A. Suhonen, A. Hamza, I. Pápai, E. Nauha, S. Yliniemelä-Sipari, M. Nissinen, P. M. Pihko, *Chem. Eur. J.* **2015**, *21*, 9493–9504.
[20] A. Suhonen, M. Kortelainen, E. Nauha, S. Yliniemelä-Sipari, P. M. Pihko, M. Nissinen, *CrystEngComm* **2016**, *18*, 2005–2013.
[21] S-conformation is based on the hydrogen bonds between C=O and pyridine-2,6-dicarboxamide NHs similarly to @ conformer, but the outmost NH group forms a hydrogen bond to a pyridine-2,6-dicarboxamide C=O (Scheme 1) or to another C=O group of the foldamer or adjacent molecule, which turns the end of the molecule away from the pyridine core. Tighter and more folded @ conformation has the outer N-H also turned towards the pyridine-2,6-dicarboxamide center with a hydrogen bond to carbonyl C=O (S7 motif).
[22] P. M. Pihko, S. Rapakko, R. K. Wierenga in *Hydrogen Bonding in Organic Synthesis* (Ed.: P. M. Pihko), Wiley-VCH, Weinheim, **2009**, pp. 43-71.
[23] a) K. Mitsui, S. A. Hyatt, D. A. Turner, C. M. Hadad, J. R. Parquette, *Chem. Commun.* **2009**, 3261-3263; b) N. T. Salzameda, D. A. Lightner, *Monatsh. Chem.* **2007**, *138*, 237–244.
[24] For anion binding properties of small analogues see: K. Helttunen, R. Annala, A. Suhonen, E. Nauha, J. Linnanto, M. Nissinen, *CrystEngComm*, **2017**, DOI: 10.1039/C7CE01109A.

[25] a) M.C. Etter, J. C. MacDonald, *Acta Crystallogr., Sect. B: Struct. Sci.*, **1990**, *46*, 256-262; b) J. Bernstein, R. E. Davis, L. Shimoni, N.-L. Chung, *Angew. Chem. Int. Ed.*, **1995,** *34*, 1555-1573.

Entry for the Table of Contents

Layout 1:

FULL PAPER

Predictability and persistence of folding: Aromatic oligoamide foldamers fold into helices and more open, folded conformations depending on the identity of central linker and solvent conditions. Pyridine-2,6-dicarboxamide units add the predictability of the conformation and lead to good persistence and comparability of conformation in solution and in the solid state.

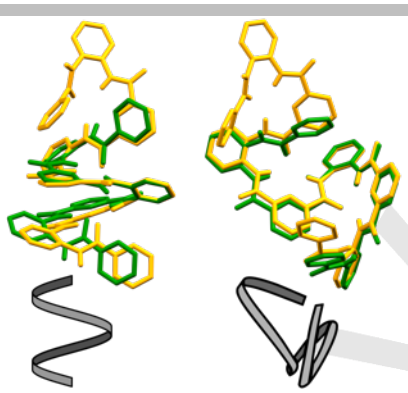

*Riia Annala, Aku Suhonen, Heikki Laakkonen, Perttu Permi, Maija Nissinen**

Page No. – Page No.

Structural tuning and conformational predictability of aromatic oligoamide foldamers

II

SUPRAMOLECULAR CHIRALITY AND SYMMETRY BREAKING OF FLUORIDE COMPLEXES OF ACHIRAL FOLDAMERS

by

Kaisa Helttunen, Riia Annala, Aku Suhonen, Elisa Nauha, Juha Linnanto & Maija Nissinen, 2017

CrystEngComm, **2017**, *19*, 5184-5187

DOI: 10.1039/c7ce01109a

Journal Name

ARTICLE

Supramolecular chirality and symmetry breaking of fluoride complexes of achiral foldamers

Received 00th January 20xx,
Accepted 00th January 20xx

DOI: 10.1039/x0xx00000x

Kaisa Helttunen,[a] Riia Annala,[a] Aku Suhonen,[a] Elisa Nauha,[b] Juha Linnanto,[c] and Maija Nissinen[*,a]

Aromatic oligoamide foldamers containing a central pyridine-2,6-dicarbonyl motif are partially preorganized to favor the binding of the fluoride anions. In the solid state the foldamer-fluoride complexes form achiral, polar and chiral crystal structures depending on the chemical structure of the foldamer. One of the six foldamers studied here, a C_{2v} symmetrical foldamer **1**, formed repeatedly chiral crystal structures when crystallized with *tetra*-butylammonium fluoride showing supramolecular bulk chirality and symmetry breaking in crystallization.

Introduction

Host-guest systems, which change conformation upon an external stimulus represent a fascinating class of responsive molecules with potential applications in sensing and as molecular machines.[1,2] Synthetic spontaneously folding molecules, or simply foldamers, form helical structures via intramolecular interactions, but also with the help of external stimulus, such as binding of guest molecules or ions within the foldamer.[3] Recently foldamers have been used as supramolecular hosts for anions.[4,5] Complexation of achiral anions (halides and sulfate) has induced a change in the helicity of foldamers,[6,7] and produced a helical fold of a linear amide receptor in the solid state.[8] Chiral guests, on the other hand, have induced chiral folding of dipyrrolyl receptors.[9] The cases where achiral foldamers adopt a chiral structure instead of racemic mixture in solution or in the solid state, however, are scarce[3,10] since single helicity is usually induced by chiral substituents within the foldamer scaffold[11] or through binding of a chiral guest[2,12].

Emergence of chiral solid state structures from flexible achiral building blocks[13] is an interesting phenomena illustrating how folding induced molecular level chirality is transferred to macroscopic scale. The induction of helical chirality from achiral components by anion binding is important, for example, in non-linear optical applications for second-harmonic generation and liquid crystals.[14] Overall, about 10 % of achiral components crystallize in chiral structures[15] but symmetry breaking, i.e. spontaneous crystallization of a homochiral crystals instead of a racemic mixture or a conglomerate, of the bulk sample is very rare. Known examples include silver helicates,[16] coordination polymers[17] and porous materials using chiral catalyst in crystallization[18]. In addition, it is postulated that number of nucleation events may affect on symmetry breaking through secondary nucleation.[17]

Herein we have investigated fluoride complexes of a family of aromatic oligoamide foldamers. The foldamers are partially preorganized for anion complexation, yet the flexibility of the molecules is evident from the versatility of molecular conformations in the solid state structures of the free foldamers and their solvates, as observed in our previous studies.[19,20] The fluoride complexes of achiral foldamers formed achiral, polar and chiral crystal structures depending on the foldamer used and one of the complexes showed bulk homochirality.

Results and discussion

An achiral C_{2v} symmetrical foldamer **1** with a central pyridine-2,6-dicarbonyl motif and four amide groups has a mirror plane running perpendicular to the central pyridine ring (Fig. 1). In the solid state foldamer **1** adopts a protohelical conformation (defined as an @-conformation) with three intramolecular hydrogen bonds to a single carbonyl group rotated towards the central pyridine ring.[19,20] In previously characterized 12 different crystal forms of **1**, the foldamer has adopted both left-handed (M) and right-handed (P) helices forming centrosymmetric structures.[20,21] The folding properties of an asymmetric foldamer derivative **2** with an electron withdrawing *p*-cyano substituent at the end of the molecule (point group C_s) are similar to **1**, except that the compound has also been found in a more open S-shaped conformation where the third intramolecular hydrogen bond forms between the inner carbonyl group and outer amide proton.[20,21]

[a] *University of Jyvaskyla, Department of Chemistry, Nanoscience Center, P.O. Box 35, FI-40014 University of Jyvaskyla, Finland. E-mail: maija.nissinen@jyu.fi*
[b] *College of Science, University of Lincoln, Joseph Banks Laboratories, Green Lane, Lincoln, LN6 7DL, UK*
[c] *Institut of Physics, University of Tartu, W. Ostwaldi Str 1, 50411 Tartu, Estonia*

Electronic Supplementary Information (ESI) available: Synthetic procedure for 3, crystallographic tables, details and additional figures, hydrogen bonding tables, UV-vis and CD spectroscopic details, computational details, and NMR spectra. CCDC1552169-1552176. For ESI and crystallographic data in CIF format see DOI: 10.1039/x0xx00000x

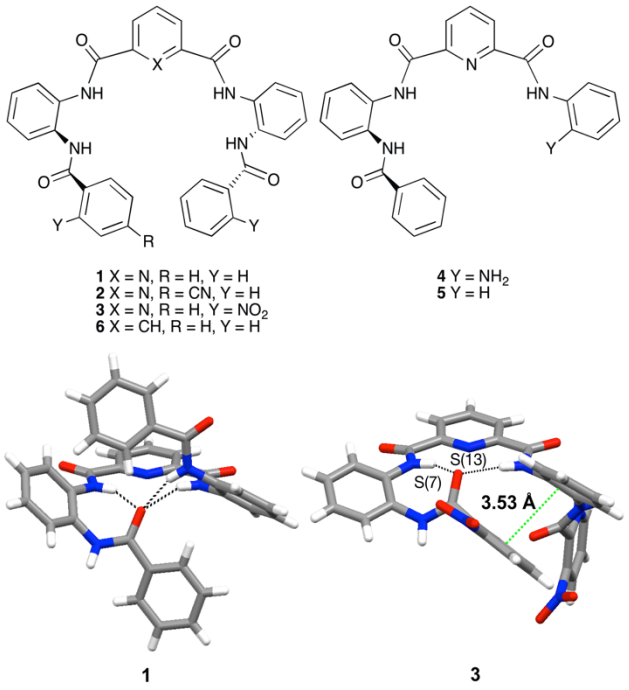

Figure 2 Schematic presentation of foldamers and the crystal structure of **1** in the protohelical *@*-conformation (CSD code MAMCAH)[21] and a new conformation obtained for foldamer **3**. Hydrogen bonds are shown with black and π···π interactions with green dashed lines.

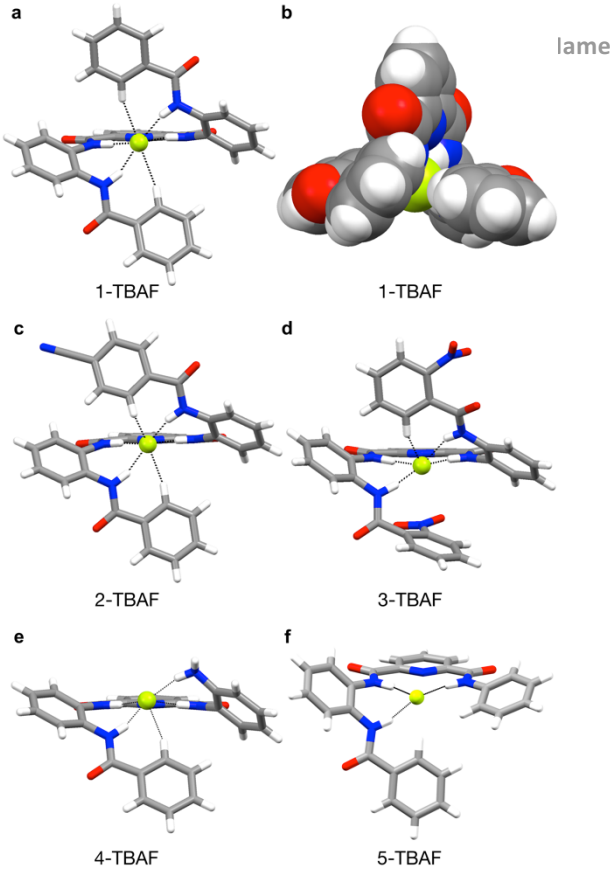

Figure 1 a-b) Complex **1-TBAF** (all M helical), c) **2-TBAF** (M helical shown), d) **3-TBAF** (M helical shown), e) **4-TBAF** (M helical shown) and f) **5-TBAF**. Intramolecular hydrogen bonds to the fluoride anion are shown with dashed lines.

In order to compare the effect of the electron withdrawing substituents to molecular folding and anion binding properties, foldamer (**3**) with *o*-nitrophenyl rings symmetrically at the both ends of the molecule was prepared. The synthesis was made by coupling 2-nitrobenzoic acid and *o*-phenylenediamine to produce *N*-(2-aminophenyl)-2-nitrobenzamide (**7**). A subsequent reaction of **7** with pyridine-2,6-dicarbonyl dichloride produced foldamer **3** with 29 % yield (see ESI for details). Foldamer **3** crystallized in a relatively open conformation with only two intramolecular hydrogen bonds to the central pyridine ring (graph set notifications S(7) and S(13); Fig. 1) and also lacking the third intramolecular bond present in S-conformation of **2**. Clearly, the nitro substituents promote π···π interactions, which have not played a major role in the structures of any other foldamers. Nitrophenyl and 1,2-diamino rings interact via intramolecular face-to-face π-stacking. In addition, several intermolecular π···π interactions stabilize the crystal packing, unlike in any other foldamers.

The complexation of fluoride anions with foldamers **1–3** was investigated by crystallizing the foldamers with *tetra*-butylammonium fluoride yielding 1:1 host-guest complexes.[†] In solution strong aggregation was observed as broadening of the NMR signals. Thus, no binding constant could be determined or detailed solution state studies done. In addition, fluoride complexes of two shorter foldamers **4** and **5** were crystallized as a reference. As expected, the fluoride is bound to the interior of the foldamers **1**-**5** by hydrogen bonding with the amide hydrogens (N···F 2.59**–**2.82 Å) organizing the foldamers into helical loops around the anion (Fig. 2). The central pyridine ring has an important role in preorganization of the inner N-H protons towards the fluoride binding site at the center of the molecule, as evidenced by the comparison to a crystal structure of analogous 1,3-dicarboxamide phenyl foldamer **6**,[19] which forms open, sandwich-like 2:2 fluoride complex (see Fig. S-7 in ESI).

Interestingly, complex **1-TBAF** formed a chiral crystal structure (space group $P2_12_12_1$) in which all foldamer molecules have folded to a left-handed direction (M helicity, Fig. 2a-b). The outermost phenyl rings of **1** contribute to the fluoride complexation by C-H···F^- interactions from the *ortho* protons H6 and H33 (C···F 3.21**–**3.25 Å, <DHA 153-162°). The individual complexes organize in zig-zag shaped chains where the terminal phenyl group points towards the anion of the adjacent complex (Fig. 3a). In order to investigate the reproducibility of homochirality of crystals, crystallization was repeated in the same conditions and with seed crystallization. The resulting crystals had the same space group and cell parameters as the reported structure, which confirmed that fluoride complex forms reliably a chiral crystal structure.

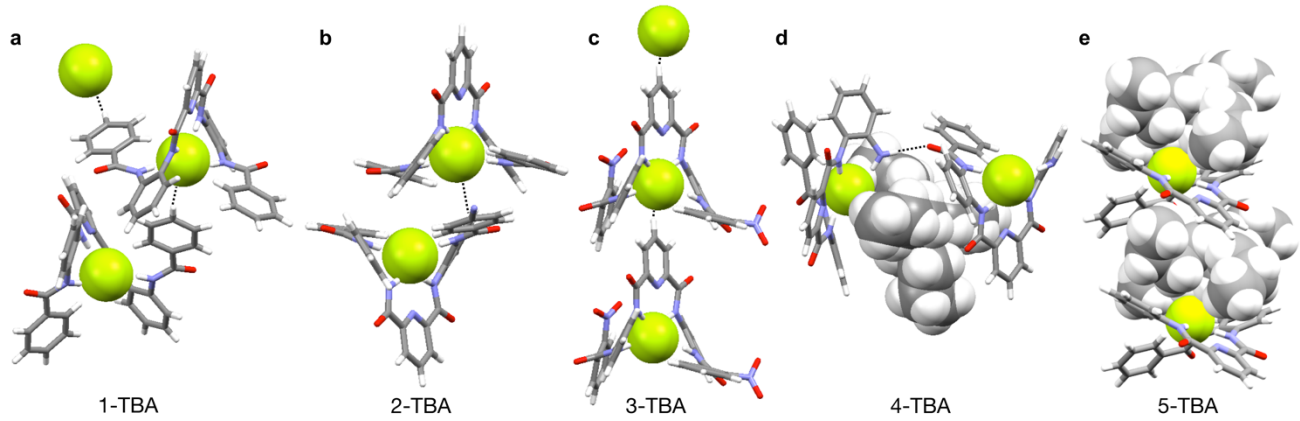

Figure 3 Selection of crystal packing showing significant interactions between two complex units: a) complex **1-TBAF** forms chains (C31···F1 3.43 Å), b) P and M helical complexes of **2-TBAF** pack by π···π interactions (anion···π marked with a dashed bond), c) **3-TBAF** forms chains via C-H···F$^-$ contact, d) intermolecular N-H···O hydrogen bond in **4-TBAF** and e) alternating layers of TBA$^+$ and foldamer in **5-TBAF**. Cations and anions are shown with space filling model.

The missing mirror symmetry and one *p*-cyano substituent of foldamer **2** had interesting effects on the centrosymmetric fluoride complex **2-TBAF**. The hydrogen bonds are similar to the hydrogen bonds in **1-TBAF** (Fig. 2c), but **2-TBAF** complexes form both P and M helical loops, which pack as dimers via π···π interactions between an electron poor *p*-cyanophenyl ring and a phenyl ring (Fig. 3b). In addition, one of the *p*-cyanophenyl groups is located at the distance of 3.90 Å from the fluoride suggesting an anion···π interaction. The complex **3-TBAF** formed a crystal structure with polar orientation (space group $Pca2_1$) of the N6 nitro groups along the crystallographic c-axis. The *o*-nitrophenyl rings have asymmetrical torsion angles and interactions with the fluoride anions since one of the rings has a C-H···F$^-$ contact of 3.09 Å like in complexes of **1** and **2**, but the other ring is rotated perpendicular to the anion (Fig. 2d). The overall structure contains M and P helical complexes, which pack in a head-to-tail fashion into chains with pyridine rings forming short C-H···F$^-$ contacts (3.10 Å, Fig. 3c).

The shorter foldamers **4** and **5** cannot completely surround the fluoride anions, which exposes the anion to the simultaneous ion pair interaction with countercation TBA (Fig. 2e-f and 3d-e). Therefore, TBA contributes to the packing of complexes unlike in **1-TBAF** – **3-TBAF**, where TBA cations fill the spaces between the foldamer chains or dimers without direct interaction with the fluoride. In the complex **4-TBAF** M and P helices alternate in chains formed by the layers of complexes and TBA. The structure of **5-TBAF**, however, constitutes of mutually disordered M and P folds. Therefore, it is not possible to say, if the complex-TBA chains constitutes of one hand only or alternating M and P folds.

Interestingly, all unsymmetrical pyridine-2,6-dicarboxamide foldamers **2**, **4** and **5** crystallize with inversion symmetry, whereas the symmetrical **1** and **3** form non-centrosymmetric crystal structures. Fluoride complexation, molecular folding and weak intermolecular interactions render especially foldamer **3** pronouncedly to an unsymmetrical conformation, whereas the binding of the fluoride increases conformational symmetry of **1** compared with the @-conformation of the free host (Fig 2a).

The supramolecular chirality of **1-TBAF** complexes in the crystal structure is likely caused by weak interactions between the adjacent complex chains and TBA cations, or the overall shape of the complex chain. Due to the achiral structure of **1** and fluoride anion and TBA cation they are expected to form a statistical 1:1 distribution of M and P helical complexes in the solution, which should produce similar distribution of M and P helical crystals. The chirality of the crystals was investigated with circular dichroism (CD) spectroscopy by comparing three single crystals and bulk sample of **1-TBAF** crystals (Fig. 4).‡ Interestingly, all samples gave a negative Cotton effect at 245–380 nm indicating symmetry breaking in crystallization promoting the crystallization of the M-helical form **1-TBAF**. A control experiment where a single crystal of **1-TBAF** was dissolved in THF did not show any Cotton effect indicating that racemic mixture forms immediately after solvation. A computer simulation of the CD spectrum was made using the crystal structure coordinates of **1-TBAF**.

Also in this case negative Cotton effect was observed corroborating the solid state CD measurements. The reasons

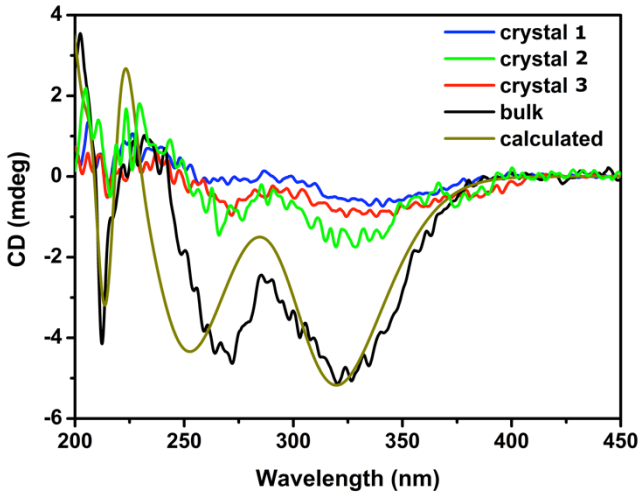

Figure 4 Calculated CD spectrum and solid state CD-spectra of **1**-TBAF bulk and three different single crystals in KCl.

for the symmetry breaking in crystallization may result from very few nucleation events (very slow crystallization) after which the chirality is transferred through the sample by secondary nucleation. Absorption spectra of the solid **1-TBAF** revealed the extension of UV-transitions to longer wavelengths compared to UV-spectra measured in solution (see Fig. S-8 in ESI). The red shift in the absorption spectra is caused by stronger intermolecular forces between complexes in the solid state than in solution.

Conclusions

The crystal structures of foldamer fluoride complexes show that the prearrangement of the pyridine-2,6-dicarboxamide foldamers to a helical conformation allows the complexation of small halide anions¶, such as fluoride, with only minor alterations to the @-shaped conformation of the foldamer. Foldamer complexes are, however, more difficult to crystallize than free foldamers or their solvates, as foldamer fluoride complexes form mainly intramolecular hydrogen bonds, whereas in free foldamer and solvate structures intermolecular hydrogen bonds facilitate the crystal packing. Therefore, several different packing modes for the complexes were found depending on the electric and steric factors of the terminal aromatic rings. This results in both centrosymmetric and intriguing non-centrosymmetric structures. The same helicity of all the **1-TBAF** complexes within the crystal structure results from weak interactions between the adjacent complex chains and TBA cations, or the overall shape of the complex chain.

Acknowledgements

Academy of Finland (project 257246) is acknowledged for funding. We thank M.Sc. Jussi Ollikka and Dr. Kirsi Salorinne for the original synthesis of **6**, and M.Sc. Juho Iloniemi for the crystallization of **1-TBAF**. Prof. Agnieszka Szumna and University of Warsaw are gratefully acknowledged for the solid state CD-measurements.

Notes and references

† Details of the crystallization experiments and crystal data of all structures are presented in ESI.

‡ Altogether 10 crystals were screened for CD measurements by determining their unit cells with single crystal X-ray diffraction. Four of these crystals were of suitable size for the CD measurements. Three of them were used for solid state measurements and one for solution studies.

¶ Complexation data with chloride will be reported elsewhere.

1 P. C. Knipe, S. Thompson and A. D. Hamilton, *Chem. Sci.*, 2015, **6**, 1630.
2 D.-W. Zhang, X. Zhao and Z.-T. Li, *Acc. Chem. Res.*, 2014, **47**, 1961.
3 E. Yashima, N. Ousaka, D. Taura, K. Shimomura, T. Ikai and K. Maeda, *Chem. Rev*. 2016, **116**, 13752.
4 H. Juwarker and K.-S. Jeong, *Chem. Soc. Rev.*, 2010, **10**, 3664.
5 For recent examples see: a) A. Borissov, J. Y. C. Lim, A. Brown, K. E. Christensen, A. L. Thompson, M. D. Smith and P. D. Beer, *Chem. Commun.*, 2016, 2483-2486; b) V. Diemer, L. Fischer, B. Kauffmann and G. Guichard, *Chem. Eur. J.* 2016, **44**, 15684; c) J. Shang, W. Zhao, X. li, Y. Wang and H. Jiang, *Chem. Commun.* 2016, 4505.
6 R. M. Meudtner and S. Hecht, *Angew. Chem. - Int. Ed.*, 2008, **47**, 4926–4930.
7 J. Suk, V. R. Naidu, X. Liu, M. S. Lah and K.-S. Jeong, *J. Am. Chem. Soc.*, 2011, **3**, 13938.
8 C. A. Johnson II, O. B. Berryman, A. C. Sather, L. N. Zakharov, M. M. Haley and D. W. Johnson, *Cryst. Growth Des.*, 2009, **9**, 4247.
9 H. Maeda, T. Shirai, Y. Bando, K. Takaishi, M. Uchiyama, A. Muranaka, T. Kawai and M. Naito, *Org. Lett.*, 2013, **15**, 6006.
10 S. Azeroual, J. Surprenant, T. D. Lazzara, M. Kocun, Y. Tao, L. A. Cuccia and J.-M. Lehn, *Chem. Commun.*, 2012, **48**, 2292.
11 N. V. Ramesh, K. M. Cheol, S. Jae-min, K. Ho-Joong, L. Myongsoo, S. Eunji, J. Kyu-Sung, *Org. Lett*., 2008, **10**, 5373.
12 a) E. Yashima, K. Maeda, *Macromolecules*, 2008, **41**, 3; b) R. B. Prince, S. A. Barnes, J. S. Moore, *J. Am. Chem. Soc.*, 2000, **122**, 2758.
13 E. Pidcock, *Chem. Commun.*, 2005, 3457.
14 J. Thisayukta, H. Kamee, S. Kawauchi and J. Watanabe, *Mol. Cryst. Liq. Cryst. Sci. Technol. Sect. A.*, 2000, **346**, 63.
15 K. Ziach and J. Jurczak, *Cryst. Growth Des.*, 2015, **15**, 4372.
16 Q. Sun, Y. Bai, G. He, C. Duan, Z. Lin, and Q. Meng, *Chem. Commun.*, 2006, 2777.
17 S.-T. Wu, Y.-R. Wu, Q.-Q. Kang, H. Zhang, L.-S. Long, Z. Zheng, R.-B. Huang and L.-S. Zheng, *Angew. Chem. - Int. Ed.*, 2007, **46**, 8475.
18 J. Zhang, S. Chen, T. Wu, P. Feng and X. Bu, *J. Am. Chem. Soc.*, 2008, **130**, 12882.
19 A. Suhonen, E. Nauha, K. Salorinne, K. Helttunen and M. Nissinen, *CrystEngComm*, 2012, **14**, 7398.
20 M. Kortelainen, A. Suhonen, A. Hamza, I. Pápai, E. Nauha, S. Yliniemelä-Sipari, M. Nissinen and P. M. Pihko, *Chem. - A Eur. J.*, 2015, **21**, 9493.
21 A. Suhonen, M. Kortelainen, E. Nauha, S. Yliniemelä-Sipari, P. M. Pihko, and M. Nissinen, *CrystEngComm*, 2016, **18**, 2005.

III

OLIGOAMIDE FOLDAMERS AS HELICAL CHLORIDE RECEPTORS – THE INFLUENCE OF ELECTRON-WITHDRAWING SUBSTITUENTS ON ANION-BINDING INTERACTIONS

by

Kaisa Helttunen, Riia Annala, Aku Suhonen, Juho Iloniemi, Elina Kalenius, Gemma Aragay, Pablo Ballester, Heikki M. Tuononen & Maija Nissinen, 2019

Chem. Asian J., **2019**, *14*, 647-654

DOI : 10.1002/asia.201801869

Oligoamide foldamers as helical chloride receptors – the influence of electron withdrawing substituents on anion binding interactions

Kaisa Helttunen,[a] Riia Annala[a] Aku Suhonen,[a] Juho Iloniemi,[a] Elina Kalenius,[a] Gemma Aragay,[b] Pablo Ballester,[b],[c] Heikki M. Tuononen,[a] and Maija Nissinen*[a]

Abstract: The anion binding properties of three closely related oligoamide foldamers were studied using NMR spectroscopy, isothermal titration calorimetry and mass spectrometry, as well as DFT calculations. The ^{1}H NMR spectra of the foldamers in acetone-d_6 solution revealed partial preorganization by intramolecular hydrogen bonding, which creates a suitable cavity for anion binding. The limited size of the cavity, however, enabled efficient binding by the inner amide protons only for the chloride anion resulting in the formation of a thermodynamically stable 1:1 complex. All 1:1 chloride complexes displayed a significant favourable contribution of the entropy term. Most likely, this is due to the release of ordered solvent molecules solvating the free foldamer and the anion to the bulk solution upon complex formation. The introduction of electron withdrawing substituents in foldamers **2** and **3** had only a slight effect in the thermodynamic constants for chloride binding compared to the parent receptor. Remarkably, the binding of chloride to foldamer **3** not only produced the expected 1:1 complex but also open aggregates with 1:2 (host:anion) stoichiometry.

Introduction

Anion binding by synthetic receptors has many important biochemical and chemical applications in membrane transport, anion recognition and sensing, and template assisted catalysis of complex molecular architectures.[1] Anion binding has also been used to control the conformation and shape of anion responsive molecules and complexes, including synthetic self-folding molecules, foldamers.[2-7] Moreover, modulation of the foldamer-anion complexes to host multiple anions has been studied. For example, aryl-triazole foldamers showed sequence dependent equilibrium between single and double helices binding chloride in 1:1 or 2:2 stoichiometries.[8] Increasing the length of the aryl-triazole foldamer chain induced complexation of two halides into a single foldamer helix accompanied with an increase in the helical pitch in comparison to the 1:1 complex.[9] The significance of the preorganized binding site for the selectivity and affinity of anion complexation has been widely demonstrated with macrocyclic and cryptand-like receptors.[10,11] In neutral acyclic anion receptors preorganization has been induced by intramolecular hydrogen bonding to reduce the entropic penalty of the complex formation.[12,13] Nevertheless, solvation/desolvation effects are known to play a significant role in anion binding in polar media.[14]

The pyridine-2,6-dicarboxamide motif has been used in many acyclic anion receptors as a conformational lock to direct the *cis*-orientation of the adjacent NH groups through intramolecular hydrogen bonding interactions with the pyridyl nitrogen atom.[15-19] Examples of this construct include selective receptors for fluoride and chloride having the central pyridine-2,6-dicarboxamide motif equipped with indole groups.[18,19]

Aromatic oligoamide foldamers have been widely studied for their ease of synthesis and conformational stability.[20] In previous studies, we investigated the conformational features of a series of oligoamide foldamers incorporating the pyridine-2,6-dicarboxamide motif.[21-23] We showed that the foldamers adopted two different conformations. In one of them, the receptor takes a proto-helical shape (so-called @-conformation) and in the other, it arranges in a more open S-shape (Fig. S-1, ESI†). The two conformations display significant differences in intramolecular hydrogen bonding patterns. Moreover, these preferred conformational features remain even when the number of pyridine-2,6-dicarboxamide units in the foldamer are doubled or tripled.[24] Remarkably, the incorporation of an electron withdrawing nitro substituent at the *ortho*-positions of the terminal phenyl groups of the foldamer promoted the observation of a new type of conformation in the solid state.[15] This latter conformation was flatter and showed the establishment of intramolecular π···π stacking interaction between the A and B' phenyl rings of the foldamer, as well as two intramolecular NH···O=C bonds. The *cis*-preorganization of the two amides groups exerted by the pyridine-2,6-dicarboxamide motif was still present in this conformer. We surmised that the *cis*-arrangement of amide groups observed in the 2,6-carboxamidepyridyl unit in all conformations of the receptor provided a suitable host preorganization for the complexation of small anions.

Herein, we describe the results obtained in binding studies of anions in solution using three structurally related oligoamide foldamers **1**–**3** (Scheme 1). Our results demonstrate that the conformation (preorganization) of the host is not substantially altered during the binding processes of the anions resulting in helical 1:1 (host:anion) complexes. On the one hand, the

[a] Dr. Kaisa Helttunen, Riia Annala, Dr. Aku Suhonen, Juho Iloniemi, Dr. Elina Kalenius, Prof. Heikki M. Tuononen, Prof. Maija Nissinen
Department of Chemistry, Nanoscience Center
University of Jyvaskyla
P.O. Box 35, FI-40014 University of Jyvaskyla, Finland
E-mail: maija.nissinen@jyu.fi
[b] Dr. Gemma Aragay and Prof. Pablo Ballester
Institute of Chemical Research of Catalonia (ICIQ), Avgda Països Catalans 16, 43007 Tarragona, Spain
[c] Prof. Pablo Ballester
Catalan Institution for Research and Advanced Studies (ICREA)
Passeig Lluís Companys 23, 08010 Barcelona, Spain

presence of an electron withdrawing CN substituent in the *para*-position of one terminal phenyl ring of the foldamer **2** provides a slight increase in the free energy of binding for the 1:1 complex compared to **1**. On the other hand, the introduction of an electron withdrawing nitro substituent at the *ortho*-position of the two terminal phenyl rings of **3** evidently favours the formation of an open complex with 1:2 (host:chloride) stoichiometry from the initially assembled 1:1 counterpart in the same range of concentrations used in the titrations of **1** and **2**.

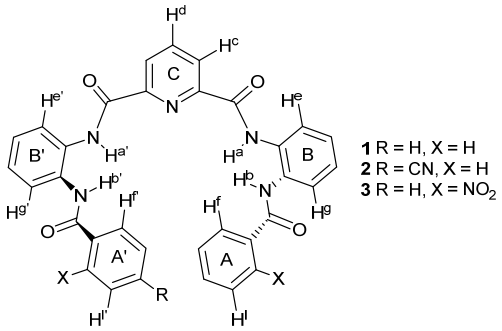

Scheme 1. Oligoamide foldamers **1**–**3** showing the corresponding proton assignment (for the symmetrical **1** and **3** A = A' etc.).

Results and Discussion

ESI-MS experiments

The oligoamide foldamer **1** has five aromatic six-membered rings and four primary amide groups. We have previously shown that in the solid-state receptor **1** forms a 1:1 complex with fluoride.[15] The bound receptor adopts a helical-like conformation featuring a sizable polar cavity suitable for the inclusion of the fluoride with the simultaneous formation of four NH···F^- hydrogen bonds and two additional CH··· F^- interactions.

Mass spectrometry was used in the screening of other potential anions that might bind to host **1** in solution. The (-)ESI-MS spectra (negative ion mode) of separate acetonitrile solutions of **1** containing three equivalents of the ammonium salts of F^-, Cl^-, Br^-, I^-, NO_3^-, $H_2PO_4^-$, SO_4^{2-}, HSO_4^- or CO_3^{2-} showed intense signals for the peaks corresponding to 1:1 complexes with chloride, bromide and nitrate, and ions [**1**+$Cl]^-$, [**1**+$Br]^-$, [**1**+$NO_3]^-$ appeared in the spectra. Less intense peaks were detected for the ion-peaks of the 1:1 complexes of iodide and hydrogen sulfate ([**1**+$I]^-$ and [**1**+$HSO_4]^-$). The mass spectra from solutions with Cl^- and Br^- also showed the peak of the deprotonated receptor [**1**-$H]^-$. This might result from the basicity of the anions (A^-) in a non-protic organic solvent and elimination of HA from the complexes. In ESI-MS spectra measured from iodide solution $[M-H]^-$ was barely detectable, but interestingly from the solution containing F^- the peak of the deprotonated receptor [**1**-$H]^-$ was exclusively observed. We interpret this result as evidence of the high basicity of F^- in a non-protic organic solvent.

We performed bilateral competition experiments involving receptor **1** and a series of halides, which included Cl^-, Br^- and I^-. Three equivalents of each competing anion (Cl^- and Br^-, Br^- and I^-) was added to an acetonitrile solution of **1**. The ESI-MS spectra showed significant differences in intensities for the 1:1 complexes [**1**+$A]^-$. In the competition between chloride and bromide, the [**1**+$Cl]^-$ complex was clearly more abundant with almost 90% relative intensity. Respectively, competition between bromide and iodide showed more abundant complex formation with bromide. Assuming that the ESI response of the three anionic 1:1 complexes is similar, the observed difference in relative intensities of the peaks can be correlated with the relative abundance of the anionic complexes in solution. In short, the abundance of the complexes with receptor 1 in competing conditions is clearly highest for chloride followed by bromide and iodide.

The evaluation of binding properties using MS was also performed for the foldamers **2** and **3**, having a cyano substituent in the *para*-position of one terminal phenyl ring and nitro groups in the *ortho*-position of both terminal phenyl rings, respectively. We limited the binding analyses to the halides that were successfully complexed by host **1**, namely, Cl^-, Br^-, and I^-. The MS spectra showed the expected peaks for the 1:1 complexes [**2**+$Cl]^-$, [**2**+$Br]^-$, [**2**+$I]^-$, [**3**+$Cl]^-$, [**3**+$Br]^-$ and [**3**+$I]^-$. These results indicated that the incorporation of the substituents in the terminal phenyl rings of the foldamers did not affect their anion binding significantly.

^{1}H NMR titrations of foldamer 1

Next, we undertook the evaluation of the anion binding properties of the three receptors using ^{1}H NMR spectroscopy. All ^{1}H NMR spectroscopy titrations of **1** with chloride, bromide, iodide and nitrate anions, as tetrabutylammonium salts, were carried out using millimolar solutions of the host in acetone-d_6.[25] The incremental addition of the anion induced significant chemical shift changes in several signals of the protons of foldamer **1**.

In particular, the gradual addition of TBACl to a millimolar solution of **1** produced significant downfield shifts in the two signals of its amide protons (Figure 1a). This observation suggests their involvement in the formation of hydrogen-bonding interactions with the chloride. The addition of 1 equiv of the TBACl induced the saturation of the chemical shift changes. These observations indicate that the binding process of the foldamer **1** with chloride shows fast dynamics on the chemical shift timescale and a complex with 1:1 stoichiometry (**1**·Cl) is formed for which a binding constant over 10^4 M^{-1} can be estimated. This value is too large to be measured accurately using ^{1}H NMR spectroscopy techniques. The complexation induced shift (CIS) experienced by the amide protons in the central 2,6-biscarboxamide pyridyl unit (H^a) and the amides connecting the terminal phenyl groups (H^b) were very similar, $\Delta\delta$ = 0.96 and $\Delta\delta$ = 1.03 ppm, respectively. This result suggested that they were involved in the binding of the anion to the same extent.[26] In addition to the amide protons, the *ortho*-protons H^f of the terminal phenyl rings (A) also shifted downfield ($\Delta\delta$ = 0.48 ppm). In contrast, the *meta*- and *para*-protons of the A phenyl ring moved slightly upfield (0.01–0.04 ppm). We interpreted these observations considering the *selective* establishment of CH···Cl^- interactions with the *ortho*-aromatic protons (H^f).

The geometry adopted by foldamer **1** in the **1**·Cl complex was inferred from the chemical shift changes experienced by the *ortho*-aromatic protons, H^e and H^g, of the diamino-phenyl ring B and the *ortho*-proton, H^c, of the 2,6-biscarboxamide pyridyl unit.

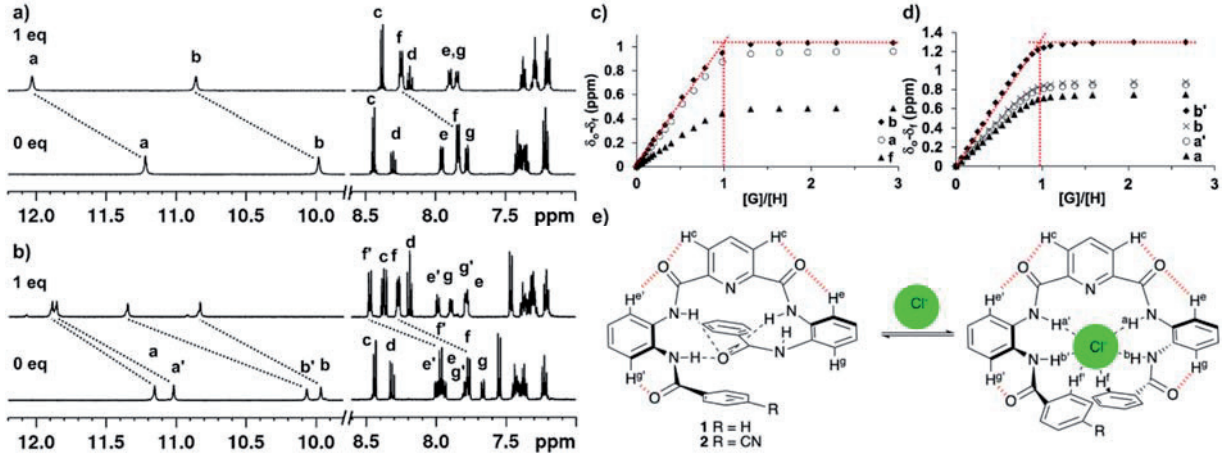

Figure 1. ^{1}H NMR spectra of foldamer 1 (a, 5 mM host) and 2 (b, 2.5 mM host) in acetone-d_6 with 0 and 1 equiv of TBACl. Chemical shift changes experienced by protons a, b and f in 1 (c) and protons a, a', b and b' in 2 (d) during the titrations. Scheme of free host (in a protohelical @-conformation) and the suggested helical chloride complexes for 1 and 2 (e). The anisotropic field induced by the oxygen lone-pairs is indicated with red dashed lines.

Protons H^e and H^c moved slightly upfield ($\Delta\delta$ = - 0.06 ppm) while proton H^g shifted minimally downfield ($\Delta\delta$ = 0.09 ppm). It is well known that the electron lone-pairs of the oxygen atom of carbonyl groups in diphenyl ureas produce an anisotropic field inducing large upfield shifts to the syn-*ortho*-aromatic proton ($\Delta\delta$ > 1.00 ppm). Owing to the reduced chemical shift changes observed for the aromatic protons *ortho* to the amide groups of **1** upon complex formation, we conclude that the bound receptor experiences a reduced conformational change to wrap around the bound anion, in comparison to the conformation adopted in solution in the free state. We putatively assign a helicoidally-shaped conformation for free **1** in solution based on our solid-state studies.

We also performed a ^{1}H NMR spectroscopy titration of **1** with the bromide TBA salt. The incremental addition of the salt produced the expected chemical shift changes for the proton signals of foldamer **1** (Figure 2). Remarkably, the addition of 1 equivalents of the bromide salt did not provoke the saturation of the chemical shift changes. The mathematical analysis of the titration data using a 1:1 theoretical binding isotherm produced a good fit and returned a binding constant value K = 281 M^{-1} (Table 1) and the complexation induced shift (CIS) values of the analysed proton signals. The downfield CIS calculated for the terminal amide protons, H^b, was $\Delta\delta$ = 0.64 ppm. The internal amide protons in **1**, H^a, also shifted downfield but to a lesser extent $\Delta\delta$ = 0.41 ppm. The *ortho*-proton, H^g, in the diamino-phenyl ring B moved downfield $\Delta\delta$ = 0.14 ppm, whereas the chemical shift change experienced by the other *ortho*-proton in the same ring, H^e, was negligible. It is worthy to note that the *ortho*-proton, H^f, in the terminal phenyl groups showed a significant downfield CIS, $\Delta\delta$ = 0.38 ppm. Altogether, the small values calculated for the CIS of the amide protons in the **1**·Br complex suggest that owing to the larger size of the bromide anion the hydrogen bonding interactions are substantially reduced. Nevertheless, the trends of the CIS support that the receptor **1** adopts a bound conformation in the **1**·Br complex that is similar to the one present in the **1**·Cl analogue.

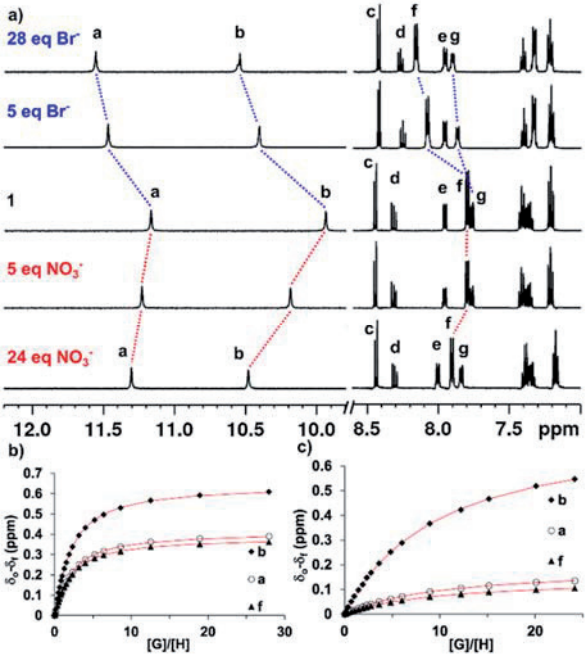

Figure 2. a) The ^{1}H NMR spectra of foldamer **1** in acetone-d_6 (2.5 mM) with incremental amounts of anions. The chemical shift changes observed by protons with addition of b) TBABr, c) $TBANO_3$ fitted to 1:1 binding isotherms (red lines).

Table 1. Binding constants for **1** and TBA salts in 1:1 stoichiometry determined by NMR titration in acetone-d_6 at 25 ˚C.

Guest	K_a (M^{-1})[a]
TBACl	> 10^4
TBABr	281[b]
TBAI	13[b]
$TBANO_3$	46[b]

[a] Global fit of 3-4 signals. [b] The average of two NMR titrations, estimated error < 25 %.

Similarly, we determined the binding constant values for the 1:1 complexes of **1** with nitrate and iodide as 46 and 13 M^{-1}, respectively (Figure 2, Fig. S-24). These results are in complete agreement with the findings of the mass spectrometry experiments (vide supra). The trend in binding constant values is the expected one for the binding of the anions using mainly hydrogen-bonding interactions. The increase in the size of the mono-charged anion has a detrimental effect in the strength of the hydrogen-bonding interaction, which is primarly of electrostatic nature (charge-dipole). Overall, the observed chemical shift changes for the protons of **1** during the titrations with iodide and nitrate suggest a change in the binding geometry adopted by the receptor in the complexes with the larger anions compared to the one expressed in the binding of chloride and bromide. Alternatively, complexes of other stoichiometry than the simple 1:1 might be assembled with the larger anions. Unfortunately, the low thermodynamic stabilities of the complexes hampered further studies.

^{1}H NMR titrations of foldamer 2

The chloride anion was selected for further binding studies with foldamer **2**. Foldamer **2** has one electron withdrawing cyano substituent at the *para*-position of one of its terminal phenyl group A' (Scheme 1). This substitution is expected to increase the anion binding affinity of **2** due to the electron withdrawing effect of the substituent, which is expected to favour NH···anion, CH···anion and anion···π interactions. Moreover, the lack of C_{2v} symmetry for foldamer **2** should allow a direct comparison of the contribution of the two different halves of the host in the chloride binding.

The complete assignment of the proton signals of foldamer **2** was based on a set of high-resolution 1D and 2D NMR spectra (^{1}H, ^{13}C, ^{1}H-^{1}H COSY, HSQC, and HMBC NMR). The ^{1}H NMR spectroscopy titration of foldamer **2** with TBACl in acetone-d_6 showed the diagnostic chemical shift changes of the protons of the host for the formation of the 1:1 complex (Figure 1) with an estimated binding constant value larger than 10^4. The amide proton, $H^{b'}$, corresponding to the *p*-cyanophenyl substituent (ring A') showed the largest CIS ($\Delta\delta$ = 1.30 ppm). In contrast, the amide proton, H^b, attached to the phenyl ring moved downfield to a lesser extent ($\Delta\delta$ = 0.88 ppm), but still in line with the shift experienced by the analogous amide protons of **1**. This observation suggested that the electron-withdrawing -CN substituent had a noticeable effect on the NH···Cl^- interaction for $H^{b'}$. Similarly, the internal amide protons H^a and $H^{a'}$ displayed reduced downfield shifts, $\Delta\delta$ = 0.75 and 0.86 ppm, compared to their counterparts in foldamer **1**. The *ortho*-protons, $H^{f'}$ and H^f, of the two the terminal aryl groups of **2** moved downfield ($\Delta\delta$ = 0.51 ppm) to a similar extent. We observed analogous chemical shift changes for the corresponding *ortho*-protons in foldamer **1**. These observations suggest that **2** adopts a similar conformation than **1** for chloride binding.

We performed a 2D NOESY experiment of the **2**·Cl complex in acetone-d_6, which showed strong NOE cross peaks between the NHs of the *ortho*-substituted amides in the two diamino rings of **2**, H^a and H^b, and $H^{a'}$ and $H^{b'}$, respectively, (Fig. S-7, ESI†). This observation supports the *syn* conformation adopted by the amides in the **2**·Cl complex.

^{1}H NMR titrations of foldamer 3

The complexation of Cl^- with foldamer **3**, possessing one strong electron-withdrawing substituent at the *ortho* position of its two terminal aryl rings (A and A'), was expected to provide a significant boost in binding affinity. The ^{1}H NMR spectroscopy titration, however, revealed that the downfield shifts experienced by the two terminal amide protons, NH^b, were similar to the one measured for foldamer **2** (Figure 3). Intriguingly, the internal amide protons, NH^a, and the *ortho*-aryl proton, H^f, of the terminal phenyl groups in **3** experienced reduced downfield shifts (0.67 and 0.11 ppm) in comparison to the ones observed for foldamers **1** and **2**. Surprisingly, both *ortho*-aryl protons H^g and H^e of the diaminophenyl ring B experienced significant downfield shifts (0.14–0.25 ppm), which can be interpreted as a change in foldamer conformation upon chloride binding compared to **1** and **2**. Furthermore, the saturation of the chemical shift changes experienced by the protons of receptor **3** was achieved after the addition of 2 equivalents of the TBACl. This finding is in striking difference to the observations made in the analogous titrations of **1** and **2** with chloride requiring only one equivalent to reach saturation. These results suggested that the binding of chloride to foldamer **3** might produce a complex with higher stoichiometry than the simple 1:1. The mathematical analysis of the titration data using a 1:1 theoretical binding isotherm produced an acceptable fit, returning a binding constant value lower than expected for the 1:1 complex, K_1 = 5800 M^{-1}. This value is one order of magnitude smaller than the ones measures for the 1:1 complexes of chloride with the **1** and **2** counterparts. As could be anticipated, a better fit of the titration data was obtained using a 1:2 (H:G) binding model containing more variables to optimise ($K_{1:1}$, $K_{1:2}$, $\delta_{1:1}$ and $\delta_{1:2}$). Remarkably, the new fit returned K_1 value for the stability of the 1:1 complex larger than 10^4 M^{-1}. This calculated magnitude for K_1 is more in line with our expectations. The fit assigned a value of 10^8 M^{-2} to the 1:2 complex. Most likely, a relative increase in the thermodynamic stability of the 1:2 complex is responsible for its formation to a significant extent during the titration rather than a destabilisation of the 1:1 precursor (see DFT calculations). We carried out a statistical F-test of the data fit to the two theoretical models to support our preferential selection of the 1:2 model.

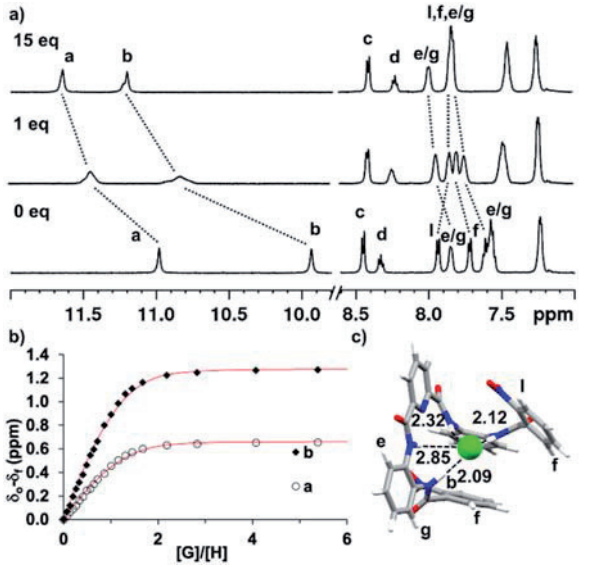

Figure 3. a) The ^{1}H NMR spectra of foldamer **3** with 0, 1 and 15 eq of TBACl in acetone-d_6 (1.2 mM host). b) The chemical shift changes observed by protons with addition of guest (up to 6 eq shown for clarity) fitted to a 1:2 binding isotherm. c) The DFT minimized structure of **3**·Cl showing hydrogen bond distances in Ångströms and NMR labels.

ITC experiments

Isothermal titration calorimetry (ITC) experiments were carried out to assess and compare the binding affinities of foldamers **1**–**3** for chloride accurately. These experiments also provided the thermodynamic enthalpy and entropy parameters of the complexation processes (Table 2, Figure 4). The measurements were performed at 25 °C by placing 0.8–2.0 mM acetone solutions of the host in the calorimeter cell and adding incremental amounts of 7.2–19 mM acetone solution of TBACl using a computer controlled microsyringe. The binding constant values determined for the **1**·Cl and **2**·Cl complexes are similar, and their binding enthalpies identical. Thus, the effect provided by incorporating one -CN group (electron withdrawing substituent) in the terminal phenyl substituent of **2** is minimal based on the ITC results.

Table 2. Thermodynamic parameters for the 1:1 foldamer:Cl^- complexes in acetone at 25 °C. The parameters are an average of 3-6 ITC measurements.

Host	K_a (×10^4 M^{-1})	$\Delta H^{[a]}$	$T\Delta S^{[a]}$	$\Delta G^{[a]}$
1	2.3 ± 0.4	-2.5 ± 0.2	3.4 ± 0.3	-5.9 ± 0.1
2	4.6 ± 0.9	-2.5 ± 0.2	3.9 ± 0.3	-6.4 ± 0.1
3	3.0 ± 0.3	-1.4 ± 0.1	4.7± 0.1	-6.1 ± 0.1

[a] in kcal×mol^{-1}

Surprisingly to us, when the interaction of foldamer **3** with chloride was probed using an ITC experiment, a single sigmoidal isotherm with an inflexion point centred at a 1:1 molar ratio was observed. Thus, the integrated and normalised heat values were fit to a theoretical 1:1 binding model. The returned K_a value was in complete agreement with the one determined using ^{1}H NMR spectroscopy titrations and considering a 1:2 binding model. On the other hand, the binding enthalpy measured for the **3**·Cl complex is slightly smaller than that obtained for the chloride complexes with the foldamers **1** and **2**. Even though only one binding event is detected by ITC we cannot rule out the formation of the 1:2 complex. Assuming that the enthalpy gain for the formation of the 1:2 complex is almost identical to the enthalpy loss during the disassembly of the 1:1 complex the net enthalpy of the binding process will be athermic and thus not detectable by ITC.

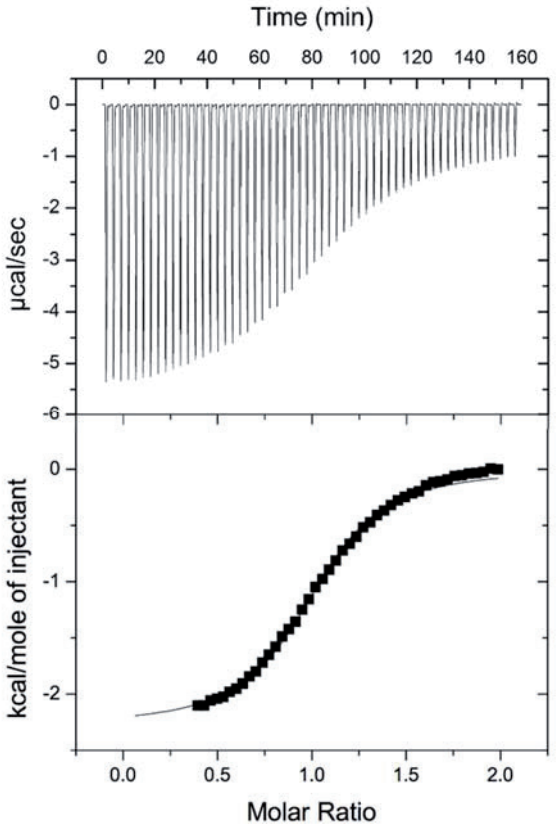

Figure 4. The ITC titration of foldamer **1** with TBACl in acetone at 25 °C, c(host) = 0.97 mM. Data below molar ratio 0.4 was omitted from the fit due to the heat of dilution of the guest.

The binding processes of chloride with the foldamer series are highly favoured by entropy. In fact, the entropic term is the main contributor to complex formation suggesting that significant solvation/desolvation processes are taking place during the binding processes. The observation of a very large and favourable entropic term for binding processes of anions with neutral receptors in polar solvents is not unprecedented.[13] The formation of 1:1 complexes of the foldamers in which the anion is almost fully solvated by the polar groups and the hydrogen atoms of the receptor, requiring a complete desolvation of the chloride and the polar groups of the receptor, would provide a sensible explanation to our observations.

These results demonstrate the important - and difficult to predict - contribution of the entropic term in binding experiments of anions performed in polar solvents. Clearly, the solvation/desolvation processes experienced by receptors **1** and **2** and their chloride complexes are different from those of the dinitro-foldamer **3**. The existence of prominent solvation/desolvation processes makes the analysis and dissection of the contributions of the enthalpy and entropic terms to binding difficult. Nevertheless, the reduced conformational change experienced by the foldamers upon chloride binding, which we derived from the ^{1}H NMR experiments, constitutes an additional factor to reduce the entropic cost of complex formation.

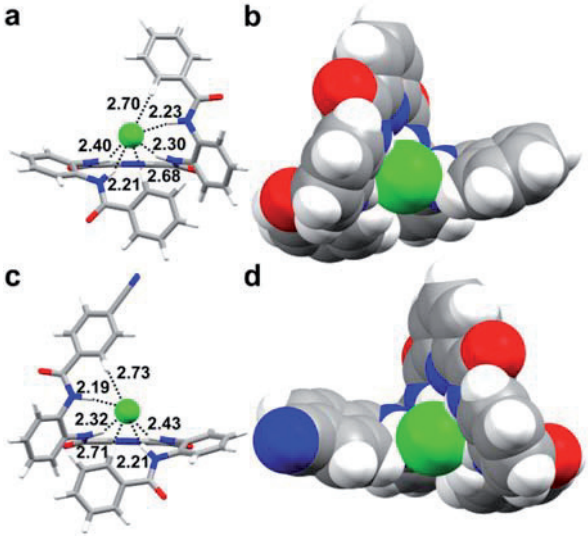

Figure 5. DFT minimized (solution state) geometries for **1**·Cl and **2**·Cl: a,c) a view showing the hydrogen bonding distances in Ångströms, b,d) a side view as a space-filling model. Atom colors: blue = nitrogen, green = chlorine, grey = carbon, red = oxygen, white = hydrogen.

DFT calculations of foldamers 1–3

The conformation adopted by the receptor **1** upon chloride binding, **1**·Cl complex, was also investigated using DFT calculations in the gas phase and in solution (see ESI† for the details and comparison of gas phase and solution state studies). The initial geometry for the energy minimization of the **1**·Cl complex consisted of the atomic coordinates of the corresponding fluoride-foldamer complex crystal structure.[15] The energy-minimized structure of the **1**·Cl complex in solution coincided well with the helical conformation deduced from the ^{1}H NMR titration data. The chloride anion is located within the polar binding site of **1** establishing four hydrogen-bonds with the amide NHs and two CH···Cl interactions with the *ortho*-protons of the terminal phenyl group (Figure 5). This confirms that the radius of the chloride is too big for the anion to be symmetrically inserted in the cavity of the helix defined by bound **1**. For this reason, the chloride shifts away from the plane defined by the atoms of the pyridine ring. The average hydrogen bond lengths for the NH^b protons (2.23 and 2.21 Å) is shorter than for the NH^a analogues (2.30 and 2.40 Å). The C-H^f···Cl^- distances of 2.68 and 2.70 Å support the existence of weak interactions with the *ortho*-protons of the terminal phenyl rings of **1**.

The DFT energy-minimized structure of the **2**·Cl complex is very similar to the calculated structure of **1**·Cl. The most significant finding is that during energy-minimization the Cl^- shifts closer to the *para*-cyano phenyl ring of foldamer **2** in contrast to the symmetrical starting geometry used in the calculation. This finding coincides well with the observed large CIS of $NH^{b'}$ in the NMR titration.

The crystal structure of **3**·F used as starting coordinates for the energy-minimized 1:1 **3**·Cl complex showed a similar helical conformation of the foldamer (Figure 3). The halide establishes four NH hydrogen bonds, a H^f···F^- interaction and a F^-···π interaction with the terminal nitrophenyl rings A (Fig. S-30). The DFT minimized structure of **3**·Cl, however, showed a π···π interaction between rings A and B and further Cl^-···π interactions between the anion and ring A. One of the NH^a···Cl^- hydrogen bonds is extended (2.85 and 2.32 Å) in comparison to **1**·Cl, whereas the NH^b···Cl^- distances are shortened (2.09 and 2.12 Å) in perfect agreement with the observed CIS in the NMR titration. Remarkably, the H^f···Cl^- interaction has been eliminated, which partially coincides with the reduced CIS observed in the NMR titration.

We also used DFT calculations to assign a putative structure to the **3**·Cl_2 complex. The resulting energy-minimized structure (Figure 6) shows two intramolecular NH^a···O=C hydrogen bonds, and two binding clefts for the anions, in which they are experiencing hydrogen bonds with NH^b and Cl^-···π interactions with the nitrophenyl rings.

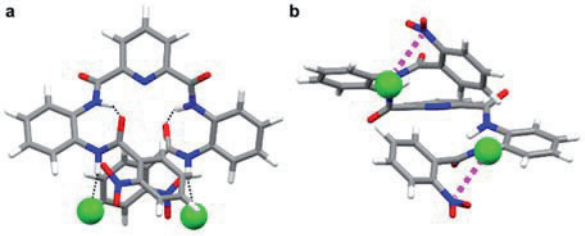

Figure 6. An energy-minimized structure of **3**·Cl_2 showing a) hydrogen bonds with black dashed lines, b) Cl^-···π interactions with magenta dashed lines. Atom colors: blue = nitrogen, green = chlorine, grey = carbon, red = oxygen, white = hydrogen.

Conclusions

Oligoamide foldamers **1**–**3** formed anionic complexes with chloride, bromide, iodide and nitrate while showing the highest binding affinity towards chloride in the order of K = 10^4 M^{-1}. The *cis*-preorganization exerted by pyridine-2,6-dicarboxamide motif was clearly assigned from the NMR experiments in solution. Based on the NMR and DFT studies, a helicoid structure for the 1:1 complexes in solution was proposed. The electron withdrawing *para*-cyano substituent at one terminal phenyl group in foldamer **2** slightly increased the binding affinity towards chloride, yet the effect was minimal. The *ortho*-nitro substituents

in foldamer **3** had an unexpected contribution to the anion binding since besides a thermodynamically stable 1:1 complex, we suggest the formation of a 1:2 host:guest complex.

All chloride complexes had a large positive entropy term, which demonstrates the important, and difficult to predict, contribution of the entropic term in binding experiments performed in polar solvents. Remarkably, the **3**·Cl complex showed the highest gain in entropy, which indicates different solvation/desolvation processes of dinitro-foldamer **3** and its complexes. This is reflected in the slightly different binding geometry supported by anion···π interactions and the likely presence of a 1:2 complex in comparison to the two counterparts. Clearly, the increase in the electrostatic interactions for the binding of charged substrates with a neutral receptor in polar solvent does not warrant a net gain in free energy of binding owing to the complex solvation/desolvation process that takes place in solution.

Experimental Section

Materials

All starting materials and chemicals were commercially available and used as such unless otherwise noted. Analytical grade solvents were used for the complexation studies. Compounds **1-3** were prepared as previously reported.[15,21-23]

Mass spectrometric studies

Mass spectrometry experiments were performed with Micromass LCT ESI-TOF and Qstar Elite ESI-Q-TOF mass spectrometers. 10 mM stock solutions of foldamers **1**, **2** and **3** were prepared in THF and 10 mM stock solutions of ammonium salts of guests were prepared in MeOH. In all measurements acetonitrile was used as solvent and the concentration of hosts **1**, **2** and **3** was 20 μM and the concentration of guests 60 μM. Competition experiments were performed with foldamer **1** and ammonium salts of halide ions Cl^- and Br^-, and Br^- and I^-, respectively.

NMR titration

The NMR spectra were measured with a Bruker Avance DRX 500 or Bruker Avance 400 spectrometer at 25 °C, and the chemical shifts were calibrated to the residual proton resonance of the deuterated solvent. For NMR titration 1.2–5.0 mM host stock solution was prepared in acetone-d_6 using Hamilton glass syringes. The guest solutions were prepared from TBAF·$(H_2O)_3$, TBACl, TBABr, TBAI or $TBANO_3$ in host solution keeping the total concentration of the host constant during titration. Titration was performed using 650 μl of host solution and adding 0.02–35 equivalents of guest in 2–240 μl aliquots. Each titration was performed twice except for foldamer **3** the titration was done once in acetone-d_6 and once in a 9:1 mixture of acetone-d_6 and $CDCl_3$. The titration data were analysed with non-linear regression of 2–4 proton signals to 1:1 binding model using MATLAB (MATLAB and Statistics Toolbox Release R2014b).[27] The analysis of **3**·Cl was made with HypNMR 2008 software Version 4.0.66.[28] The fitting of the titration data was made by optimizing the chemical shifts of the complex species ($\delta_{1:1}$, or $\delta_{1:1}$ and $\delta_{1:2}$ of the same four protons) by non-linear regression.

ITC measurements

The ITC measurements were performed on a MicroCal VP-ITC microcalorimeter at 25 °C. A host stock solution of 0.8–2.0 mM in acetone was titrated with a TBACl solution of a concentration of $c_{guest} = 9 \times c_{host}$. Each titration was performed 3–6 times. A blank experiment was done by titrating the guest solution to the pure solvent, and the heat of dilution was reduced from the experiment before fitting the data to a binding isotherm.

Calculations

The gas phase and solution state geometry optimisations were performed for the foldamer complexes **1**·Cl, **2**·Cl and **3**·Cl with the Turbomole program package[29] using the PBE1PBE density functional[30-33] together with Ahlrichs' def2-TZVP basis sets[34] and Grimme's GD3BJ empirical dispersion correction.[35,36] The effect of the solvent (acetone, ε = 20.5) was taken into account using a conductor-like continuum solvation model COSMO.[37] The initial geometries of complexes **1**·Cl, **2**·Cl, and **3**·Cl were taken directly from the single-crystal X-ray diffraction data of the corresponding fluoride complexes.[15] The initial geometry for **3**·Cl_2 was envisaged by analysing the observed CIS in the NMR titration. Full frequency calculations were performed for the optimised structures in the gas phase to ensure that they correspond to true minima on the potential energy hypersurface.

Acknowledgements

Funding from Academy of Finland (projects 257246, 284562, 278743 and 312514) and University of Jyvaskyla (mobility funding for KH) are acknowledged. M.Sc. Esa Haapaniemi is gratefully acknowledged for assistance with the NMR measurements and Minna Kortelainen and Anniina Aho for providing foldamer **2**.

Keywords: Anions • Foldamers • Host-guest systems • Receptors • Supramolecular chemistry

[1] N. H. Evans and P. D. Beer, *Angew. Chem. Int. Ed.,* **2014**, *53*, 11716–11754.
[2] I. Saraogi and A. D. Hamilton, *Chem. Soc. Rev.*, **2009**, *38*, 1726–1743.
[3] M. J. Kim, H.-W. Lee, D. Moon and K.-S. Jeong, *Org. Lett.*, **2012**, *14*, 5042–5045.
[4] V. Diemer, L. Fischer, B. Kauffmann and G. Guichard, *Chem. Eur. J.*, **2016**, *22*, 15684–15692.
[5] U.-I. Kim, J. Suk, V. R. Naidu and K.-S. Jeong, *Chem. Eur. J.*, **2008**, *14*, 11406–11414.
[6] H. Juwarker, J. M. Lenhardt, D. M. Pham and S. L. Craig, *Angew. Chem. Int. Ed.*, **2008**, *47*, 3740–3743.
[7] R. Wechsel, J. Raftery, D. Cavagnat, G. Guichard and J. Clayden, *Angew. Chem. Int. Ed.*, **2016**, *55*, 9657–9661.
[8] Y. Liu, F. C. Parks, W. Zhao and A. H. Flood, *J. Am. Chem. Soc.*, **2018**, *140*, 15477–15486.
[9] Y. Wang, J. Xiang and H. Jiang, *Chem. Eur. J.*, **2011**, *17*, 613–619.
[10] S. O. Kang, J. M. Llinares, V. W. Day and K. Bowman-James, *Chem Soc Rev*, **2010**, *39*, 3980–4003.
[11] M. J. Chmielewski and J. Jurczak, *Chem. Eur. J.*, **2005**, *11*, 6080–6094.
[12] S. Lee, Y. Hua, H. Park and A. H. Flood, *Org. Lett.*, **2010**, *12*, 2100–2102.
[13] R. Tepper, B. Schulze, H. Görls, P. Bellstedt, M. Jäger and U. S. Schubert, *Org. Lett.*, **2015**, *17*, 5740–5743.
[14] H. Juwarker, J. M. Lenhardt, J. C. Castillo, E. Zhao, S. Krishnamurthy, R. M. Jamiolkowski, K.-H. Kim and S. L. Craig, *J. Org. Chem.*, **2009**, *74*, 8924–8934.
[15] K. Helttunen, R. Annala, A. Suhonen, E. Nauha, J. Linnanto and M. Nissinen, *CrystEngComm*, **2017**, *19*, 5184–5187.
[16] E. Wagner-Wysiecka and J. Chojnacki, *Supramol. Chem.*, **2012**, *24*, 684–695.

[17] C. Caltagirone, C. Bazzicalupi, A. Bencini, F. Isaia, A. Garau and V. Lippolis, *Supramol. Chem.*, **2012**, *24*, 95–100.

[18] G. W. Bates, P. A. Gale and M. E. Light, *Chem. Commun.*, **2007**, 2121–2123.

[19] T. Zieliński, P. Dydio and J. Jurczak, *Tetrahedron*, **2008**, *64*, 568–574.

[20] See for example: a) Y. Hamuro, S. J. Geib and A. D. Hamilton *J. Am. Chem. Soc.,* **1996**, *118*, 7529–7541. b) V. Berl, I. Huc , R. G. Khoury, M. J. Krische and J. ‐ M. Lehn, *Nature* **2000**, *407*, 720−723. c) J. Zhu, R. D. Parra, H. Zeng, E. Skrzypczak-Jankun, X. C. Zeng and B. Gong, *J. Am. Chem. Soc.*, **2000**, *122*, 4219–4220. d) H. Jiang, J.-M. Léger and I. Huc, *J. Am. Chem. Soc.*, **2003**, *125*, 3448–3449. e) Z.-Q. Wu, X.-K. Jiang, S.-Z. Zhu, and Z.-T. Li, *Org. Lett.,* **2004**, *6*, 229–232.

[21] A. Suhonen, E. Nauha, K. Salorinne, K. Helttunen and M. Nissinen, *CrystEngComm*, **2012**, *14*, 7398–7407.

[22] M. Kortelainen, A. Suhonen, A. Hamza, I. Pápai, E. Nauha, S. Yliniemelä-Sipari, M. Nissinen and P. M. Pihko, *Chem. Eur. J.*, **2015**, *21*, 9493–9504.

[23] A. Suhonen, M. Kortelainen, E. Nauha, S. Yliniemelä-Sipari, P. M. Pihko and M. Nissinen, *CrystEngComm*, **2016**, *18*, 2005–2013.

[24] R. Annala, A. Suhonen, H. Laakkonen, P. Permi and M. Nissinen, *Chem. Eur. J.*, **2017**, *23*, 16671–16680.

[25] Preliminary studies with TBAF suggested aggregation and either H/D exchange or deprotonation of the host (see ESI†). Thus, complexation with fluoride was not investigated further in solution.

[26] Most likely, the small difference measured in the CIS is related to different acidity and positioning in the resulting 1:1 complex; the pKa = 23.3 for benzamide and pKa = 22.0 for 3-picolinic amide (see refs. [38] and [39]). We also performed electrostatic surface potential calculations to compare the hydrogen bonding abilities of the amide protons (see Fig. S-32, ESI†).

[27] P. Thordarson, *Chem. Soc. Rev.*, **2011**, *4*, 1305–1323.

[28] C. Frassineti, S. Ghelli, P. Gans, A. Sabatini, M. S. Moruzzi and A. Vacca, *Anal. Biochem.*, **1995**, *231*, 374–382.

[29] *TURBOMOLE V7.3 2018, a development of University of Karlsruhe and Forschungszentrum Karlsruhe GmbH, 1989-2007, TURBOMOLE GmbH, since 2007; available from http://www.turbomole.com*., 2018.

[30] C. Adamo and V. Barone, *J. Chem. Phys.*, **1999**, *110*, 6158–6170.

[31] P. Perdew, John, K. Burke and M. Ernzerhof, *Phys. Rev. Lett.*, **1997**, *78*, 1396.

[32] P. Perdew, John, K. Burke and M. Ernzerhof, *Phys. Rev. Lett.*, **1996**, *77*, 3865–3868.

[33] J. P. Perdew, M. Ernzerhof and K. Burke, *J. Chem. Phys.*, **1996**, *105*, 9982–9985.

[34] F. Weigend and R. Ahlrichs, *Phys. Chem. Chem. Phys.*, **2005**, *7*, 3297–3305.

[35] S. Grimme, S. Ehrlich and L. Goerigk, *J. Comput. Chem.*, **2011**, *32*, 1456–1465.

[36] S. Grimme, J. Antony, S. Ehrlich and H. Krieg, *J. Chem. Phys.*, **2010**, *132*, 154104.

[37] A. Klamt and G. Schüürmann, *J. Chem. Soc. Perkin Trans.* **1993**, *2*, 799–805.

[38] F. G. Bordwell and G.-Z. Ji, *J. Am. Chem. Soc.*, **1991**, *113*, 8398–8401.

[39] F. G. Bordwell, H. E. Fried, D. L. Hughes, T.-Y. Lynch, A. V. Satish and Y. E. Whang, *J. Org. Chem.*, **1990**, *55*, 3330–3336.